UNIVERSITÀ DI PISA

Scuola di Dottorato in Ingegneria "Leonardo da Vinci"

Corso di Dottorato di Ricerca in
SICUREZZA NUCLEARE E INDUSTRIALE

Tesi di Dottorato di Ricerca

Characterization of the Mixed Radiation Fields for BNCT

Autore:

Nafiseh Mirzajani _____

Relatori:

Prof. Francesco d'Errico _____

Prof. Giorgio Curzio _____

Dr. Riccardo Ciolini _____

Anno 2013

Acknowledgements

I would like to express best gratitude and most sincere thanks to my tutors Prof. Francesco d'Errico, Prof. Giorgio Curzio and Dr. Riccardo Ciolini for their encouragement, supervision and profound enthusiasm, discussion, patience for reading and their comment on this thesis.

I am also grateful to Prof. Walter Ambrosini for his guidance and helpful advice during my work.

I wish to thank Dr. Angela Di Fulvio, Dr. Dahmane Mazed, Chiara Romei, Daniele Del Serra, Aldo Del Gratta and Fabio Pazzagli for collaboration and advice during this project.

I would like to acknowledge the kind, care and support of all staff of departments of Civil and Industrial Engineering (DICI), University of Pisa.

I must sincerely thank my parents, my lovely sister, my family and all of my friends in Pisa whose support and encouragement have helped me throughout my studies.

Ringraziamenti

Vorrei esprimere la mia gratitudine e i più sinceri ringraziamenti ai miei tutori Prof. Francesco D'Errico, Prof. Giorgio Curzio e il Dott. Riccardo Ciolini per l'incoraggiamento, la supervisione, il profondo entusiasmo, le discussioni e nonché la pazienza per la lettura e i loro preziosi commenti su questa tesi.

Sono anche grato al Prof. Walter Ambrosini per la sua guida e consigli utili provveduti durante lo svolgimento di questo lavoro.

Desidero ringraziare il Dott. Angela Di Fulvio, Dr. Dahmane Mazed, Chiara Romei, Daniele Del Serra, Aldo Del Gratta e Fabio Pazzagli per la collaborazione e la consulenza nel corso di questo progetto.

Vorrei riconoscere anche in genere, la cura e il sostegno di tutto il personale del Dipartimento di Ingegneria Civile e Industriale (DICI), Università di Pisa.

Devo sinceramente ringraziare i miei genitori, mia bellissima sorella, la mia famiglia e tutti i miei amici a Pisa per il sostegno e l'incoraggiamento e l'aiuto provveduto durante i miei studi.

Index

Introduction

Mixed radiation fields are normally encountered in the treatment of tumors with ionizing radiations in Boron Neutron Capture Therapy (BNCT). BNCT is a binary treatment modality for a variety of tumors, mainly high-grade primary brain tumors (glioblastoma multiforme), skin malignant melanoma, hepatic metastases and other cancers. Several hundred patients have been treated in the United States of America, Europe, Argentina and Japan. Survival times are comparable with those obtained with standard radiation therapy but improved patients' quality of life have been reported as a result of several of these BNCT treatments (Stupp, 2005; Menendez, 2009; Skold, 2010; Barth, 2012).

The BNCT facilities use research reactors or accelerator-based neutron beams with a broad epithermal energy spectrum, ranging from few eV up to about 30 keV, which also includes fast neutrons and gamma rays as contaminants. Before delivering this type of therapy, it is necessary to obtain detailed information on the neutron energy spectrum of the BNCT facility and evaluate the neutron dose delivered to the tumor and also to the adjacent healthy tissues of the patient, because the effectiveness of neutrons beams varies greatly depending on their energy. Thus, one of the major challenges of BNCT is to characterize the neutron beam in terms of intensity and energy spectrum.

The main aim of the present research is the definition of a suitable methodology for a complete neutron characterization of mixed field BNCT facilities, but the developed method applies generally also to other type of mixed fields, as found in the LINAC irradiation rooms. These neutron fields are complex to characterize because normally their energy extends from thermal (about 10-8 MeV) up to tens of MeV. Different neutron spectrometric techniques are available, which differs from what concerns their limitation and specific energy response, but only multi sphere systems (Bonner sphere Spectrometers, BSS) were found to have a wide energy range of application with an isotropic response (Alevra, 2003; Thomas, 2002). This type of neutron spectrometer consists of a set of moderating Bonner spheres with different diameters, typically made of polyethylene with a neutron thermal detector (passive or active) positioned at the center of each Bonner sphere. The accuracy of the resulting spectral neutron fluence is related to the application of an unfolding procedure to the experimental readings of the BSS and the availability of accurate spectrometer response matrix. Very precise response matrixes have been calculated solving the neutron transport equation or using Monte Carlo methods (Mares, 1994; Vega-Carrillo, 2008). The unfolding process is one of the most complicated parts of the BSS-based spectrometry. Most of the commonly employed unfolding codes rely on mathematical convergence algorithms, thus requiring a guess spectrum as similar as possible to the one to be determined (Matzke, 1994). The FRUIT (Bedogni, 2007) and MAXED (Reginatto, 2002) unfolding code were selected as a proper tool to obtain the neutron energy spectrum from the experimental data.

Neutron scattering contribution in the neutron energy spectrum profile is generally present due to the interactions of neutrons with accelerator room structures (walls, air and the ancillary experimental apparatus). To evaluate this contribution, the shadow cone technique (Eisenhauer, 1985; ISO, 2000; IAEA, 2000) was applied with BSS for the measurement of neutron spectra in the considered mixed radiation fields. The main item of this technique was counting the scattered neutrons contribution in the considered neutron installation. For this purpose, three shadow cones were realized and positioned between the source and BSS. Experiments were performed to select the optimal source to shadow cone distance by using an unfolding code to determine the neutron spectrum. The difference between the unfolded spectra obtained by using the shadow cones and the ISO reference spectra was considered as a parameter to select the optimum condition in the shadow cone technique application.

BSS and shadow cone method were applied for the investigation of neutron spectrum for an under construction BNCT facility. In particular, in this work, experimental activities were performed at INFN Legnaro National Laboratories (LNL) (Padua, Italy) aimed at angular-dependence neutron energy spectra measurements produced by the ^{9}Be (p,xn) reaction, under 5 MeV proton beam. Such a work was performed in the framework of the INFN TRASCO-BNCT project. In this work, a BSS based on ^{6}LiI(Eu) scintillator, named from now on BSS-UNIPI, coupled with the shadow cone technique was applied. The response function matrix for the set of BSS-UNIPI Bonner spheres and bare ^{6}LiI(Eu) detector was calculated by MCNPX code (Pelowitz, 2008) for an extended neutron incidence energy range from 1 meV to 100 MeV. To obtain the neutron spectrum from measurements, the response function determined for each Bonner sphere was used and both the FRUIT and MAXED unfolding codes were applied to obtain the final spectra. The results are in agreement. This thesis is organized as follows:

Chapter 1 is an overview of physical bases, history and present status of BNCT, with a description of the applications of different available neutron sources for this type of therapy.

Chapter 2 introduces neutron spectrometry detectors and technique with special attention dedicated to BSS, with the more common active or passive detectors. Moreover, BSS based on ^{6}LiI(Eu), which are selected for measuring the neutron spectrum in BNCT facility in this work, are described.

Chapter 3 describes a general review of Monte Carlo methods, Monte Carlo calculation response function and matrix of BSS-UNIPI based on ^{6}LiI (Eu), the response function of BSS-UNIPI based on activation foils.

Chapter 4 gives a general review of the unfolding method and the description of the selected unfolding codes, FRUIT, version 5, and MAXED.

Chapter 5 describes the experimental calibration of BSS and the set-up of the shadow cone technique.

Chapter 6 is devoted to the application of BSS-UNIPI for the determination of the angular neutron energy spectrum produced by the ^{9}Be (p,xn) reaction, under 5 MeV proton beam, to be applied for an accelerator-based BNCT facility at INFN-LNL.

Chapter 7 reports the summary, conclusions and prospects.

References

Alevra, A.V and Thomas, D. J. (2003). Neutron spectrometry in mixed fields: multisphere spectrometers. *Radiation Protection Dosimetry*, 107 (1–3), pp. 37-72.

Barth, R.F., et al. (2012). Current status of boron neutron capture therapy of high grade gliomas and recurrent head and neck cancer. *Radiation Oncology,* 7, 146, pp. 8-21.

Bedogni, R., et al. (2007). FRUIT: an operational tool for multisphere neutron spectrometry in workplaces. *Nuclear Instruments and Methods A*, 580, pp. 1301–1309.

Ceballos, C., et al. (2009). The BSA modeling for the accelerator-based BNCT facility at INFN LNL for treating shallow skin melanoma. *Applied Radiation and Isotopes,* 67 (7-8), pp. S274-S277.

Eisenhauer, C.M., et al. (1985). Calibration techniques for neutron personal dosimetry. *Radiation Protection Dosimetry*, 10, pp. 43–57.

IAEA, Safety Reports Series No. 16, 2000.

ISO 8529-2, 2000. Reference neutron radiations—part 2: calibration fundamentals of radiation protection devices related to the basic quantities characterizing the radiation field, International Organization for Standardization, Geneva, Switzerland.nt with other authors.

Mares, V and Schraube, H. (1994). Evaluation of the response matrix of a Bonner sphere spectrometer with Lil detector from thermal energy to 100 MeV. *Nuclear Instrumental Method A*, 337, pp. 461-473.

Matzke, M. (1994). Unfolding Methods, *Report D38116, Physikalisch-Technische Bundesanstalt*, Germany.

Menendez, P.R., et al. (2009). BNCT for skin melanoma in extremities: Updated Argentine clinical results. *Applied Radiation and Isotopes,* 67(S), pp. S50–S53.

Pelowitz, D.B. (2008). MCNPX User's Manual, 2.6.0 ed., LA-CP-07-1473.

Pisent, A., et al. (2006). Progress on the accelerator based SPES-BNCT project at INFN Legnaro. *Journal of Physics: Conference Series,* 41, pp. 391-399.

Prete, G., et al. (2008). Selective production exotic Species, Chapter XII – SPES applied Science, BNCT and LENOS. Technical design report. INFN-LNL-224, pp. 181-214.

Reginatto, M., et al. (2002). Spectrum unfolding, sensitivity analysis and propagation of uncertainties with the maximum entropy deconvolution code MAXED. *Nuclear Instruments and Methods A*, 476, pp. 242-246.

Skold, K., et al. (2010). Boron neutron capture therapy for newly diagnosed glioblastoma multiforme: An assessment of clinical potential. *British Journal* of *Radiology*, 83(991), pp. 596-603.

Stupp, R.M., et al. (2005). Radiotherapy plus concomitant and adjuvant temozolomide for glioblastoma. *The New England* Journal *of Medicine*, 352(10), pp. 987-996.

Thomas, D.J., et al. (2002). Bonner sphere spectrometers—a critical review. *Nuclear Instruments and Methods in Physics Research*, A 476, pp. 12-20.

Vega-Carrillo, H.R., et al. (2008). Calculation of Response matrix of a BSS with ^{6}LiI scintillator. *Revista Mexicana de Física S*, pp. 54-57.

1. Boron Neutron Capture Therapy

Boron neutron capture therapy (BNCT) is one of the experimental types of radiotherapy treatments cancers. BNCT has started to show its ability to treat types of cancers. It has traditionally been used to treat the malignant brain tumour called glioblasoma multiforme (GBM) and then melanomas since the mid-1980s. There are some reports about successful trial BNCT about especially head and neck tumors, but it hasn't become a conventional therapy yet. Thus, BNCT is still in the trial stage now (Barth, 2012; Kankaanranta, 2011; 2012; Miyatake, 2012).

In recent years, BNCT also has been used to treat recurring of primary or recurrent cancers such as liver, lungs, thyroid and skin cancers (Emiliano, 2012; Masunaga, 2012; Pisarev, 2012; Gonzalez, 2004).

Fig. 1.1 shows a patient with a recurrent mucoepidermoid carcinoma neck cancer after 22 months of the first BNCT session treatment. Three treatment sessions caused not only a beneficial reduction in tumor size with BNCT, but also resolution of a cutaneous ulcer and reepithelization were recovered from normal skin. These results clearly demonstrate that BNCT is a highly tumor-selective treatment modality, and the patient lived for 7 years more before die.

Figure 1.1: In the left a patient with a recurrent mucoepidermoid carcinoma cancer of the parotid gland and on the right patient after 22 months of the first BNCT (Kato, 2004).

BNCT has some advantages and disadvantages in comparison to external photon radiotherapy. The advantages included are: first, BNCT has the ability to selectively deliver a high radiation dose to the tumor with a much lower dose to surrounding normal tissues. This is an important feature that makes BNCT particularly attractive for salvage therapy of patients who have been treated to tolerance with chemotherapy and radiotherapy; second, it has the potential to more effectively target multicentric deposits of tumor than is possible with stereotactic radiosurgery of primary and metastatic brain tumors. Third, although it may be only palliative, it can produce striking clinical responses, as evidenced by the experience of several groups treating patients with recurrent, therapeutically refractory head and neck cancer (Diaz, 2003; Busse, 2003; Barth, 2012); finally, median survival times of patients (GBM) have been increased who were treated by BNCT combining with conventional fractionated photon radiotherapy (BNCT-XRT) and temozolomide in comparison with using BNCT alone (Kawabata, 2011; Yamamoto, 2011; Nakai, 2011).

However, there are few disadvantages of using BNCT. There are only few of neutron beams which has quality required for BNCT (Catharine, 2005): nuclear reactors, charged-particle accelerators, compact neutron generators and hospital radiotherapy facilities (Photo Neutron Source (PHONES)) for BNCT that can produce the required low-energy neutron beam for BNCT (Burian, 2006; Prest, 2010; Autrerinen, 2001; 2005; 2012). Moreover BNCT facilities of the radiation are required to support medical facilities. While there are many research reactors around the world, only a few of them were modified to develop BNCT. Then, there are not yet available boron compounds with a sufficiently high ratio of boron delivery tumor to healthy tissue, to ensure that healthy tissues will not be affected by BNCT treatment.

A third disadvantage is due to the additional undesirable dose components which will be produced as an unavoidable side-effect, the most significant of these being the gamma ray and fast neutron contamination components which come from the neutron source. Also a supplementary gamma dose is generated via neutron capture in hydrogen of the tissues during patient irradiation. These doses, which are not directed at the tumor cells, place a limit on the total dose which can be delivered to the region of the body.

Although the research to the concept of BNCT is going on about seventy years, all the current work is still under investigation. The major challenges for the BNCT research include improving the beam quality of incident neutrons, developing new boron delivery agents, devising better methods to accurately calculate dose, finding alternative sources of neutrons, and creating beams with epithermal neutrons (he energy range 1 eV-10 keV), that are capable of reaching deep seated tumors without the need for surgery.

This chapter describes the fundamental of BNCT, an overview of the BNCT history and present status, and then neutron sources which were used or under development for BNCT.

1.1 The fundamental of BNCT

BNCT is based on thermal neutrons interaction with ^{10}B (~20 μg/g weight or ~10^9 atoms/cell), injected to the patient's tumor, the reaction produces two high LET[1] particles: ^{7}Li isotope (6 μm) and ^{4}He (α) (9 μm) particle and their ranges are comparable to a cell diameter (10 μm) as (Figs. 1.3 and 1.4). Nuclear reactions take place inside a tumor cell in the following (Walker, 1998):

$$^{10}B + ^{1}n\ (0.025\ eV) \rightarrow ^{11}B^* \rightarrow ^{7}Li^*\ (0.84\ MeV) + \alpha\ (1.47\ MeV) \qquad (94\ \%)$$

$$^{7}Li^* \rightarrow ^{7}Li + \gamma\ (0.48\ MeV)$$

$$^{10}B + ^{1}n\ (0.025\ eV) \rightarrow ^{11}B^* \rightarrow ^{7}Li\ (1.01\ MeV) + \alpha\ (1.78\ MeV) \qquad (6\ \%)$$

The cross section of the $^{10}B(n,\alpha)^{7}Li$ reaction is very high (about 3837 barns) at thermal energy, the Q-value is 2.790 MeV. When the ^{10}B nucleus captures a thermal neutron it becomes ^{11}B nucleus in the excited state for a very short time (~ 10^{-12} s). Then the excited boron ($^{11}B^*$) decays by producing an alpha particle, and an excited-state lithium ($^{7}Li^*$) with a probability of 94%. In the sequence, $^{7}Li^*$ decays to its fundamental level with a gamma ray emission (0.478 MeV) (Chadwick, 2006) (Fig. 1.2).

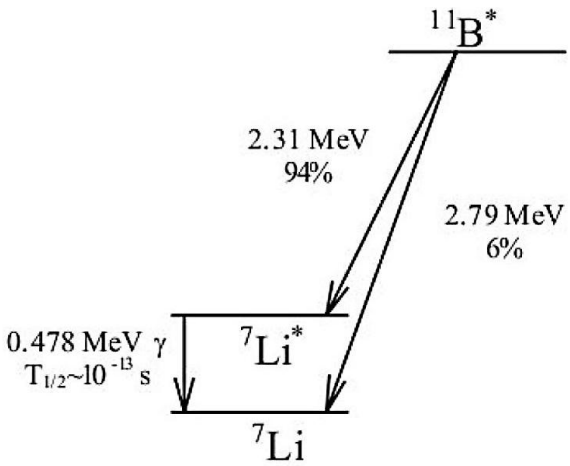

Figure 1.2: Energy level diagram for $^{11}B^*$ showing its decay scheme (Chadwick, 2006).

[1] linear energy transfer

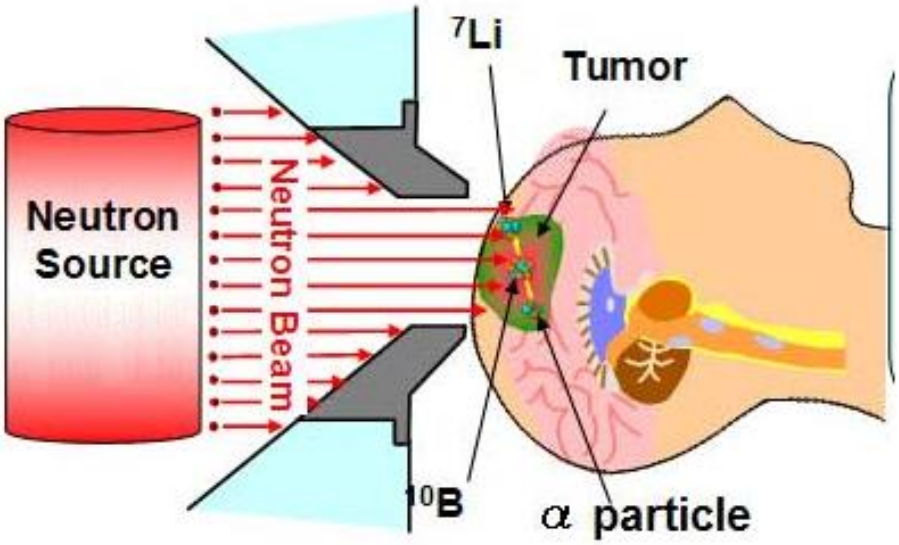

Figure 1.3: Schematic method of BNCT like the one performed by Hatanaka in Japan (Takayanagi, 2012).

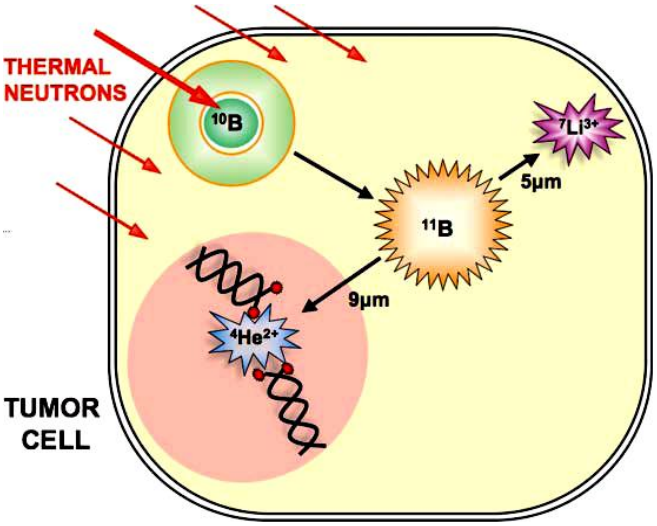

Figure 1.4: The process of thermal neutrons interaction with ^{10}B inside the tumor cell which are producing two particles (^{7}Li and $^{4}He(\alpha)$).

When the reaction takes place inside a cell, the two ionizing particles leave the nucleus of tumor cells and can cause non repairable damages to the DNA, as double strand breaks. Because of their short ranges and high LET, the lethal damage is largely restricted to the tumor cells (Fig. 1.4) (Soyland, 2000; Pouget, 2001; Hall, 2000; Soloway, 1998). The energy of the neutrons which should be used depends on the depth of the tumour in BNCT. Thermal neutrons (0.025 eV) were used to irradiate shallow tumors, while epithermal neutrons (1 eV - 10 keV) were applied for treating deep tumors because they penetrate farther into the body before being slowed down to thermal energies.

Thermal neutrons have little effect on normal cells, since the capture cross-sections of the major tissue elements ^{16}O, 1^2C, ^1H, and ^{14}N are only 1.9×10^{-4} b, 3.4×10^{-3} b, 3.32×10^{-1} b and 7.5×10^{-2} b, respectively (Chadwick, 2006). This is one advantage for BNCT because the surrounding healthy cells would be spared from radiation damages coming from the capture reactions occurring in tumor cells. By fluence of 10^{12} neutrons/cm^2 and 10^9 boron atoms per cell would be enough to produce 2 to 3 neutron captures. Thus, the cell would be damaged. The proper borate compound such as (L)-4-dihydroxy-borylphenylalanine, referred to as boronophenylalanine (BPA), and $Na_2B_{12}H_{11}SH$, known as sodium borocaptate (BSH), have been used in clinical trials (Barth, 2012). These two compounds represent two different approaches to delivering boron to the tumours. BSH relies on passive diffusion from the blood into brain tumours. Brain tumors disrupt the blood brain barrier (BBB), and as a result BSH is able to diffuse into cancerous cells but not into healthy areas of the brain where the blood brain barrier is still intact.

In recent years, the development of novel improved boron carriers for BNCT has focused on nanoparticles (Steen Paterson, 2008; Mandal, 2011), porphyrin type (Shinji, 2011), nucleosides (Byun, 2006) and amino acids (Kabalka, 2003; Semioshkin, 2007) which are still used in the BNCT research programs for their ability to concentrate the boron atoms preferably in tumor cells.

Whilst the most of attention world-wide has focused on ^{10}B as the neutron capture isotope in BNCT but there are other possibilities to use isotopes (^{11}B, ^{12}C, ^1H, ^{14}N, ^{23}Na, ^{35}Cl, ^{235}U, ^{153}Gd and ^{157}Gd). Gadolinium-157 (^{157}Gd) has the highest neutron cross section (248,000 barns) for thermal neutrons among the stable nuclides and produces the neutron capture reaction (n,γ) as follows (nth is a thermal neutron):

$$^{157}Gd + n_{th}\ (0.025\ eV) \rightarrow {}^{158}Gd^* \rightarrow {}^{158}Gd + \gamma + 7.94\ MeV$$

Thus, ^{157}Gd have been proposed as Gadolinium Neutron Capture Therapy (GdNCT) for brain cancer in the 1980's. The released energy of ^{157}Gd interaction with neutron thermal is more than 90% (~ 7.5 MeV) deposited by prompt gamma rays that reduce the local energy deposition. The emitted gamma rays partially interact with tumors but mainly diffuse in the body damaging healthy tissues. Also different Gd nuclear reactions and the generated Auger electrons in particular, cause a high local energy deposition, which results in a tumour cell inactivation. DNA single and double strand breaks from Auger electrons emitted during $^{157}Gd(n,\gamma)$ events (Cerullo, 2009; Goorley, 2004).

Some research was done on *In vivo* experiments and toxicity studies for this new compound in GdNCT (De Stasio, 2001; 2005; Cerullo, 2009; Crossley, 2010). There are very few studies demonstrating the efficacy of GdNCT in experimental animal tumor models (Tokumitsu, 2000). Gadolinium such as Gd-DTPA currently is widely used to enhance images in MRI[2] (Geninatti-Crich, 2011). Nowadays, it is commonly assumed the use of gadolinium instead of boron in neutron capture therapy and it is under investigation in worldwide.

Recently an investigation was done about using components H_2TCP and H_2DCP as carboranyl porphyrins instead of boronophenylalanine. The result showed that it can be used as delivery agents for BNCT of an experimental brain tumor. In addition they have enhanced cellular uptake and improved therapeutic efficacy (Kawabata, 2011). However BNCT needs to develop new delivery agents in future. In following section an overview of BNCT history and present status will be described.

1.2 The BNCT history and present status

Two years after the discovery of neutrons in 1932 by Chadwick, the first research about the interaction of thermal neutron with boron which produces charged particle (^{7}Li and ^{4}He) was done at Cambridge University (Goldhaber, 1986). BNCT was first proposed by a biophysicist, Locher, of the Franklin Institute in Pennsylvania in 1936. He suggested treating tumors with thermal neutron irradiation and ^{10}B which has a high reaction cross section (Locher, 1936). Then, the first radiobiological studies by using the $^{10}B(n,\alpha)^7Li$ reaction was performed at the University of Illinois in 1938 (Kruger, 1940). During the years 1951 to 1961, the first clinical application of BNCT was done for a group of malignant glioma patients at Brookhaven National Laboratory (BNL) in USA. At the same time, other clinical application of BNCT was done for 18 patients (brain cancer) at Massachusetts Institute of Technology (MIT) in USA. BNL and MIT used the thermal neutron beams extracted from the reactors of the two laboratories and applied a borate compound named Borax (^{10}B-enriched) for trials. These trials were not successful because of the thermal neutrons penetrated insufficiently into the deep tumors, damaging the scalp and the ^{10}B carrier accumulated inadequately in the tumor cells. In additional, an induced tumor was found at depth following doses that exceeded the tolerance of normal surface tissues. Thus, all clinical trials in the USA had been stopped in 1961 (Farr, 1954; Soloway, 1967; Slatkin, 1991).

In 1960, Hatanaka confirmed that BNCT has advantages for the patient's treatment of brain cancers in comparison between BNCT and conventional chemo-immuno – radiotherapy in Japan (Hatanaka, 1986). After that he applied new borate compounds BSH that were able to deliver a higher boron concentration inside the tumor cells for avoiding thermal neutron penetration problem. His trial had three processes: First, the tumor was removed as much as possible by surgery. Second,

[2] Magnetic resonance imaging

BSH was slowly injected into the residual tumor that was able to deliver a higher boron concentration inside the tumor cells. Third, half a day later, the residual tumor was irradiated by a thermal neutron beam at the Hitachi Training Reactor (HTR) (Hatanaka, 1973; 1991; Hawthorne, 2003).

In the 1980s, BPA was utilized for intravenous administration in cutaneous and intracerebral melanoma, combined still with the thermal neutron beams in Japan. The application of BNCT for treating brain tumors gave better results, even if the mean survival was no longer than the one obtained with conventional radiotherapy.

Nevertheless the high number of patients treated (120 patients in Japan) pushed the research to go on and improve the clinical results during the years 1960 to 1990. (Mishima, 1989 ; Hatanaka, 1994; Nakagawa, 1997).

In 1980, a preliminary clinical BNCT was started on glioblastoma multiforme and supported by the BIOMED I program of the European commission. In this program the BNCT facility was the high flux reactor (HFR) for treating patients at Petten in the Netherlands. At the time, a European team of experts worked in collaboration of German radiotherapist of the University of Essen (Germany) (Gabel, 1990; Moss, 1990; Sauerwein, 1997).

In 1984 a great multidisciplinary program of research started on application of BNCT to treatment of cancer at the University of Pavia in Italy, with the following goals: 1) to define the conditions under which the neutron irradiation could obtain a therapeutic result on an explanted organ bearing areas of neoplastic populations; 2) to verify the possibility to achieve these conditions in the liver; 3) to apply the BNCT procedure both in cell cultures and in the experimental animal (Zonta, 2006). Previously, the trials which were done in USA and Japan applying thermal neutron beams in the treatment by BNCT; however, the next trials have shifted, USA using of higher energy epithermal neutron beams, while in Japan, both epithermal and thermal-epithermal neutron beams are being used in BNCT facilities (Savolainen, 2012).

During 1994 to1999, a new clinical trial started at the BNL, USA: it was the first time that the higher energy epithermal neutrons using for the treatment of 53 GBM patients. The method allowed reaching a better penetration, to spare the skin and to deliver a higher BNCT dose in the tumor. While the neutron was passing the layers of tissue, it is thermalized in the first layers of tissue (skin, scalp). Moreover, a new generation of borate compounds BPA-f (borophenylalanine-fructose complex) was used, which was able to carry the boron atoms inside the cells penetrating their membrane (Coderre, 1997; Chanana, 1997; Diaz, 2003). In 1996 to 1999, at MIT a trial started for the treatment of 20 GBM patients with orally taken BPA and using epithermal neutron beams and 2 years later another trial was done for intra-cerebral melanoma or lioblastoma in the same laboratory (Madoc-Jones, 1999; Busse, 2003).

In 1996, the first configuration of an epithermal neutron beam for BNCT was constructed at the Finnish research reactor FiR1 in Otaniemi, Espoo (Finland). After the final configuration, FiR1 was used for radiobiological studies and patient

treatments in 1997. Two years later, over hundred patient irradiations have been performed (Auterinen, 2001).

During 1997 to 2002, the first clinical trial of BNCT was started at HFR in Petten (Netherlands) by the collaboration EORTC[3] (BNCT group). 26 GBM patients have been treated by combining BSH and epithermal neutron beams, in collaboration with at the Academic Hospital of the Free University (AZVU) in Amsterdam (NL) and the Department of Radiotherapy of the University of Essen (Germany) within the BIOMED II Program (Sauerwein, 1999). The aims of this study were to investigate the systemic toxicity of i.v. administration of BSH, the maximum tolerated radiation dose and the dose limiting toxicity of BNCT. However, dose limiting toxicities were observed in this study (Hideghéty, 1999; Sauerwein 2002; Capala, 2003; Vos, 2005; Nievaart, 2007).

In 1997, the Japanese clinical BNCT group started to use BPA and epithermal neutrons for brain cancer treatments in Japan (Imahori, 1998).

In Finland, from 1999 to 2001, trials started with BPA and epithermal neutrons for 18 GBM patients at Helsinki University Central Hospital and VTT (Technical Research Center). In additional, the patients had surgery before BNCT (Joensuu, 2003).

From 1999 to 2005, preliminary study of clinical trial BNCT for high grade gliomas was done that was carried out using BPA and an epithermal neutron beam at Studsvik (Sweden) (Capala, 2003). Next investigation was done for increasing the infusion time boron concentrations in invading tumor cells in glioma bearing rats (Smith, 2001). Then, the higher dose and longer infusion time of the BPA were well tolerated by 29 patients and the result showed improved survival data. Using a 6-hour infusion time and a higher dose of BPA it could represent a significant step forward in BNCT of brain tumors, especially if combined with a photon boost. Moreover, all the patients had surgery before BNCT. BNCT facility was closed at Studsvik (Sweden) in 2006 (Sköld, 2010; Hopewell, 2011).

During 2000 to 2002, the first BNCT trails was performed in nine GBM patients with using BSH and the epithermal neutron facility of LVR-15[4] reactor at NRI Rez Reactor in Czech Republic (Burian, 2002).

From 2001 until 2003, two liver cancer patients were successfully treated with the TAOrMINA[5] method by BNCT in Pavia (Italy). In the method, the patient had surgery and the liver removed from the body. Then, BPA was injected into the liver. Later then, the liver transported to a reactor for irradiation with thermal neutrons in the thermal column of the TRIGA Pavia research reactor. After irradiation, the liver was autotransplanted to the patient. Both patients were treated successfully with the TAOrMINA method. This success showed that BNCT could be a beneficial

---

[3] European Organization for Research and Treatment of Cancer

[4] light-water research reactor

5 Trattamento Avanzato d'Organi Mediante Irraggiamento Neutronico e Autotrapianto

option for a large number of patients suffering from liver cancer by using the TAOrMINA method (Pinelli, 2002; Zonta, 2006).

In 2001, the firstly application of BNCT was done to treat patients with cancers of the head and neck (HN) region who had failed all other therapies at the Kyoto University Research Reactor Institute (KURRI) in Japan (Kato, 2004). During 2002 to 2004 an additional investigation for BNCT was done in Japan about the possibility of applying BNCT to treat liver tumors. This research was done by using normal liver cells in mice. BNCT with the use of boron-lipiodol was evaluated to have the potential to treat VX2 liver tumor (Lin, 2002; Suzuki, 2004).

In 2001, in Argentina, BNCT was demonstrated in treating oral cancers. In the research, because of oral cancers could be easily exposed to the neutron beams, the oral cancer of hamsters was carried out and human oral mucosa tumors were transplanted in the hamsters. BPA was proven to be an effective boron-carrying agent for oral cancer in Argentina (Kreimann, 2001). Another investigation was done for using BNCT on treating skin melanoma in 2003. A phase I/II clinical trial was made using BPA and a mixed thermal-epithermal neutron beam at a RA-3 nuclear reactor in Bariloche (Argentina) (Gonzales, 2004; Menéndez, 2009).

In 2002, the first animal trail started for investigating treatment of lung cancer in the mice by using BNCT at the Ohio State University in USA. In the research, $Na_3B_{20}H_{17}NH_3$ was selected as indirect boron-10 delivery agent for the treatment of murine lung carcinoma in mice by using BNCT. The results showed that folate receptor tumor targeting was not significantly enhance overall tumor localization but may improve boron delivery at the cellular and subcellular levels (Pan, 2002).

In 2003, the WIDEST[6] project is studying the feasibility of the in situ BNCT treatment of lung metastases from colon adenocarcinoma. As the indispensable condition for the treatment implementation, the selective ^{10}B uptake of the tumour cells with respect to the normal parenchima was investigated in a small animal model of lung metastases induced in BD-IX rats and treated with the ^{10}B carrier BPA-fructose (Bortolussi, 2011).

In 2004, a research group of MIT and Harward (USA) by collaboration with Oxford (UK) started to demonstrate the treatment of lung cancer using rats which were irradiated with X-rays, thermal neutrons, or thermal neutrons in the presence of p-boronophenylalanine (BPA). The result indicated a positive breathing rate response. It was defined as a 20% increase in breathing rate using thermal neutron and BPA at any time during the period of 40–80 days after irradiation (Kiger, 2004).

In 2004, the Argentinian research group studied BPA-BNCT which induced control of experimental squamous cell carcinomas (SCC) of the hamster cheek pouch mucosa with no damage to normal tissue. They explored the feasibility and safety of treating spontaneous head and neck tumors, with particular focus on SCC, of

[6] WIDE Spread Tumours

terminal feline patients with a low dose BPA-BNCT applying the thermal beam of the RA-1 Reactor within a preclinical context in Argentina (Rao, 2004).

In 2004 and 2005, the second trial clinical of BNCT was performed for treating malignant melanoma using the boron carrier BPA (EORTC protocol 11011) at HF in Petten (Netherlands) by the collaboration with the University of Essen (Germany) (Wittig, 2006).

In 2006, the first investigation was carried out on the liver tumor with BNCT at Kyoto University Research Reactor (KUR) in Japan: a patient multiple hepatocellular carcinomas (HCCs) was treated with BNCT without surgical procedure, using a newly developed boron delivery system: intra-arterial administration of the boron compound with a vessel-embolizing agent, lipiodol, in the hepatic arteria. The first patient has been treated successfully by BNCT (Suzuki, 2007).

At the same time, Suzuki demonstrated the feasibility of BNCT for lung cancer, malignant pleural mesothelioma (MPM), for 3 patients from a viewpoint of dose distribution analysis using Simulation Environment for Radiotherapy Applications (SERA). In this study, the ^{10}B concentrations were assumed in the tumor and normal lung from data observed in clinical trials. The maximum, mean, and minimum doses to the tumors and the normal lung were assessed for each plan. The results were obtained from the analysis of the dose-distribution, indicated that BNCT has the possibility to be a promising treatment for MPM patients who are inoperable because of age and other medical illnesses (Suzuki, 2006).

In 2006, interest some BNCT researchers increased to treat lung cancer (MPM) by BNCT in Italy.

In 2006, It was the first study using a rat model for exploring post-irradiation damage to the healthy lung after the irradiation of whole-thorax in Italy by BNCT. The investigations were planned for three kinds of experiments using rat by BNCT. Firstly, the rat colon carcinoma cells which incubation in BPA was followed by *in vitro* thermal neutron radiation. The half of the post-irradiation boron was to assist the biological effectiveness of BNCT. Secondly, it was *in vitro* post-irradiation boron rich cells injected through the inferior vena cava of rat to stimulate lung metastases and determine the survival endpoint. Thirdly, there were injections through the inferior vena cava of the rat to determine the histological characterization of metastatic tumor (Bortolussi, 2006).

In 2006, the preliminary treatment of liver cancer studied by BNCT and using the autotransplant method. The projects have been created to modify the thermal column of TRIGA reactors and to accomplish irradiation facilities around epitermal beams at the HFR Petten, Netherlands (Nievaart, 2006).

In Japan, during 2004 to 2008, BPA and BSH were applied simultaneously with epithermal neutrons in brain tumor and also HN cancer BNCT (Kato, 2004; Miyatake, 2005; Aihara, 2006; Yamamoto, 2008). In 2007, the other investigation was done about simulation depth-dose distributions for cancers of liver, lung,

pancreatic, prostate osteosarcoma by Monte Carlo calculation. The result showed that BNCT has the potential to be applied for treating those cancers under certain conditions in Japan (Matsumoto, 2007). In 2008, the first study was performed for treating of lung cancer patients a malignant pleural mesothelioma (MPM) using both BPA and BSH with an epithermal neutron beam. The same study for other malignant short spindle cell tumor with BPA by BNCT in Japan (Suzuki, 2008).

During 2003 to 2006, a BNCT trial was performed using BPA and epidermal neutron at the FiR 1 BNCT facility in Finland for patients who had recurred inoperable head and neck cancer. Most patients responded despite prior conventional radiation therapy in history, and most responses lasted for several months. Four (33%) patients were alive without cancer recurrence after a follow-up time exceeding 1 year, suggesting that some patients treated with BNCT may achieve a durable treatment response (Kankaanranta, 2007).

In 2009, BNCT was combined with conventional fractionated photon radiotherapy in primary treatment of brain tumors In Japan (Matsumura, 2009).

In 2009 and 2011, the other Italian research group had some investigation about the application of BNCT for treating lung cancer. The research was done about the possibility to apply boron neutron capture therapy (BNCT) for lung tumors. In the study, some rats are considered to be irradiated in the thermal column of the TRIGA reactor of the University of Pavia. Before the irradiation, lung metastases were induced in BDIX rats, which subsequently were infused with boronophenylalanine (BPA). During the irradiation, the rats were positioned in a box designed to shield the whole animal except the thorax area (Baking, 2009; Protti, 2009; Bortolussi, 2011). In the other research, small animal treatment planning and *in vivo* BNCT was performed at the Pavia reactor. The Monte Carlo treatment plan optimizations and validations for several animal models are presented together with some very preliminary *in vivo* tests to prove the suitability of the irradiation chamber of the Pavia reactor in 2011 (Protti, 2011).

During 2007 to 2012, BNCT was applied as the last salvage therapy for heavily pretreated HN patients with recurrent cancer and also was successfully applied as the first-line treatment of a large inoperable HN tumor in combination with intensity-modulated chemoradiotherapy in Finland (Kankaanranta, 2011; 2012).

During 2009 to 2011, the research of BNCT project was focused on the treatment of liver tumors applying BNCT to auto-transplanted livers at the University of Mainz. Consequently, a clinical trial was performed in four patients, suffering from liver metastases of colorectal carcinoma. Additionally, *in vitro* experiments have been initiated to investigate radiobiological effects of radiation generated during BNCT. For the *in vitro* experiments, as well as for the treatment of liver cancer, a reliable dosimetry system is necessary. At the same time, the other preclinical study was carried out for investigation the uptake of the neutron capture pharmaceutical (^{10}B) under conditions identical to the proposed therapy for 15 patients at the Department of Transplantation Surgery of the University Mainz. Moreover, all experiments were done with human hepatoma cell lines to expand the research on the treatment for liver cancer in the BNCT. The other study investigated the

dosimetric feasibility BNCT of explanted livers in the thermal column of the research reactor in Mainz by Monte Carlo method. The simulation results showed that dosimetry should guarantee effective BNCT treatment of the organ to be better shielded from all gamma radiation (Hampel, 2009; Blaickner, 2012).

In 2011, Japan research group demonstrated patients (GBMs) which had surgery before treatment by BNCT with XRT conventional fractionated photon radiotherapy (BNCT-XRT) and temozolomide in combination with BSH. The result showed that they were treated successfully by the method and the median survival times of patients increased in comparison to the method that just uses BNCT (Kawabata, 2011; Yamamoto, 2011; Nakai, 2011).

In 2010-2011, ten patients with recurrent, late stage cancer of the head and neck region have been treated at the National Tsing Hua University THOR reactor in Taiwan using BPA (Wang, 2011).

In 2012, a Japanese research group evaluated the effects of employing a (10) B-carrier and manipulating intratumour hypoxia on local tumour response and lung metastatic potential in BNCT by measuring the response of intratumour quiescent (Q) cells. The result showed that BPA-BNCT, especially in combination with nicotinamide treatment, and the potential to reduce the number of metastases in lung more than BSH-BNCT (Masunaga, 2012).

A recent report about BNCT research activities and clinical trials was published in the proceedings of the 15th International Congress on Neutron Capture Therapy, held at Tsukaba, (Japan) in September 2012. A detailed description of the current status of BNCT of high grade gliomas and recurrent head and neck cancers has been reported by Barth in 2012 (Barth, 2012).

Today some countries such as USA, Argentina, Japan, England, Australia, Italy, Germany, Sweden, Netherlands, Slovakia, Czech Republic, Russia, and Taiwan developed wide BNCT research activities and clinical trials. Moreover, many of Institutes with the objective to develop neutron beams for medical applications in the world wide. Nowadays, current or recently completed clinical trials have been carried out in Japan, Filand, Argentina and Taiwan. In the hope that progress BNCT could be success in the treatment of many kinds of tumors in the future. BNCT should be on the development of new drugs, which would ensure a higher boron concentration ratio between tumour and healthy tissue. In additional, the possibility to irradiate larger targets which mean shorter irradiation times and, with a high dose delivery to the tumour and an almost total sparing of neutron sources for BNCT.

1.3 Application of neutron sources for BNCT

The required neutron beams for BNCT facilities must to provide and are difficult to achieve in practice. One of the major problems for the BNCT technique is to obtain

a suitable beam of neutrons in terms of intensity and energy spectrum. The characteristics of the neutron beam are given below:

1. The thermal neutron flux must have high intensity at the tumor cell for reducing irradiation time and the epithermal neutron flux usually is about 10^9 neutron·$cm^{-2}sec^{-1}$;
2. The optimum neutron beam energy for treating deep-seated tumors with BNCT is from the 4 eV to 40 keV energy spectrum peaking at 10 keV.

Neutrons were produced by neutron sources which are classified according to its energy as follows in Table 1.1.

Table 1.1: Classification of neutron in term of the kinetic energy.

Classification	Energy
Thermal	Around 0.025 eV and below 0.5 eV
Slow	< 1keV
Epithermal	0.5 eV – 10 keV
Resonance	1 keV - 0.5 MeV
Fast	0.5 MeV - 10 MeV
High energy	> 10 MeV

Thermal neutron and epithermal neutron can be very effective for the treatment of tumors in BNCT (Daquino, 2008; IAEA, 2001; Chadwick, 2006).

Neutron sources for BNCT currently have been limited to specially modified nuclear reactors, which are available in Japan, United States, European countries (Finland, Netherlands, Germany, Czech Republic), Argentina and Taiwan. Accelerators producing epithermal neutron beams also could be used for BNCT and these are being developed in several countries. It is anticipated that the first Japanese accelerator will be available for therapeutic use in 2013.

1.3.1 Nuclear reactors

Reactors are the most suitable type for neutron source because of it provides a suitable energy neutron spectrum with high intensity thermal neutron flux. Neutrons are generated by the fission reaction occurring in the core, mean energy is 1.98 MeV, in a nuclear reactor. It requires suitable moderator in order to obtain the epithermal neutron. From the beginning of BNCT history, the nuclear experimental reactors have been used as the only neutron sources to provide correct energy spectrum and adequate thermal neutron flux. Today, BNCT move from using

thermal neutron beam to the use of a more energetic, epithermal neutron beam. In principle epithermal neutrons have the capability to penetrate deep into the tissue by reducing the skin exposure and thermalizing at the same time. Thus, epithermal neutrons are useful for BNCT treatments of different tumor types. In addition epithermal thermal neutrons can be easily moderated further to be less penetrating by using a tissue-equivalent (TE) material on the patient's skin (Seppälä, 2004).

A number of reactors, with a very good neutron beam quality have been developed and applied clinically for BNCT, are shown in Table 1.2 (Hatanaka, 1973; Storr, 1992; Auterinen, 2001; Burian, 2002; Pinelli, 2002; Capala, 2003; Kato, 2004; Wittig, 2006; Nigg, 2006; Sauerwein, 2009; Wang, 2011; Gustavo, 2012).

Table 1.2 : Reactor- based neutron source for BNCT.

USA
The Brookhaven Graphite Research Reactor (BGRR) at Brookhaven National Laboratory
The Massachusetts Institute of Technology Research Reactor (MITR)
Europe
The TRIGA II in Mainz, Germany
The TAPIRO reactor in Rome, Italy
The TRIGA in Pavia, Italy
JRC-HFR reactor at Petten, Netherlands
The Finnish TRIGA reactor, FiR 1, as clinical reactor in Helsinki, Finland
LVR reactor, Czech Republic
The R2-0 Reactor, Studsvik Medical in Nyköping, Sweden
Light Water Reactor (LWR) in Budapest, Hungary
The WWR-M Kyiv Research Reactor (KRR) in Kyiv, Ukraine
The research reactor IRT-2000 in Sofia, Bulgaria
The MARIA reactor in Świerk, Poland
Japan
The Hitachi Training Reactor (HTR)
Kyoto University Research Reactor (KURR) in Kumatori
JRR4 at the Atomic Energy Research Institute (JAERI)
The Musashi Institute of Technology Reactor (MuITR)
Elsewhere
The High Flux Australian Reactor (HIFAR) at Lucas Heights (Australia)
RA-6, RA-3, RA-1 CNEA reactor at Bariloche (Argentina)
The National Tsing Hua University THOR reactor (Taiwan)
In-hospital compact nuclear reactor in Beijing (China)

In following, two facilities, FiR 1 (Finland) and MITR (USA) which can be applied as a epithermal neutron source for BNCT, will be described.

In order to generate epithermal neutrons, the moderator block consisting of Al+AlF_3 (Fluental™) was developed and produced in Technical Research Centre of Finland (VTT). The Fluental™ neutron moderator was installed into the space of the thermal column at FiR 1. The epithermal neutrons are produced from the irradiation the fast fission neutrons by The Fluental™ neutron moderator at 250 kW power. The epithermal neutron fluence has been obtained about 1.1 $\times 10^9$ $n/cm^2 \cdot sec$. The undesired fast neutron dose per epithermal fluence is 2 $Gy/10^{13}\, cm^{-2}$ and the corresponding gamma contamination 0.5 $Gy/10^{13}\, cm^{-2}$.

The epithermal neutron fluence was suitable for BNCT purposes. A 14 cm diameter collimator has been installed for directing the neutrons into the tumor area (Auterinen, 2001, 2005 and 2012) (Fig. 1.5).

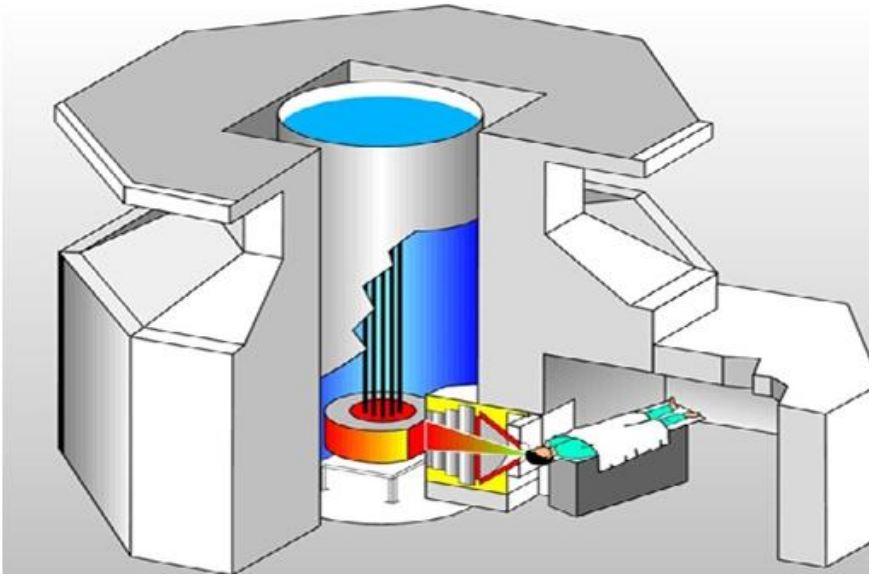

Figure 1.5: Diagram of requirements for BNCT treatment at FiR 1 nuclear research reactor in Otaniemi, Finland (Auterinen, 2001).

The fission converter based epithermal neutron irradiation (FCB) facility is placed in the experimental hall of the MITR and operates in parallel with other user applications. The FCB contains an array of 11 MITR-II fuel elements cooled by forced convection of heavy water coolant. The converter power is 120 kW at 6 MW reactor power. A shielded horizontal beam line contains an aluminum and Teflon filter-moderator to tailor the neutron energy spectrum into the desired epithermal

energy range. A patient collimator defines the beam aperture and extends into the shielded medical room to provide circular apertures ranging from 16 to 8 cm in diameter. The in-air epithermal flux is 6.2×10^{9} n/cm^{2}s at the patient position with the 12 cm collimator (Fig. 1.6) (Barth, 2005; 2007; 2012).

The measured specific absorbed doses were constant for all field sizes and below the inherent background of 2.8×10^{-12} GyWcm^2/n produced by epithermal neutrons in tissue. The dose distributions were achieved by using the FCB approach and the theoretical optimum for BNCT. This facility is useful for clinical studies for superficial cancers and small animal studies (Harling, 2002; Riley, 2003). However, the application of nuclear reactors is limited and most of them are not located near the hospital. Thus, it would be necessary to have hospital-based neutron sources (Barth, 2007). Finally, an “in-hospital” compact nuclear reactor, which will be used exclusively for BNCT, has been designed and built in Beijing, China (Yiguo, 2010). But the new idea of the small reactors is not attractive for BNCT due to its low acceptability of such structure in a hospital environment and the high investment cost. Hence, the potential utility of accelerators provides an attractive idea in a real hospital environment. Nowadays, a number of groups around the world are involving their research toward into this topic.

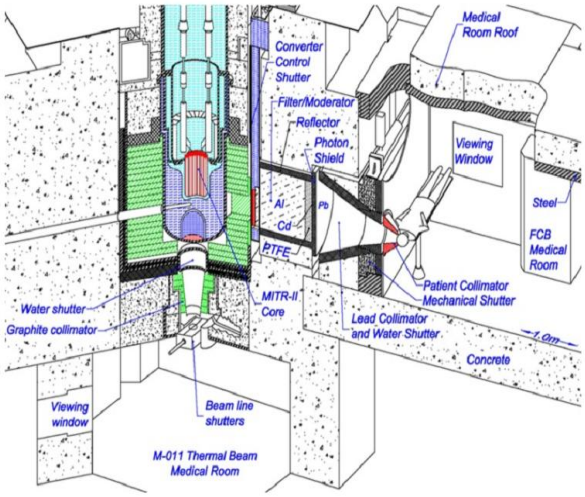

Figure 1.6: Diagram of the BNCT facility at the Massachusetts Institute of Technology Reactor (MITR) in USA (Barth, 2012).

1.3.2 Accelerator-based neutron sources (ABNS)

Accelerator speed up the charge particles (protons, heluim-4, deuterons, tritons and electrons) with defined energy and let them interact to suitable target such as ^{7}Li, ^{9}Be, ^{13}C, ^{12}C, ^{2}H and ^{3}H nuclei (Howard, 2001; Thomas, 2003). Consequently,

the neutrons are produced from nuclear reactions. Some reactions used for generating neutrons by accelerator are listed in Table 1.3.

As can be seen in Table 1.2, there are different target materials and different incident particles but generally attention has been focused on low energy proton accelerators with the choice of either lithium or beryllium as the target material.

In an investigation, total neutron yields have been calculated based on cross sections which are obtained from the thick target lithium bombarded by proton beam (Listen, 1975; Randers-Pehrson, 1998). Campbell with collaborators has measured direct total neutron yields from thick beryllium targets bombarded by proton beam (Campbell, 1977). The both results are shown in Fig. 1.7. In Fig. 1.7 the neutrons yields are high and, additionally, the kinetics are such that the secondary neutron spectrum has relatively low energy. Because of these /advantages, early designs for accelerator based BNCT systems focused on lithium targets (Randers-Pehrson, 1998).

Table 1.3 Characteristics of the charged particle, targets and nuclear reactions which are considered for ABNS-BNCT.

Reaction	Bombarding energy (MeV)	Average neutron energy (MeV)	Maximum neutron energy (MeV)	Neutron production rate ($n \cdot mA^{-1}s^{-1}$)
$^{7}Li(p,n)^{7}Be$	2.5	0.55	0.79	$9.1 \cdot 10^{11}$
$^{9}Be(p,n)^{9}B$	4.0	1.06	2.12	$1.0 \cdot 10^{12}$
$^{9}Be(p,n)^{10}B$	1.5	2.01	5.08	$3.3 \cdot 10^{11}$
$^{13}C(d,n)^{14}N$	1.5	1.08	6.77	$1.9 \cdot 10^{11}$
$^{2}H(d,n)^{3}He$	0.15	2.5	4.7	$4.7 \cdot 10^{8}$
$^{3}H(d,n)^{3}He$	0.15	14.1	14.1	$5.0 \cdot 10^{10}$

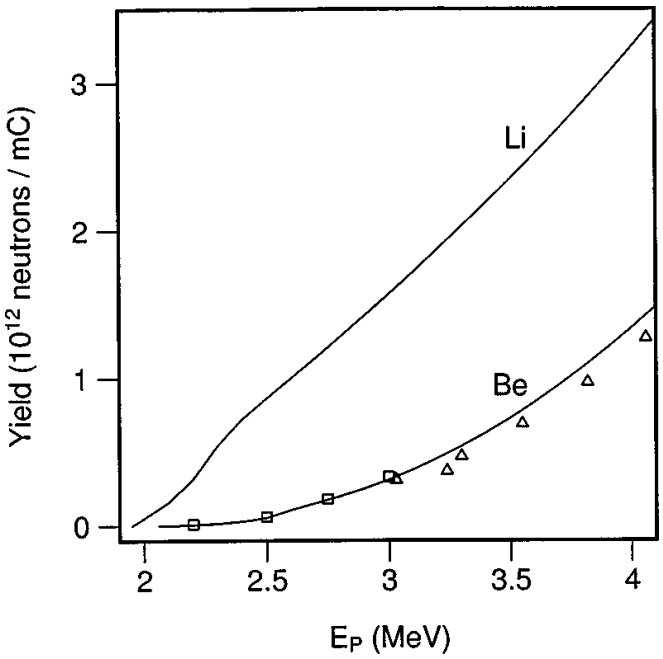

Figure 1.7: The total neutron yields after proton bombardment of thick lithium and beryllium targets as a function of incident proton energy.

Moreover, fusion reaction (D-T and D-D) can be used for generating neutron and are also considered as a neutron source. However, according to bombarding engineers, type of the charged particle and targets, the accelerator will be capable to generating the currents neutron needed to deliver therapy for BNCT in reasonable times.

Accelerators can generally be classified to linear (electrostatic quadrupole (ESQ) and radio frequency quadrupole (RFQ), Tandem cascade accelerator (TCA) and recirculating (cyclotron). Mostly these types of accelerator are suitable for producing neutron as ABNS which are applied for BNCT research and clinical trials (Green, 1998; Thomas, 2003; Culbertson, 2004; Kreiner, 2007; Pisent, 2006; Forton, 2009; Mitsumoto, 2010; Aleynik, 2011; Tanaka, 2009).

Theoretically RFQ accelerators have the capacity to be used as a neutron source in BNCT (Pisent, A. 2006).

Some of ABNS developed and applied clinically for BNCT are shown in Table 1.4 (Green, 1998; Thomas, 2003; Culbertson, 2004; Yonai, 2004; Kreiner, 2007; Pisent, 2006; Forton, 2009; Chiojdeanu, 2009; Sauerwein, 2009; Mitsumoto, 2010; Aleynik, 2011).

Table 1.4: ABNS for BNCT.

USA
The proton-cyclotron-based accelerator facility, Washington in Seattle
The proton linear accelerator facility at Fermi National Accelerator Laboratory in Illinois
The deuteron cyclotron facilities at Harper Hospital in Detroit
Europe
The proton-RFQ under investigated in Legnaro, Italy
The proton-cyclotron-based in Louvain-La-Neuve, Belgium
The proton-Tandem in Bucharest-Mãgurele, Romania
Dynamitron proton accelerator facility in Birmingham, England
The proton-cyclotron-based facility in Bratislava, Slovak Republic
Japan
The proton-cyclotron-based at Sumitomo Heavy Industries in Sumitomo
The proton-cyclotron-based at Tohoku University in Sendai
Elsewhere
The proton Tandem-Electro- Static-quardapol (ESQ) facility in Buenos Aires, Argentina
The proton Tandem in Novosibirsk, Russia

Two ABNS-BNCT facilities (the dynamitron proton accelerator facility of the University of Birmingham in Birmingham, England, and the proton-RFQ under investigate at the National Institute of Nuclear physics (INFN) in Legnaro (Italy) will be described.

The dynamitron proton accelerator facility of the University of Birmingham was the first clinical accelerator-based BNCT facility in the world. The accelerator had proton currents (1 mA) by bombarding a ^{7}Li target via ^{7}Li(p,n)^{7}Be reaction with high energy protons (2.8 MV) generated thermal neutron flux $1.37 \cdot 10^{12}$ n·s^{-1}. The facility used the Fluental TM as moderator to obtain the neutron beam in appropriate therapy energies as well as epitermal neutron. The proton beam with a Fluental TM, graphite reflector, lead filter, lithium target and shield (delimiter) Li-polyethylene was shown in Fig. 1.8 (Green, 1998; Culbertson, 2004).

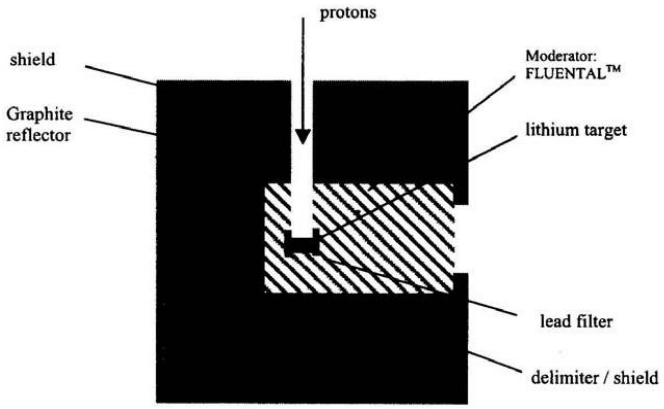

Figure 1.8: University of Birmingham accelerator-based neutron source system.

The RFQ is a unique facility in worldwide at INFN Legnaro (Italy). It's able to deliver 30 nA with 5 MeV proton beam which is useable in research project SPES-BNCT. The beryllium target (^{9}Be) is bombarded by 30 nA proton via ^{9}Be(p,xn)^{9}B reaction, generating neutrons which are moderated via heavy water and graphite. Consequently the neutron flux of thermal neutrons is obtained about $2.5 \cdot 10^{9}/(s \cdot cm^{2})$ which are suitable for therapy (Figs. 1.9 and 1.10).

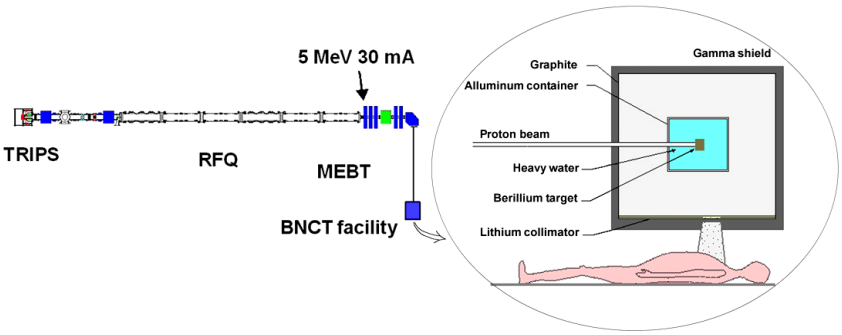

Figure 1.9: Schematic layout of SPES-BNCT irradiation facility.

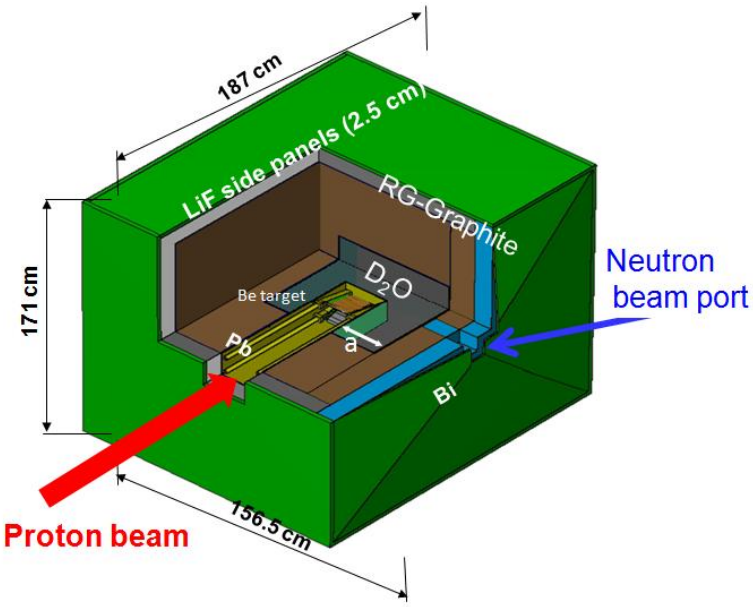

Figure 1.10: Schematic layout of neutron source at irradiation facility INFN-LNL.

The LNL-BNCT facility is foreseen to explore the treatment of extended skin melanoma with such a therapeutic modality and, at the next stage, hepatic metastases in the explanted liver (Agosteo, 2001; Prete, 2008; Ceballos, 2009). The main items of the research program are being mainly focused on the neutron irradiation facility design, involve quality neutron beam, the development of a new boron carrier and a new, on-line, biological dose monitoring in both tumor and healthy tissues (Pisent, 2006).

The new application of neutron source for BNCT is using of process photoneutron production by a linear electron accelerator.

When medical electron accelerator (LINACs) works with acceleration potentials above 10 MV, they could generate secondary neutrons via photon-neutron (γ, n) and electron-neutron reaction (e, e′n) giant dipole resonance reactions of incident photons and electrons, respectively, with all the heavy materials present inside the gantry and along the beam line.

During the mid-1990s, the Idaho National Laboratory and Idaho State University has been involved in the first idea about the photoneutron production process driven by an electron accelerator which could be applied for BNCT in futures. In this research, relativistic electron beams impinge upon heavily-shielded tungsten targets located at the outer radius of a small cylindrical tank of circulating heavy water (D_2O). A fraction of the energy of the electrons is converted in the tungsten targets into radially-inward-directed bremsstrahlung radiation. Neutrons

subsequently generated by photodisintegration of deuterons in the D_2O within the tank are directed to the patient through a suitable beam tailoring system. Initial proof-of-principal tests using a low-current benchtop prototype of the epithermal photoneutron source concept for BNCT were conducted (Nigg, 1997 and 2006). The results of these experiments demonstrated that on the basis of neutronic performance, the proposed photoneutron device could offer as an approach for the production of epithermal neutrons in BNCT.

Another research was done as PhoNeS (PhotoNeutron Source) project at Trieste University with collaboration Turino University in Italy. In this study, the photo-reaction model assumed which can be applied as a neutron source. Thus, a photoconverter has been designed. In order to increase the photoneutron production inside the moderating materials, the photoconverter materials have been selected: graphite blocks for the external moderator, lead target, moderators in polyethylene, PMMA box, 5 cm thick volumes filled with heavy water (D_2O 99%), and irradiation cavity. Finally, the photoconverter placed at off-axis points of photon beam with 18 MV at medical electron accelerator (Varian Clinac 210). As consequently, thermal and/or epithermal neutron beam with neutron fluence rate about $1.06 \cdot 10^8$ $cm^{-2}s^{-1}$ has been obtained and could be used for BNCT treatment of shallow tumors (as melanoma or limb sarcoma) (Fig. 1.11) (Giannini, 2006).

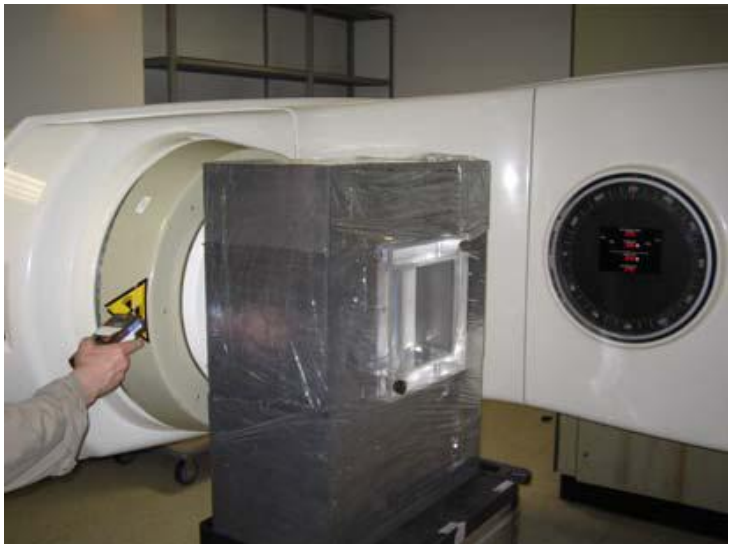

Figure 1.11: The small prototype photoconverter at Mauriziano Hospital (Torino, Italy).

Accelerator-based neutron sources (ABNS) have potential advantages over reactor-based neutron sources for clinical applications. First, ABNS can be easily turned off when the neutron field is not required during therapy. But the fast neutrons are not stopped via a critical assembly of fissile material, what means that licensing and regulations associated with maintaining the neutron source are substantially simplified. Second, the variety of neutron producing reactions that are accessible to accelerators, allows a number of neutron energy source spectra to be produced. Consequently, for some accelerator types, epithermal neutron beams can be produced the neutron flux energy spectrum can be tailored to the spatial characteristics of a particular patient's tumor. Third, the capital expenses of an accelerator-based BNCT system will be substantially lower than those associated with the installation of a reactor system in or near a hospital. And finally, accelerators have been prominent features of radiotherapy departments in hospitals for years; clinicians have a longstanding and comfortable experience with such devices for patient irradiation. It is likely that accelerator hardware for BNCT irradiations could be sited within an existing radiotherapy room with the addition of extra shielding.

References

Aihara, T., et al. (2006). First clinical case of boron neutron capture therapy for head and neck malignancies using ^{18}F-BPA PET. *Head Neck,* 28, pp. 850-5.

Agosteo, S., et al. (2001). Advances in the INFN-Legnaro BNCT Project for Skin Melanoma. In Proceedings of *International Physical and Clinical Workshop on BNCT Candiolo (Torino)*, February 7, 2001.

Aleynik, V., et al. (2011). BINP accelerator based epithermal neutron source. *Applied Radiation and Isotopes,* 69, pp. 1635-1638.

Auterinen, I., et al. (2001). Metamorphosis of a 35 years old Triga reactor into a modern BNCT facility. In: Frontiers in Neutron Capture Therapy, Plenum Press, New York, 1, 267-275.

Autrerinen, I., et al. (2005). Fir 1 Reactor in service for boron neutron capture therapy (BNCT) and isotope production. STI/PUB/1212. IAEA, pp. 313-324.

Autrerinen, I. (2012). Introducing the BNCT option in a national health care system-the Finnish experience. In proceedings of 15 international congress on neutron capture therapy, 10-14 September, Tsukuba, Japan.

Bakeine, G.J., et al. (2009). Feasibility study on the utilization of boron neutron capture therapy (BNCT) in a rat model of diffuse lung metastases, *Applied Radiation and Isotopes, 6*7, pp. S332-S335.

Barth, R.F., et al. (2005). Boron Neutron Capture Therapy of Cancer: Current Status and Future Prospects. *Clinical Cancer Research*, pp. 3987-4002

Barth, R.F., et al. (2007). Boron neutron capture therapy for the treatment of glioblastomas and extracranial tumors: As effective, more effective or less effective than photon irradiation? *Radiation Oncology, 8*2, pp. 119-122.

Barth, R.F., et al. (2012). Current status of boron neutron capture therapy of high grade gliomas and recurrent head and neck cancer. *Radiation Oncology, 7*, 146, pp. 8-21.

Blaickner, M., et al. (2012). Dosimetric feasibility study for an extracorporeal BNCT application on liver metastases at the TRIGA Mainz. *Journal of Applied Radiation and Isotopes,* 70, pp. 139-143.

Bortolussi, S., et al. (2011). Boron uptake measurements in a rat model for Boron Neutron Capture Therapy of lung tumours. *Applied Radiation and Isotopes, 6*9, pp. 394-398.

Byun, Y., et al. (2006). Anti-Cancer Agents in Medicinal Chemistry*,* 6, pp. 127-144.

Burian, J., et al. (2006). Physics for BNCT. *Journal of Physics Conference Series,* 41, pp.174-186.

Burian, J., et al. (2002). Report on the first patient group of the phase I BNCT trial at the LVR-15 reactor. In proceedings of Conference Research and Development in Neutron Capture Therapy, Bologna*,* pp. 1107-1112.

Busse, P.M., et al. (2003). A critical examination of the results from the Harvard-MIT NCT program phase I clinical trial of neutron capture therapy for intracranial disease. *Neuro-Oncology,* 62, pp. 111-121.

Campbell, J., et al. (1977). Absolute neutron yield measurements for protons on Li, Cu, Co, and Be from threshold to 3 MeV. *In Proceedings of the 4th Conference on the Scientific and Industrial Applications of Small Accelerators,* IEEE, New York*,* pp. 517-521.

Capala, J., et al. (2003). Boron neutron capture therapy for glioblastoma multiforme: clinical studies in Sweden. *Journal of Neuro-Oncology,* 62(1-2), pp. 135-144.

Catharine, M., et al. (2005). Boron neutron capture therapy for glioblastoma multiforme. *Journal of Pharmacy World* & *Science,* 27, pp. 92-95.

Ceballos, C., et al. (2009). The BSA modeling for the accelerator-based BNCT facility at INFN LNL for treating shallow skin melanoma. *Applied Radiation and Isotopes, 6*7 (7-8), pp. S274-S277.

Cerullo, N., et al. (2009). Progress in the use of gadolinium for NCT. *Applied Radiation and Isotopes,* 67, pp. 157-160.

Chadwick, M. B., et al. (2006). *ENDF/B-VII.* Next Generation Evaluated Nuclear Data Library for Nuclear Science and Technology. *Nuclear Data Sheet* pp. 107.

Chanana, A. D., et al. (1997). Boron neutron capture therapy for glioblastoma multiforme: interim results from the phase I/II dose escalation studies. *Neuro-Oncology,* 44, pp. 1182-1192.

Chiojdeanu, C.F., et al. (2009). Boron neutron capture therapy set up for a linear accelerator, *Romanian Journal Physics,* 54, (7–8), pp. 641-648.

Coderre, J.A., et al. (1997). Boron neutron capture therapy for glioblastoma multiforme using boronophenylalanine and epithermal neutrons: trial design and early clinical results. *Neuro-Oncology,* 33**,** pp. 141-152.

Crossley, E.L., et al. (2010). Selective aggregation of platinum-gadolinium complex within a tumor cell nucleus. *Angewandte Chemie International Edition,* 49, pp. 1231-1233.

Culbertson, C.N., et al. (2004). In-phantom characterization studies at the Birmingham Accelerator-Generated epithermal Neutron Source BNCT facility. *Applied Radiation and Isotopes,* 61, pp. 733-738.

Daquino, G., et al. (2008). A Review of the Recommendations for the Physical Dosimetry of Boron Neutron Capture Therapy (BNCT). *JRC technical reports,* EUR 23632 EN.

De Stasio, G., et al. (2001). Gadolinium in human glioblastoma cells for gadolinium neutron capture therapy. *Cancer Research,* 61, pp. 4272-4277.

De Stasio, G., et al. (2005). Are gadolinium contrast agents suitable for gadolinium neutron capture therapy. *Neurological Research,* 27, pp. 387-398.

Diaz, A.Z., et al. (2003). Assessment of the results from the phase I/II boron neutron capture therapy trials at the Brookhaven National Laboratory from a clinician's point of view. *Neuro-Oncology,* 62, pp. 101-109.

Emiliano, C.C., et al. (2012). Boron neutron capture therapy (BNCT) for liver metastasis: therapeutic efficacy in an experimental mode. *Radiation and Environmental Biophysics,* 51, pp. 331-339.

Farr, L.E., et al. (1954). Neutron Capture Therapy with Boron in the treatment of Glioblastoma Multiforme*. American Journal of Roentgenology, 7*1, pp. 279-291.

Forton, E., et al. (2009). Overview of the IBA accelerator-based BNCT system. Applied Radiation and Isotopes*,* 67, pp. S262-265.

Gabel, D., et al. (1990). Approach boron neutron therapy in Europe: Goals of a European Collaboration on Boron Neutron Capture Therapy. *In proceeding 2nd European Particle Accelerator Conference. 12 - 16 Jun, Nice, France.*

Geninatti-Crich, S., et al. (2011). MRI-Guided Neutron capture therapy by use of a dual gadolinium/boron agent targeted at tumor cells through unregulated low-density lipoprotein transports. *Chemistry – A, European Journal,* 17, 30, pp. 8479-8486.

Gustavo, A., et al. (2012). BNCT in Argentina : An Interdisciplinary Approach. *In proceedings of 15 international congress on neutron capture therapy, 10-14 September , Tusukaba , Japan.*

Giannini, G., et al. (2006). Photoneutron Source for In-Hospital BNCT Treatment: feasibility study. In proceedings 12th International Congress on Neutron Capture Therapy. Takamatsu. Japan.

Goldhaber, M., et al. (1986). Introductory remarks. *In: Proceeding of a Workshop on Neutron Capture Therapy. Reports BNL-51994. NY: Brookhaven National Labortory*, pp. 1-2.

Gonzalez, S.J., et al. (2004). First BNCT treatment of a skin melanoma in Argentina: dosimetric analysis and clinical outcome. *Applied Radiation and Isotopes,* 61(5), pp. 1101-1105.

Goorley, T., et al. (2004). Calculated DNA damage from gadolinium Auger electrons and relation to dose distributions in a head phantom. *International Journal of Radiation Biology*, 80 (11-12), pp. 933-940.

Green, S., et al. (1998). Developments in accelerator based boron neutron capture therapy. *Radiation Physics Chemistry,* 51, 4-6, pp. 561-569.

Hall, E. J., et al. (2000). Radiobiology for the Radiologist, Lippincott Williams &Williams, *Philadelphia, 5th edn.*

Harling, OK., et al. (2002). The fission converter based epithermal neutron irradiation facility at the Massachusetts Institute of TechnologyReactor. *Nuclear Science Engineering,* 140, pp. 223-240.

Hampel, G., et al. (2009). Irradiation facility at the TRIGA Mainz for treatment of liver metastases. *Applied Radiation and Isotopes,* 67, pp. S238-S242.

Hatanaka, H., et al. (1973). A revised boron-neutron capture therapy for malignant brain tumors. I. Experience on terminally ill patients after cobalt-60 radiotherapy. *Neurology,* 204, pp. 309-332.

Hatanaka, H., et al. (1986). Clinical experience of boron-neutron capture therapy for gliomas: a comparison with conventional chemo-immuno-radiotherapy. *Boron Neutron Capture Therapy for Tumors*. Niigata, Japan.

Hatanaka, H., et al. (1991). Boron neutron capture therapy for brain tumors, In: Karin ABMF, Laws E, editors, Glioma. Berlin: Springer-Verlag, pp. 233.

Hatanaka, H., et al. (1994). Clinical results of long-surviving brain tumor patients who underwent boron neutron capture therapy. *International Journal of Radiation Oncology, Biology, Physics,* 28, pp. 1061-1066.

Howard, W.B., et al. (2001). Measurement of the thick-target ^{9}Be(p,n) neutron energy spectra. *Nuclear Science Engineering,* 138 (2), pp. 145-160.

Hawthorne, M.F., et al. (2003). A critical assessment of boron target compounds for boron neutron capture therapy. *Neuro-Oncology,* 62, pp. 33-45.

Hideghéty, K., et al. (1999). Postoperative treatment of glioblastoma with BNCT at the Petten irradiation facility. *EORTC protocol 11961*. *Journal of Strahlentherapie Und Onkologie, 1*75 S, pp. 111-114.

Hopewell, J.W., et al. (2011). Boron neutron capture therapy for newly diagnosed glioblastoma multiforme: an assessment of clinical potential. *Applied Radiation and Isotopes,* 69, pp. 1737–1740.

IAEA-TECDOC-1223 (2001). Current status of neutron capture therapy.

Imahori, Y., et al. (1998). Positron emission tomography-based boron neutron capture therapy using boronophenylalanine for high-grade gliomas: part II. *Clinical Cancer Research,* 4 pp. 1833-1841.

Joensuu, H., et al. (2003). Boron neutron capture therapy of brain tumors: clinical trials at the Finnish facility using borophenylalanine. *Neuro-Oncology,* 62 (1-2), pp. 123-134.

Kabalka. G.W., et al. (2003). Synthesis of a potential boron neutron capture therapy agent: 1-aminocyclobutane-1-carboxylic acid bearing a butylboronic acid side chain, *Synthesis*, 18, pp. 2890-2893.

Kankaanranta L., et al. (2007). Boron neutron capture therapy in the treatment of locally recurred head and neck cancer.*International Journal of Radiation Oncology, Biology, Physics,* 69**,** pp. 475-482.

Kankaanranta, L., et al. (2011). L-BPA- mediated BNCT for malignant glimoa progressing after external radiation beam therapy. *International journal of radiation Oncology, Biology*, *Physics,* 1, 80 (2), pp. 369-376.

Kankaanranta, L., et al. (2012). Boron neutron capture therapy in the treatment of locally recurred head-and-neck cancer: final analysis of a phase I/II trial. *International Journal of Radiation Oncology,* 82, pp. 67–75.

Kato, I., et al. (2004). Effectiveness of BNCT for recurrent head and neck malignancies. *Applied Radiation and Isotopes,* 61, pp. 1069-1073.

Kawabata, Sh., et al. (2011). Phase II clinical study of boron neutron capture therapy combined with X-ray radiotherapy/temozolomide in patients with newly

diagnosed glioblastoma multiforme–study designed current status report. *Applied Radiation and Isotopes,* 69, pp. 1796-1799.

Kawabata, Sh., et al. (2011). Convection enhanced delivery of carboranylporphyrins for neutron capture therapy of brain tumors. *Neurology,* 103, pp. 175-185.

Kiger, J.L., et al. (2004). Effects of boron neutron capture irradiation on the normal lung of rats. *Applied Radiation and Isotopes,* pp. 969-973.

Kreiner, A.J., et al. (2007). Tandem ESQ for Accelerator- Based Boron neutron capture therapy. The Lawrence Berkeley National Laboratory.

Kreimann, E.L., et al. (2001). The hamster cheek pouch as a model of oral cancer for boron neutron capture therapy studies: selective delivery of boron by boronophenylalanine*. Cancer research,* 61, pp. 8775-8781.

Kruger, P.G., et al. (1940). Some biological effects of nuclear disintegration products on neoplastic tissue. Proceedings of the National Academy of Sciences of the USA, 26, pp. 181-192.

Locher, G.L., et al. (1936). Biological effects and therapeutical possibilities of neutrons. *Roentgenology,* 36, pp. 1-13.

Lin, W.Y., et al. (2002). Boron-lipiodol: a potential new drug for the Treatment of liver tumors. *Anticancer Research,* 22, pp. 3989-3992.

Listen, H., et al. (1975). Neutron production cross-sections and energies for the reactions ^{7}Li(p,n)^{7}Be and ^{7}Li(p,n)^{7}Be*(431 keV). Data Nuclear Tables*,* 15, pp. 57-84.

Mandal, S., et al. (2011). Design, development and characterization of multi-functionalized gold nanoparticles for biodetection and targeted boron delivery in BNCT applications. *Applied Radiation and Isotopes,* 69, 12, pp. 1692-1697.

Madoc-Jones, H., et al. (1999). A Phase–I dose escalation trial of Boron Neutron Capture Therapy for subjects with metastatic subcutaneous melanoma of the extremities *In : Cancer Neutron Capture Therapy,* (New York: Plenum Press) pp. 707.

Matsumoto, T., et al. (2007). Nuclear Instruments and Methods in Physics Research Section A: Accelerators, Spectrometers, Detectors and Associated Equipment*., 5*80, 1, pp. 552-557.

Matsumura, A., et al. (2009). Current practices and future directions of therapeutic strategy in glioblastoma: survival benefit and indication of BNCT. *Applied Radiation and Isotopes, 6*7, pp. 12-14.

Masunaga, S., et al. (2012). Effects of employing a ^{10}B-carrier and manipulating intratumour hypoxia on local tumour response and lung metastatic potential in boron neutron capture therapy. British Journal of Radiology*,* 285,(1011), pp. 249-258.

Menéndez, P.R., et al. (2009). BNCT for skin melanoma in extremities: updated Argentine clinical results. *Applied Radiation and Isotopes,* 67, pp. S50-53.

Mishima, Y., et al. (1989). Treatment of malignant melanoma by single thermal neutron capture therapy with melanoma-seeking ^{10}B-compound *Lancet,* 2, pp. 388-389.

Miyatake, S., et al. (2005). Modified boron neutron capture therapy for malignant gliomas performed using epithermal neutron and two boron compounds with different accumulation mechanisms: an efficacy study based on findings on neuroimages. *Neurosurgery,* 103, pp. 1000-1009.

Miyatake, S-I., et al. (2012). Bevacizumb for progressive radation necrosis: preliminary results and ongoning clinical trial. *Proceedings of 15 international congress on neutron capture therapy, 10-14 September – Tusukaba – Japan.*

Mitsumoto, T., et al. (2010). Cyclotron-based neutron source for BNCT. New Challenges in Neutron Capture Therapy: *Proceedings of the 14th International Congress on Neutron Capture Therapy,* pp. 519-522.

Moss, R.L., et al. (1990). Progress towards boron capture therapy at the High Flux Reactor Petten", *Basic Life Sciences,* 54, pp. 169-183.

Nakagawa et al. (1997). Boron neutron capture therapy: clinical brain tumor studies. *Neuro-Oncology, 3*3, pp. 105-115.

Nakai, K., et al. (2011). Boron neutron capture therapy combined with fractionated photon irradiation for glioblastoma: a recursive partitioning analysis of BNCT patients. *Applied Radiation and Isotopes, 6*9, pp. 1790-1792.

Nievaart, V.A., et al. (2006). Design of a Rotating Facility for Extracorporal Treatment of an Explanted Liver with Disseminated Metastases by Boron Neutron Capture Therapy with an Epithermal Neutron Beam", *Radiation Research, 1*66, pp. 81-88.

Nievaart, V.A., et al. (2007). Spectral Tailoring for Boron Neutron Capture Therapy. *IoS Press. ISBN 978-1-58603-762-8.*

Nigg, D.W., et al. (1997). Experimental Investigation of Filtered Epithermal Photoneutron Beams for BNCT. In proceedings of Advances in Neutron Capture Therapy, Volume 1, Elsevier, Amsterdam, pp. 477.

Nigg, D.W., et al. (2006). Neutron Sources and Applications in Radiotherapy - A Brief History, and Current Trends. *In proceedings of 12th International Symposium on Neutron Capture Therapy.*

Pan, X.Q., et al. (2002). Boron delivery to a murine lung carcinoma using folate receptor-targeted liposomes. *Anticancer Research*, 22, pp. 1629-1633

Pinelli, A., et al. (2002). TAORMINA: From the first idea to the application to the human liver. *In proceedings of Conference Research and Development in Neutron Capture Therapy*. Bologna, pp. 1065-1072.

Pisarev, M.A., et al. (2012). Studies on the Possible Application of BNCT to Thyroid Cancer. *Neutron Capture Therapy,* pp. 425-431.

Pisent, A., et al. (2006). Progress on the accelerator based SPES-BNCT project at INFN Legnaro. Journal of Physics: Conference Series, 41, pp. 391-399.

Prest, M., et al. (2010). In-hospital BNCT and the PhoNeS project: status and perspectives. *Proceedings* of 12th Vienna Conference on Instrumentation.

Prete, G., et al. (2008). Selective production exotic Species, Chapter XII – SPES applied Science, BNCT and LENOS. *Technical design report.* INFN-LNL-224, pp. 181-214.

Pouget, J.-P., et al. (2001). General aspects of the cellular response to low- and high-LET radiation, *European Journal of Nuclear Medicine and Molecular Imaging, 28,* pp. 541-561.

Protti, N., et al. (2009). Calculations of dose distributions in the lungs of a rat model irradiated in the thermal column of the TRIGA reactor in Pavia. *Applied Radiation and Isotopes,* 67 (7-8), pp. S210-S213.

Protti, N., et al. (2011). The efficacy of boron neutron capture therapy in small animal models. Ph.D. thesis, Universita degli studi di Pavia, Pavia, Italy.

Randers-Pehrson, G., et al. (1998). A practical target system for accelerator-based BNCT which may effectively double the dose rate. *Medical Physics,* 25, 6, pp. 894-896.

Riley, KJ., et al. (2003). Performance characteristics of the MIT fission converter based epithermal neutron beam. *Physics in Medicine and* Biology, 48, pp. 943-958.

Savolainen, S., et al. (2012). Boron neutron capture therapy (BNCT) in Finland: Technological and physical prospects after 20 years of experiences. *Medical Physics,* pp. 1-16.

Sauerwein, W., et al. (1997). Postoperative treatment of glioblastoma with BNCT at the Petten irradiation facility. 1. Phase I clinical trial. *EORTC Protocol 11961.*

Sauerwein, W., et al. (1999). Postoperative Treatment of glioblastoma with BNCT at the Petten irradiation facility", *EORTC Protocol 11961.*

Sauerwein, W., et al. (1999). Organization and management of the first clinical trial of BNCT in Europe (EORTC Protocol 11961), *Strahlenther Onkologie, 1*75, II, pp. 108-111.

Sauerwein, W., et al. (2002). The EORTC Boron Neutron Capture Therapy (BNCT) Group: achievements and future projects. *European Journal of Cancer,* 38, pp. S31-34.

Sauerwein, W. (2009). Requirements for Boron Neutron CaptureTherapy (BNCT) at a Nuclear Research Reactor.Report, EUR 23830 EN.

Semioshkin, A., et al. (2007). Reaction of oxonium derivatives of $[B_{12}H_{12}]_{2-}$ with amines : Reactions of oxonium derivatives of : Synthesis and structure of novel B_{12}-based ammonium salts and amino acids. *Organometallic* Chemistry*,* 692, pp. 4020-4028.

Seppälä, T., et al. (2004). A dosimetric study on the use of bolus materials for treatment of superficial tumors with BNCT. *Applied Radiation and Isotopes, 6*1, pp. 787-791.

Shinji, K., et al. (2011). Convection enhanced delivery of carboranyl porphyrins for neutron capture therapy of brain tumors. *Neuro-Oncology,* 103, pp. 175-185.

Soloway, A. H., et al. (1998). The chemistry of neutron capture therapy. *Chemical* Reviews*,* 98, pp. 1515-1562.

Slatkin, D.N., et al. (1991). A history of boron neutron capture therapy of brain tumors. Postulation of a brain radiation dose tolerance limit, *Brain,* 114, pp. 1609-1629.

Smith, D.R., et al. (2001). Quantitative imaging and microlocalizaton of boron-10 in brain tumors and infiltrating tumor cells by SIMS ion microscopy: Relevance to neutron capture therapy. *Cancer Research,* 61, pp. 8179-8187.

Sköld, K., et al. (2010). Boron neutron capture therapy for glioblastoma multiforme: advantage of polonged infusion of BPA-f. *Acta Neurol Scand,* 122, pp. 58-62.

Soloway, A.H., et al. (1967). Penetration of brain and brain tumor. VII. Tumor-binding sulfhydryl boron compounds. *Medicinal Chemistry,* 10, pp. 714-717.

Soyland, C., et al. (2000). Survival of Human Lung Epithelial Cells Following *In Vitro* Alpha-particle Irradiation with Absolute determination of the number of Alpha-particle Traversals of Individual Cells" *International Journal* of *radiation biology,* 76, 1 pp. 315-1322.

Steen patersen, M., et al. (2008). Boron Nanoparticles Inhibit Tumor Growth by Boron Neutron Capture Therapy in the Murine B16-OVA Model. *Journal of anticancer research, 28*, pp. 571-576.

Storr, G. J., et al. (1992). Design Considerations for the Proposed Hifar Thermal and Epithermal Neutron Capture Therapy Facilities. *Progress in Neutron Capture Therapy for Cancer,* pp. 79-82.

Suzuki, M., et al. (2004). Dosimetric study of boron neutron capture therapy with borocaptate sodium (BSH) /lipiodol emulsion (BSH/lipiodol-BNCT) for treatment of multiple liver tumors, *International Journal of Radiation Oncology, Biology, Physics,* 58, pp. 892-896.

Suzuki, M., et al. (2006). Feasibility of boron neutron capture therapy (BNCT) for malignant pleural mesothelioma from a viewpoint of dose distribution analysis *International Journal of Radiation Oncology, Biology, Physics,* 66, pp. 1584-1589.

Suzuki, M., et al. (2007). First attempt of boron neutron capture therapy (BNCT) for hepatocellular carcinoma. *Japanese Journal of Clinical* Oncology*,* 37, pp. 376-381.

Suzuki, M., et al. (2008). A novel concept of treatment of diffuse or multiple pleural tumors by boron neutron capture therapy (BNCT). *Radiation Oncology,* 88, pp. 192-195.

Takayanagi, M. (2012). Boron Neutron Capture Therapy Irradiation Technology Forum, http://www.jaeri.go.jp.

Tanaka H., et al. (2009). Characteristics comparison between a cyclotron-based neutron source and KUR-HWNIF for boron neutron capture therapy. *Nuclear Instruments and Methods in Physics Research Section B,* 267, pp. 1970-1977.

Tokumitsu, H., et al. (2000). Gadolinium neutron-capture therapy using novel gadopentetic acid-chitosan complex nanoparticles: *in vivo* growth suppression of experimental melanoma solid tumor. Cancer Letters*,* 150, pp. 177-182.

Thomas, E., et al. (2003). Accelerator-based epithermal neutron sources for boron neutron capture therapy of brain tumors, *Neuro-Oncology,* 62. pp. 19-31.

Vos, M.J., et al. (2005). Radiologic findings in patients treated with boron neutron capture therapy for glioblastoma multiforme within EORTC trial 11961, *International Journal of Radiation Oncology, Biology, Physics,* 61, pp. 392-399.

Walker, S.J., et al. (1998). Boron Neutron Capture Therapy: *Principles and Prospects, Radiography,* 4, 3, pp. 211-219.

Wang, LW., et al. (2011). BNCT for locally recurrent head and neck cancer: preliminary clinical experience from a phase I/II trial at Tsing Hua open-pool reactor. *Applied Radiation and Isotopes,* 69, pp. 1803-1806.

Wittig. A., et al. (2003). Early phase II study on BNCT in metastatic malignant melanoma using the boron carrier BPA. *EORTC Protocol 11011.*

Wittig, A., et al. (2006). Early phase II study on BNCT in metastatic malignant melanoma using the boron carrier BPA (EORTC protocol 11011). In Advances in Neutron Capture Therapy. Takamatsu, Japan: *International Society for Neutron Capture Therapy*; pp. 284-287.

Wu, G., et al. (2007). Nanotechnology for Cancer Therapy, CRC Press, Boca Raton, FL, pp. 77-103.

Yamamoto, T., et al. (2008). Boron neutron capture therapy for glioblastoma, *Cancer Letters*, 262, pp. 143-52.

Yamamoto, T., et al. (2011). The status of the Tsukuba BNCT trial: BPA-based boron neutron capture therapy combined with X-ray irradiation. *Applied Radiation and Isotopes,* 69, pp. 1817-1818.

Yiguo, L., et al. (2010). Start-up of the first in-hospital neutron irradiator (IHNI-1) & Presentation of the BNCT development status in China. New Challenges in Neutron Capture Therapy: *In proceedings of the 14th International Congress on Neutron Capture Therapy,* pp. 371-374.

Yonai, S., et al. (2004). Benchmark experiments for cyclotron-based neutron source for BNCT. *Applied Radiation and Isotopes*. 61, pp. 997-1001.

Zonta, A., et al. (2006). Clinical lessons from the first applications of BNCT on unresectable liver metastases*. Physics,* 41, pp. 484-495.

2. Neutron spectrometry application, detectors and technique

2.1 Neutron spectrometry

When neutrons were discovered in 1932 by Chadwick, the development of neutron spectrometry techniques was started in nuclear physics (Chadwick, 1932). In additional, neutron spectrometry techniques become an important tool in several other fields such as nuclear technology, fusion plasma-diagnostics, radiotherapy and radiation protection for investigation neutron spectrum in the fields. Thus, different instruments and neutron spectrometry techniques have been developed to fulfill the requirements of the intended applications.

Neutron spectrometry deals with measuring the energy distributions of neutrons. All neutron spectrometry techniques based on the detection of secondary particles like charged particles or photons which are generated via the interaction of neutrons with matter.

These techniques can be classified into seven groups based on the principle used for measuring the neutron energy:

1. Measurements of the energy of a recoiling nucleus via scattering neutrons.
2. Measurements of the energies of charged particles which are released in neutron-induced nuclear reactions.
3. Measurements of the velocity of the neutron as the time-of-flight (TOF) method.
4. Threshold methods, in which a minimum neutron energy is indicated by the appearance of the induced neutron effect, such as radioactivity or other effects.
5. Methods in which the neutron energy distribution is determined by unfolding or deconvolution of a set of readings of detectors which differ in the energy-dependence of their response to neutrons.
6. Neutron diffraction methods.
7. Measurement of the time-distribution of the slowing down of a short burst of high-energy neutrons in a suitable medium.

Groups 6, 7 and some of the methods in group 3 use pulsed neutron source, while other methods applied to the continuous neutron beam.

2.2 History

Three main periods times can be identified in the evolution of neutron spectrometry that include 1932-1959, 1960-1979 and 1980-now. Today most applications of neutron spectrometers are based on methods that were introduced before 1960 which consist of recoil telescopes, proportional counter, ionization chambers, organic scintillators, nuclear emulsions, cloud chambers and double-pulse (capture-gated) neutron spectrometers (Brooks, 2002). At the same time, methods

based on measuring the energies of charge reaction products included the ^{3}He-proportional counter spectrometer (Batchelor, 1960) and the ^{6}LiI(Eu) scintillation crystal. Also, other methods such as time-of-flight methods (Spaepen, 1961) and threshold radioactivation methods (Byerly, 1960) have been used.

During 1960 and 1979 a notable development occurred with introduction Bonner sphere Spectrometer (BSS, group 5). In addition, the advances made in neutron spectrometry techniques based on gaseous ionization detectors (Grosshoeg, 1979) and scintillation detectors (Harvey, 1979). During this period, an important development was the advent of computer unfolding methods for determining neutron spectrum from measurements by detector (Perey, 1978). During this period, other notable developments were the first applications of semiconductor detectors for neutron spectrometry (Dearnaley, 1963) and Apfel firstly introduced the superheated drop detector (Apfel, 1979).

Since 1980's, considerable technological progress but most emphasizes on computer programming and tools in neutron spectrometry. Monte Carlo codes were applied for calculating the response matrix of the detector for unfolding process. Also, iterative algorithms were used to unfold the neutron spectra from spectrometer measurements.

2.3 Current techniques

In the following section will be reviewed especially some techniques and BSS which are widely applied at present.

2.3.1 Recoil nuclei spectrometers

Recoil nuclei spectrometers based on the production of secondary charged particles by interaction neutrons with the spectrometer material and collect recoils at all angles to the incident neutron a direction which are accepted for measurement. On the other hand, recoil telescopes collect recoils at a particular angle which are selected for analysis. The spectrometer response function (pulse height spectrum resulting from the bombardment with monoenergetic neutrons) is typically a broad continuum for the first category and a narrower group in the case of a telescope. Recoil telescope spectrometers strive to achieve a simple response function, ideally a single sharp peak at a pulse height uniquely related to the neutron energy. Typically the energy ranges are about 50 keV to 4 MeV and pulse height resolution is about 10% (FWHM) for 1 MeV recoil ions. A wide variety of designs have been used to do this. The best performance in terms of energy range (up to 200 MeV) can be obtained with telescope detectors or scintillators based instruments. Reviews of spectrometers based on proportional counters and liquid scintillators have been published in 2003 by Tagziria and Klein (Tagziria, 2003; Klein, 2003).

2.3.2 Nuclear reaction as neutron spectrometer

The nuclear reactions include $^{3}He(n,p)^{3}H$ (Q= 0.764 MeV), $^{6}Li(n,\alpha)^{3}H$ (Q= 4.79 MeV), $^{10}B\ (n,\alpha)^{7}Li$ (Q= 2.79 MeV), $^{12}C(n,\alpha)^{9}Be$ (Q= - 5.70 MeV) and $^{28}Si(n,\alpha)^{25}Mg$ (Q= -1.65 MeV), which are the main candidates for using in spectrometers. The neutron spectrometer is applied to determine the neutron energy by measuring the energies of charged reaction products which are generated by neutron interaction on it via nuclear reactions. The most of $^{3}He(n,p)^{3}H$ reaction is used for neutron spectrometry in the energy range from 50 keV to 5 MeV. Many types of ^{3}He-spectrometer are used such as proportional counters, gridded ionization chambers and sandwich spectrometers (Dietz, 1993; Takeda, 1999; Shalev, 1973; Seghour, 1999). For example, ^{3}He-filled gridded ionization have pulse height resolutions of 15–40 keV (FWHM) for neutron energies 2.5 MeV (Hawkes, 1993; Iguchi, 1994). In addition, ^{3}He-sandwich spectrometers are used in an energy neutron range from 100 keV to 15 MeV with pulse height resolutions about 50 keV (Kluge, 1982; Marsh, 1995).

The $^{6}Li(n,\alpha)^{3}H$ reaction has been used in scintillation spectrometers and sandwich detectors (Murray, 1958; Seghour, 1999). Moreover, the applying scintillation spectrometers have been limited by factors such as their sensitivity to gamma rays, non-linear pulse height response and contributions to the response function arising from neutron interactions with other constituents of the scintillator. The $^{10}B(n,\alpha)^{7}Li$ reaction is not suitable for spectrometry because it populates both the ground state and first excited state (0.48 MeV) of ^{7}Li with similar probability. Neutron spectrometers based on the $^{12}C(n,\alpha)^{9}Be$ and $^{28}Si(n,\alpha)^{25}Mg$ reactions were used in diamond and silicon semiconductor crystals which in applications for plasma diagnostics. This type of spectrometer for incident neutron energies below about 20 MeV can obtain a pulse height resolution of about 2% (FWHM) (Elevant, 1986).

2.3.3 Time-of-flight (TOF) method

In this method neutron energy is determined by measuring the time spent in traveling neutron at a known distance. When the neutron source is not pulsed, detectors such as scintillator detector are needed to register both, the start and termination, of the neutron flight. Two methods are used to generate the start signal. In the first method the neutron is scattered in a start detector, for example an organic scintillator, and the time of flight to a second detector at a known distance and the angle is measured. In the second method the start signal is provided by an associated particle or quantum that is emitted from the neutron source at the same time as the neutron. The typical range neutron is from 1 to 15 MeV with a pulse height resolution about 5% at 2.5 MeV (Elevant, 2002; Brooks, 2002).

2.3.4 Threshold detectors spectrometers

This spectrometer is based on an appropriate set of nuclear reactions with well-known threshold energy (Q<0). The observation of a radioactive product or daughter resulting from such a reaction indicates that the neutron energy must

exceed the threshold for the reaction. Thus the energy spectrum of a neutron field may be determined by comparing measurements of several different neutron-induced activities (with different threshold energies), made by irradiating an appropriate set of target foils in the field (Kuijpers, 1977). The response matrix is then based on the evaluated excitation functions of the reactions employed (Baard, 1989). Another type of threshold method is based on measurements of gamma rays or internal conversion electrons excited by neutron inelastic scattering in a germanium semiconductor crystal or in a suitably selected scattering material surrounding such a crystal (Ejiri, 1991). Activation foil techniques and superheated drop detectors spectrometry are based on threshold method. Superheated drop (bubble) detector can be used in the energy ranges from 0.1 to 20 MeV (d'Errico, 1997; 2003). In following, this chapter, activation foil techniques and superheated drop detectors will be described.

2.3.5 Bonner sphere spectrometer (BSS)

2.3.5.1 Overview

The BSS was firstly introduced as an instrument for neutron spectrometry in 1960 (Bramblett, 1960). From fifty years ago it became one important tool in neutron spectrometer and today it's widely used by many institutes and laboratories especially in BNCT facilities more than other techniques for the aims neutron spectrometry. It has an almost isotropic response, can cover the energy range from thermal to several GeV neutrons, and is easy to operate. BSS has some drawbacks, such as the weight and the poor energy resolution, which does not allow appreciating fine structures as narrow peaks in the neutron spectrum: Moreover they need to sequentially irradiate for long times a set of Bonner spheres having different diameters (Brooks, 2002; Alevra, 2003; Thomas, 2002). This spectrometer consists of a set of moderating Bonner spheres with different diameters, typically made of polyethylene with a neutron thermal detector (active or passive detector) positioned at the center of each Bonner sphere. The combination of a thermal detector plus moderating of Bonner sphere has a sensitivity to neutrons over a broad energy range. However, the sensitivity of each Bonner sphere depends on the particular neutron energy range and by increasing the Bonner sphere diameter response of BSS shifted to higher neutron energy. Thus an accurate knowledge of the energy dependence of the response of each Bonner sphere is necessary to reconstruct the neutron spectrum from the measurement (counts or activities) of a set of Bonner spheres in the neutron field through an “unfolding” procedure.

In the following, Table 3.1, there are some laboratories in Europe which are using a set of Bonner spheres for measuring the neutron spectrum at neutron field (Marek, 1998; Alevra, 2002; Thomas, 2002; Lacoste, 2004; Gressier, 2005; Bedogni, 2006; Chiojdeanu, 2009; Mirzajani, 2009; Amgarou, 2010).

An idea was using of shells with different thickness of the materials (B, Cd and Li) which are absorbed thermal neutron (Fig. 2.1). It has an effect on the response of the detector for higher the energy range as the thickness is increased (Silari, 2001; Howell, 2010; Garny, 2011). For example, PE (Polyethylene)-insert, the gold foil

was placed with and without a Cd shield inside 2.5 in. Bonner sphere for measuring neutron thermal. Thus, Cd captures neutrons with low energies while being almost transparent for neutrons with higher energies (Fig.2.1).

Table 2.1: Laboratories in Europe use BSS.

PTB[7], Braunschweig, Germany
Bare (^{3}He), bare+Cd, 3, 3.5, 4, 4.5, 5, 6, 7, 8, 10, 12, 15 and 18 in.
NPL[8], UK
Bare (Gold foil), 2, 2.5, 3, 3.5, 4, 5, 6, 7, 8, 10 and 12 in.
University of Barcelona, Spain
Bare (Gold foil), 2.5, 3, 4.2, 5, 6, 8, 10 and 12 in. plus 2.5 in. plus 1 mm Cd, 3 in. plus1 mm Cd, 4.2 in. plus 1 mm Cd.
IRSN[9] Cadarache, France
Bare (^{3}He and Gold foil), 2.5, 3, 3.5, 4.2, 5, 6, 7, 8, 10, 11 and 12 in. plus 1 mm Cd for five smaller Bonner sphere.
Nuclear Research Institute, Rez, Czech Republic
Bare (^{6}LiI(Eu)), 2, 3, 4, 5, 8, 10 and 12 in.
NIPN[10], Romania
Bare (^{3}He), 3, 4, 5, 8, 10 and 12 in.
INFN[11] Frascati National Laboratory, Italy
Bare (^{6}LiI(Eu)), 2, 3, 5, 8, 10 and 12 in.
University of Pisa, Italy
Bare (^{6}LiI(Eu)), 3, 4, 5, 6, 7, 8, 10, 12, and 15 in.

[7] Physikalisch-Technische Bundesanstalt
[8] National Physical Laboratory
[9] Institut de Radioprotection et de Surete Nucleaire
[10] National Institute for Physics and Nuclear Engineering
[11] Istituto Nazionale di Fisica Nucleare

Figure 2.1: PE-insert, the gold foil was placed with and without a Cd shield inside 2.5 in. Bonner sphere (Garny, 2011).

a)  b) 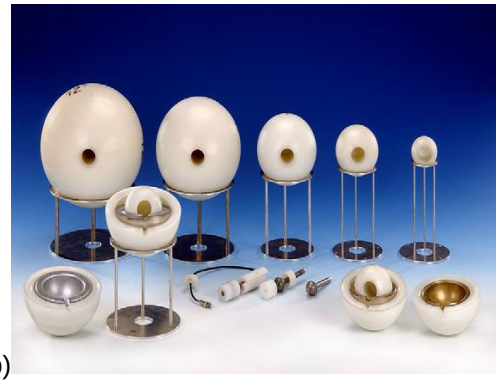

Figure 2.2: a) An Al shell (7.62 cm inner diameter) and Pb shell (12.7 cm outer diameter) and outer 3 in. polyethylene Bonner sphere for measuring in high energy neutron (Howell, 2010); b) Instrument of PTB-NEMUS which consist of five polyethylene Bonner spheres (from left to right: 12, 10, 7, 5 and 3 in. Bonner sphere). In the ground, on the left side an opened modified Bonner sphere containing a 2.54 cm thick lead shell, on the right side an opened modified Bonner sphere containing a 1.27 cm thick copper shell. In the ground center, ^{3}He proportional counter of type SP9 with additional parts to fill the drill holes of the Bonner spheres (Wiegel, 2009).

Some laboratories have added internal metal shell (Pb, Cu, W, Fe, etc.) with high atomic number inside the Bonner sphere to extend the response of the detector for the energy range to GeV neutron. For example, PTB has added four Bonner spheres (maximum diameter 8 in.) with copper and lead inlets (Figs. 2.2a,b). The responses to high energy neutrons increase with energy due to high cross-section the reaction (n,xn) of copper and lead. Thus the set can be used by the neutron energy range 10 GeV (Wiegel, 2002, 2009).

In a recent investigation, the cylindrical polyethylene was used as moderator for Bonner spectrometer. The different thicknesses of moderator were created by inserting one cylinder into another. Simulations and measurements showed that, despite its shape, the device can be made to offer for angular isotropic response to neutrons and that unfolded neutron fission spectra were in agreement with those

obtained with the more traditional BSS (Dubeau, 2010; Atanackovic, 2012). However, the accuracy of the resulting spectral neutron fluence, derived by the application of an unfolding procedure to the experimental readings of the BSS, is limited by the accuracy of the spectrometer response matrix and the unfolding process itself.

2.3.5.2 BSS response and efficiency

The response of a BSS with an active or passive thermal neutron detector is generally defined as the ratio reading A_i of the *i-th* Bonner sphere is given in counts to the neutron fluence ($\varphi(E) = d\varphi/dE$) which is known the fluence response $R_i(E)$. $R_i(E)$ depends on energy neutrons E is defined by:

$$R_i(E) = \frac{A_i}{\varphi(E)} \tag{2.1}$$

where $\varphi(E)$ is the neutron fluence (cm^{-2}) at the point where the center of the Bonner sphere is placed (but in the absence of the Bonner sphere). Thus the fluence response is expressed in terms of counts/(neutrons·cm^{-2}). The subscript *d* is an index identifying the Bonner sphere. As the diameter of a Bonner sphere may be large, it should be stressed here that the definition includes the requirement that the Bonner sphere must be uniformly irradiated by neutron beams, i.e. that the neutron fluence at any point of impact on the Bonner sphere equals the fluence at the center of the Bonner sphere (with the Bonner sphere removed). This requirement is obviously fulfilled for measurements in a homogeneous plane parallel neutron field. Because of the near spherical symmetry of a Bonner sphere, and hence isotropic response, undirectionality of the neutrons is not a condition. However, the illumination homogeneity of the Bonner sphere is an important condition, and one which is not satisfied for instance by irradiation with a point neutron source placed at small distances from the Bonner sphere (the normal calibration arrangement), or in collimated neutron beam whose cross sections are smaller than the Bonner sphere diameter.

The efficiency $\varepsilon_i(E)$ of BSS to neutrons of energy E is the ratio of the reading A_i to the number of neutrons of energy E entering the Bonner sphere. Taking into account the requirement for a homogeneous illumination of the Bonner sphere, the number of neutrons of energy E entering the Bonner sphere is $\Phi(E)\pi D_i^2/4$, where D_i is the diameter of the Bonner sphere. From this and Eq. (2.1), the following efficiency (dimensionless number) is obtained:

$$\varepsilon_i = \frac{4R_i(E)}{\pi D_i^2} \tag{2.2}$$

2.3.5.3 The principle of BSS operation

The most frequent interactions of neutrons entering to a BSS are shown in Fig. 2.3. Neutron 1 escapes from the Bonner sphere after its first interaction, usually an elastic collision with a hydrogen or carbon nucleus (this is a history of type h1). Neutron 2 escapes the Bonner sphere after being slowed down (possibly thermalized) through several interactions with the polyethylene (history of type h2). This category includes neutrons of relatively high energies which undergo (n,p), (n,d) or (n,α) reactions with carbon nuclei (see Fig. 2.4 for the corresponding cross sections). Neutron 3 undergoes many interactions with the polyethylene and is finally thermalized, but before getting a chance to enter the detector it is captured by a hydrogen nucleus (history of type h3). The resulting 2.2 MeV gamma rays in most cases escapes the Bonner sphere, but can also produce an electron in the detector or in the detector wall or mounting. Neutron 4 is thermalized and enters the detector, where the probability of detection approaches unity (history of type h4). The probability of each particular interaction process is dictated by their cross sections. Fig. 2.4 shows the energy variation of the cross sections for various interaction processes of neutrons with carbon nuclei, and also the scattering cross section. The neutron elastic scattering cross section of hydrogen as a function of neutron energy is shown in Fig. 2.5.

The proportion in which the four types of neutron histories (h1, h2, h3, and h4) occur depends on the incident neutron energy and diameter of the Bonner sphere. In smaller Bonner spheres, the low-energy neutrons follow all four types of history, and a non-negligible fraction of them enters the detector and are detected (h4), while the high-energy neutrons mostly escape (h1, h2). For larger Bonner spheres there is considerably more moderate: for the low-energy neutrons which do not escape, history h3 dominates and consequently the response is low. It is in the large Bonner spheres that the high-energy neutrons have the greatest probability of being thermalized and then detected in the detector (h4).

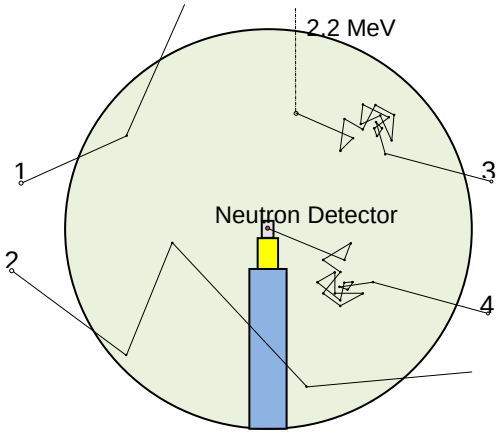

Figure 2.3: Scheme of the main neutron interaction taking place within BSS. The thermal neutron detector is located at the center of the polyethylene Bonner sphere (Alevra, 2003).

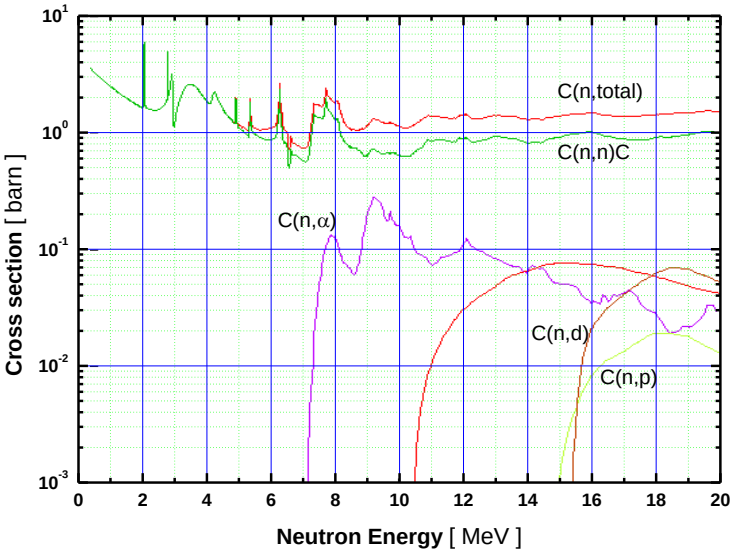

Figure 2.4: Cross sections of various interaction processes of neutrons with carbon nuclei (from ENDFB 6.1 data library).

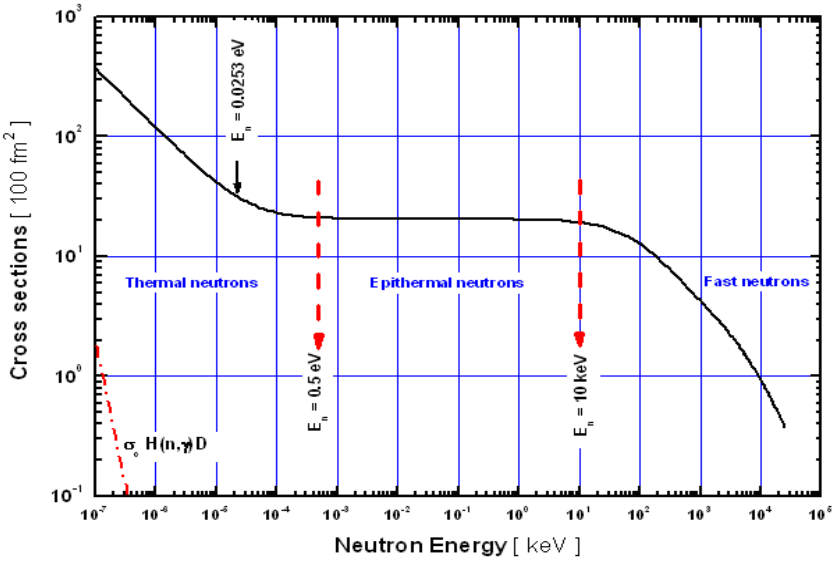

Figure 2.5: Neutron elastic scattering cross section of hydrogen as function of neutron energy.

By taking into the response of the detector the neutron fluence spectrum $\varphi(E)$ can be obtained by solving folding or convolution integrals as known linear Fredholm integral or mathematically underdetermined Eq. (2.3):

$$A_i = \int_{E_{\min}}^{E_{\max}} \varphi(E) R_i(E) dE \qquad (i = 1, 2, ..., n) \tag{2.3}$$

In Eq. (2.3), A_i is the number of counts of BSS, $R_i(E)$ is the response of the i-th Bonner sphere for mono-energetic neutron of energy E (the so-called "response function") while $E_{\min}$ and $E_{\max}$ are energy limits given by the range of the response function. On the other hand, the discrete form Eq. (2.3) and for purposes of calculating, the following approaches as unfolding algorithms are applied:

$$A_i = \sum_{i=1}^{n} R_{ij} \varphi_j \qquad \varphi_j = \varphi(E) \Delta E_j \tag{2.4}$$

where $\varphi_j = \varphi_E(E_j)\Delta E_j$ is the neutron fluence rate at energy j-th with group of width ΔE_i and $R_{ij} = R_i(E_j)$ which is response function the i-th the Bonner sphere for E_j energy of the incident neutron.

Response functions could be achieved by using Monte Carlo particle transport codes and have not experimentally validated.

Extraction of the neutron spectrum from undetermined Eqs. (2.3) or (2.4) are termed "deconvolution" or "unfolding" process. The equations are undetermined and do not have a unique solution (Matzke, 1994). For this purpose, many computerized BSS unfolding codes have been developed. Therefore an appropriate neutron spectrum is determined from the measured data (the count rate for each Bonner sphere) via mathematical deconvoution unfolding process using the response matrix. The detail about response matrix and unfolding process will be discussed in the next chapter.

2.3.5.4 Thermal neutron detector

Many types of thermal detector have been used inside of BSS at the center of BS. The choice of the thermal neutron detector depends heavily on the following elements which characterize the workplace neutron field:

1. Intensity of the field;
2. Time structure of the field;
3. Presence of electromagnetic noise;
4. Photon component.

Thermal detectors are included active or passive detectors. Active detectors are such as cylindrical ^{6}LiI(Eu) scintillator, ^{3}He filled proportional counter, BF_3, spherical SP9 counter and organic scintillator. Passive detectors included superheated drop detectors, thermoluminescent dosimeters (TLD), activation foils

and track detectors. In the following chapter some of the most important active or passive detectors which are used in neutron fields are described.

2.3.5.5 Active neutron detectors

Active detectors are types of detector which the most commonly are applied in neutron fields. They are placed in the center of Bonner spheres to detect thermal neutrons. Active detectors defined as real-time detectors, because the quantity of measurements is displayed during the experiments in the workplace. Detection is achieved via reactions in nuclei resulting in ionizing charged particles which share the reaction energy *Q*.

The cross sections of the three most-used reactions are shown in Fig. 2.6. For neutron energies below 1 keV, all these cross sections follow the 1/*v* law and reach large values in the thermal region. This allows detectors to be relatively small in size, while still attaining efficiencies close to unity for thermal neutrons.

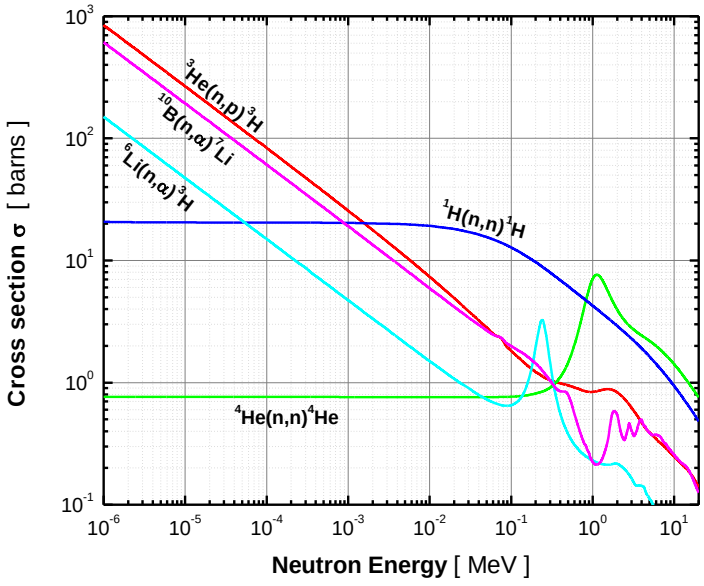

Figure 2.6: Cross sections of some reactions most commonly used to detect thermal neutrons shown as functions of neutron energy (using ENDFB 6.1 data library).

2.3.5.6 The ^{6}LiI(Eu) scintillator

The cylindrical ^{6}LiI(Eu) scintillator mostly is used by type of 4 mm diameter and 4 mm height in the original Bonner sphere set (Bramblett, 1960). While the neutrons incident to detect the following reaction takes place inside the crystal:

$$^{6}\mathrm{Li} + {}^{1}n_{th} \rightarrow {}^{3}\mathrm{H} + {}^{4}\mathrm{He} + 4.780\ \mathrm{MeV} \tag{2.5}$$

The cross section of reaction ^{6}Li(n,α)^{3}H is 940 barn at thermal energy, which combined with the high mass density of the ^{6}LiI crystal makes it the smallest scintillator which can attain 100% efficiency to thermal neutrons. Although the small size favors neutron detection (mainly a surface effect) rather than gamma detection (a volume effect), the high density and atomic number of iodine determines some problems in the discrimination between the gamma and neutron radiation.

Fig. 2.7 shows a pulse-height spectrum obtained from a ^{6}LiI(Eu) scintillator (Mares, 1994). The reaction energy of 4.780 MeV is shared by the resulting alpha particle and Triton and appears in the pulse-height spectrum as the broad quasi-Gaussian full-energy peak. The shape of this peak is determined by the poor pulse-height resolution and edge effects when alpha particles or Tritons partly escape. The quasi-Gaussian distribution due to thermal neutrons is superimposed on an exponential distribution of pulse heights due to gamma events. As the light output of the scintillator for heavy charged particles is much lower than that for electrons of the same energy, pulses due to photoelectrons and Compton electrons induced by gamma rays have pulse heights comparable with the neutron induced pulses. A separation between neutron and gamma induced events can be made by fitting the pulse-height spectrum with a Gaussian combined with an exponential function, as illustrated in Fig. 2.7.

It is important to mention here that the relative contribution of the photon background in the pulse-height spectrum changes with Bonner sphere size in a particular field, and for a particular Bonner sphere is different in different fields. The consequence of this fact is that the photon subtraction must always be performed as shown in Fig. 2.7, and it cannot be acceptable to just set a discriminator level in the pulse-height spectrum at some point below the peak and expect the photon component in all measurements to be the same as in the calibration measurements. This last approach can lead to very significant distortion in any measured spectrum.

Where high sensitivity is required larger scintillator crystal sizes can be used, e.g. 4 mm high by 8 mm diameter (Jacobs, 1980; Marek 1998), 2mm by 10 mm (Mazrou, 2008), 8 mm by 8 mm, or 12.7 mm by 12.7 mm (Sanna, 1973; Hertel, 1985), but the subtraction of gamma events becomes more difficult. The ^{6}LiI crystal needs to be connected to a photomultiplier, which is usually done via a light pipe, and this tends to compromise the isotropic response of Bonner spheres.

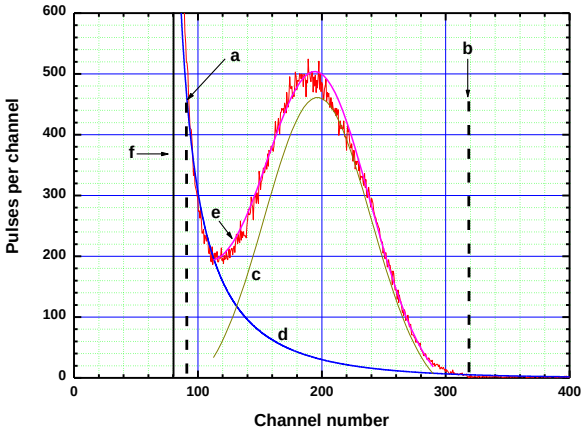

Figure 2.7: An example of a pulse-height spectrum obtained with a 4 mm high, 4 mm diameter ^{6}LiI(Eu) scintillator within a 10 in.Bonner sphere: a–b) range of fitted data; c) Gaussian peak; d) photon background; e) sum of fitted components; f) lower discriminator limit.

2.3.5.7 The $^{10}BF_3$ filled proportional counter

BF_3 proportional counter is widely used for measuring thermal neutrons. In this detector, boron trifluoride, particularly ^{10}B enriched as well as its high concentration of boron as a proportional gas makes resulting efficiency around five times greater than the one that gas contains only natural boron. It is superior properties of the detector can be an alternative to a ^{6}LiI crystal. Bonner sphere sets based on the BF_3 proportional counter does not common to use for the purpose neutron spectrometry. A spherical proportional counter by diameter 50.8 mm has been applied for measuring the neutron spectrum respectively, (Harvey, 1993; Liu, 1990). The nuclear reactions take place inside the BF_3 proportional counter as follows:

$$^{10}\mathrm{B} + n_{th} \rightarrow \begin{cases} \rightarrow {}^{4}\mathrm{He} + {}^{7}\mathrm{Li}^{*} + 2.314\ \mathrm{MeV}\ \ (93.7\%) \\ {}^{7}\mathrm{Li}^{*} \rightarrow {}^{7}\mathrm{Li} + \gamma + 478\ \mathrm{keV} \\ \rightarrow {}^{4}\mathrm{He} + {}^{7}\mathrm{Li} + 2.792\ \mathrm{MeV}\ \ (6.3\%) \end{cases} \qquad (2.6)$$

This reaction has a cross section of 3843 barns for thermal neutrons and produce exciting-state lithium (^{7}Li*) with a probability of 94%, which decay to the fundamental level by emission of gamma ray (0.478 MeV). At thermal neutron energies, 6.3% of the reactions produce stable ^{7}Li.

Fig. 2.8 shows a pulse-height spectrum obtained from a proportional counter filled with BF_3 gas. The main peak (channel 421) is due to the 2.314 keV full-energy

dissipation in the counter gas from the resulting alpha particle and ^{7}Li recoil nucleus. The small distribution (peaked at channel 513) above the main peak is due to full-energy dissipation of particles resulting from transitions to the ground state of ^{7}Li. The pulse-height distribution below the full-energy peak is due to the partial escape of the alpha particle and/or ^{7}Li recoil nucleus (wall effect); the lower limit of the neutron induced events corresponds to the full escape of the alpha particle, implying the full energy dissipation of the ^{7}Li recoil nucleus (841 keV, channel 155) in the gas. Another edge, around channel 300, is due to the full energy deposition of the alpha particle (1473 keV). The pulse-height distribution below channel 100 is due to gamma events and noise.

The separation of the neutron-induced events from pulses because of noise or gamma ray induced events can be achieved simply by introducing a discrimination threshold just below the lower limit of the neutron induced pulse-height distribution. BF_3 proportional counter cannot be operated at pressures higher than 0.5-1.0 atm due to the poor gas performance of at higher pressures.

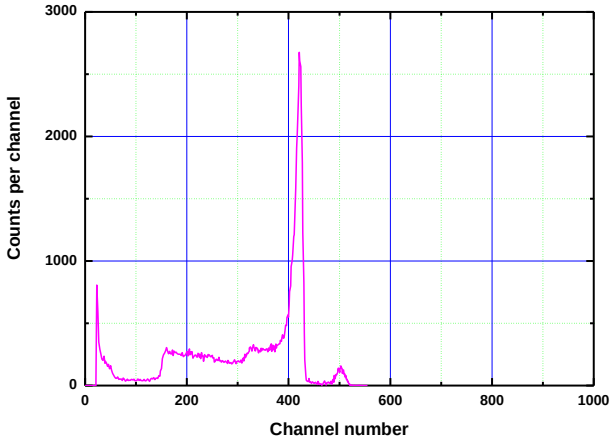

Figure 2.8: Typical pulse-height spectrum that could be obtained from a proportional counter filled with $^{10}BF_3$ gas.

2.3.5.8 The ^{3}He filled proportional counter

French researchers published several papers for performance the use of a 10 mm high by 9 mm diameter cylindrical ^{3}He proportional counters (type 0.5NH10) as thermal detectors in the 1970s and early 1980s (Caizergues, 1973 ; Mourgues, 1974 ; Zaborowski, 1981). The use of this counter, which contains nominally 8 kPa of ^{3}He, provides a system with a response approximately double in comparison to the 4 mm by 4 mm ^{6}LiI system (Alevra, 1988). Although it is less sensitive to

gamma rays than the ^{6}LiI scintillator, the low gas amplification can make it difficult to set a discriminator level which allows all the neutron-induced events to be counted while excluding noise and gamma ray events. However, this counter is still in using by several research groups (Aroua, 1992; Kralik, 1997; Muller, 2002). It can be applied in more intense neutron fields and provides a useful lower-response alternative.

Centronic Ltd., UK, manufactured the large spherical ^{3}He proportional counter (the type SP9) and in the 1980s and early 1990s several groups started to investigate the application of SP9 (Thomas, 1994; Alevra, 1992; Mares, 1994). This has a low gas pressure, of about 200 kPa, but has a diameter of 3.2 cm, resulting in a larger geometrical cross section. Consequently, the overall fluence responses of Bonner spheres based on the counter are about a factor of 14 higher than the 4 mm by 4 mm ^{6}LiI detector. According to characterization of the system such as depending on the Bonner sphere size and neutron energy, the discrimination gamma rays and noise are excellent but pile-up effects become a problem if it applies in the high-intensity gamma ray fields. For overcoming this problem increase the pressure of the gas and add a small amount of a heavier gas such as CO_2 or Ar which cause decreasing the charged particle range thus reduce the pile-up effects (Shalev, 1969).

Bonner spheres based on this counter requires the response functions coupled with unfolding tools for the aims neutron spectrometer.

The reaction takes place in the counter which strongly depending on the incident neutron energy E (1/√E dependence):

$$^{3}\mathrm{He} + n_{th} \rightarrow {}^{3}\mathrm{H} + {}^{1}\mathrm{H} + 0.764\ \mathrm{MeV} \qquad (2.7)$$

The ^{3}He(n,p) reaction has a cross section about 5321 barns for thermal neutrons. A typical pulse-height spectrum obtained with a ^{3}He proportional counter is shown in Fig. 2.9.

The full-energy peak (at about channel 430) corresponds to the reaction energy of 764 keV. Due to the partial wall effect suffered by the proton and/or the Triton, the lower-amplitude pulses are generated. The lower limit of the neutron induced events, at about channel 100, corresponds to the full wall effect of the proton (573 Kiev) implying the full Triton energy transfer (191 Kiev) to the sensitive gas. About 100 kPa (~ 1 atm) of krypton is admixed with the ^{3}He gas to increase the stopping power and hence to reduce wall effects. A simple threshold placed at about channel 80 allows the consistent separation of the neutron induced events from noise and gamma ray induced events.

The simple and efficient separation of the neutron events from a pulse-height spectrum obtained with a ^{3}He filled proportional counter makes it suitable for measurements in neutron fields with very low fluence rates (e.g. the neutron natural background induced by the cosmic radiation at ground level, or even inside buildings with thick concrete shielding).

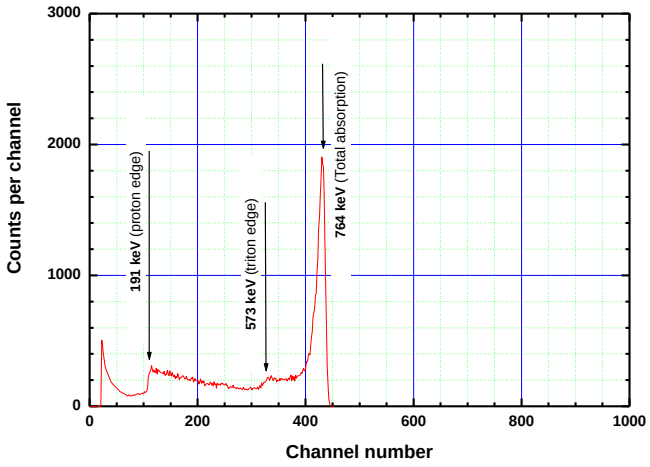

Figure 2.9: Typical pulse-height spectrum obtained using a ^{3}He proportional counter in a neutron field.

In some situations, where the dose rates are particularly intense, the relatively high response of the ^{3}He proportional counter to thermal neutrons is a problem because of the high count rates for all Bonner spheres. In an attempt to devise a well-characterized lower-response system, investigations have been made for the effects of covering the counter with a thin close-fitting cadmium shell. Reductions were obtained by factors of 6 to 8, but these proved to be dependent on energy and Bonner sphere size so that an appropriate fluence response matrix could not be derived simply by renormalizing the matrix elements for the conventional system using this counter. An alternative approach, not yet fully explored, might be to use an SP9 counter with a reduced gas filling. Bonner sphere systems based on even larger ^{3}He counters have been developed, including ones using a 50.8 mm diameter spherical counter filled with 1 MPa of ^{3}He (Uwamino, 1985; Goldhagen, 2002).

2.3.5.9 Passive neutron detectors

Not only BSS based on active detectors could be used to measure neutron fields but also BSS based on many passive detectors such as activation foils, TLD, superheated drop detectors, and track detectors which are placed at the central of Bonner sphere in a BSS.

Passive detectors have advantages compared with active detectors, and the choice type of detector depends on the characteristics of the workplace in which the measurement was made in general to avoid dead-time problems and sensitive to gamma rays, which can be of concern for active detectors in intense neutron fields. In additional they can be used especially in pulsed fields, high photon background, high dose rate and high electromagnetic noise. By concern for the their properties, for example if needed for long time measuring they can be used, in

the case of activation foils, that the half-life of the activation product is not too short. One of advantage is no electronic connection to Bonner spheres and it makes easy to position Bonner spheres in the field quickly, thus reducing the dose rate to the user. The Bonner sphere can also be wrapped in thin plastic bags protecting them from contamination in areas where radioactive contamination is a potential problem.

2.3.5.10 Activation foils

The activation foil technique relies on activation method. The activation method based on the neutron-induced nuclear reactions such as (n,p), (n,γ), (n,α), (n,f), etc., by irradiating foils or wires in a reactor or accelerator. As a result the reaction products radioactive material which most of them decays usually by gamma emission. Moreover the cross-section of each of these reactions depends on the neutron energy. Hence, the total activity gives a measure of the neutron fluence in a given energy range. The irradiated foils or wires are counted separately after the irradiation, generally by using gamma spectrometric methods (Knoll, 2000). A high resolution HPGe detector could be applied for the purpose. Neutron flux distributions are usually determined in reactors, accelerators and neutron fields by the method through the specificity of the reaction, simplicity of measurement, insensitivity to gamma components, and the using response matrix for the unfolding purposes (Tripathy, 2007). Bonner sphere set based on activation foil (In, Au, Mn, Ni, Al, Cu, Dy, Co, Zn and Fe) can be applied for determining neutron flux distributions (Figs. 2.10a,b and 2.11) (Ueda, 2011).

a) 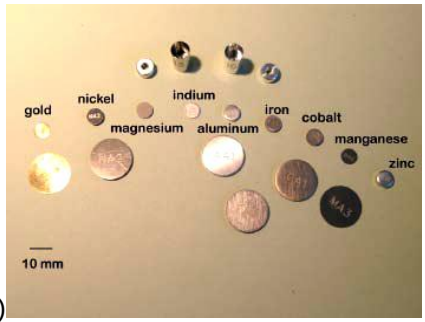

b) 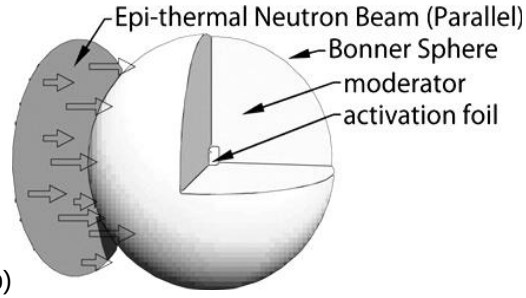

Figure 2.10: a) Activation foils which are used for measuring neutron flux distributions in a nuclear facility; b) Geometrical modeling by simulation for BSS based on Au (Ueda, 2011).

BSS based on activation foils such as gold (Thomas, 2002; Amgarou, 2009; Domingo, 2010), indium (Sannikov, 1994) and dysprosium foils (Bedogni, 2009) usually have been used for determining the unwanted secondary neutrons which are generated via photon-neutron (γ,n) and electron-neutron reaction (e,e'n) giant dipole resonance reactions of incident photons and electrons, respectively, with all

the heavy materials present inside the gantry and along the beam line of high-energy LINACs used in radiotherapy medical treatments. These activation foils are almost insensitive to gamma rays and so can be used in intense photon fields. For example gold activation sensors the ^{196}Au produced by (γ,n) reactions must be separated from the ^{198}Au produced by (n,γ) reactions, but this is relatively straight forward because of the different half-lives. Indeed, above about 18 MeV the (γ,n) reactions take place in the carbon in the polyethylene of the Bonner sphere and should be considered it (Thomas, 2002; Amgarou, 2009, 2011).

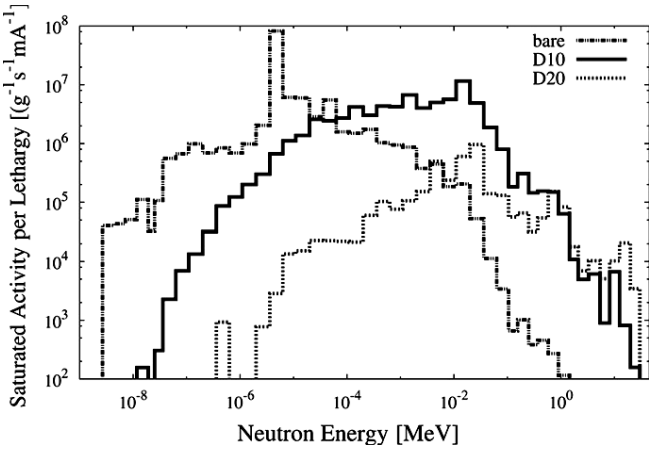

Figure 2.11: The saturated-activities of ^{197}Au, calculated on the assumption of the R0- 2.5 spectra, for the Bonner sphere using water including ^{10}B of 1wt%.''D10'' represents the 10 cm diameter Bonner sphere, and ''bare'' corresponds to the case without the Bonner sphere (Ueda, 2011).

2.3.5.11 Thermoluminescent dosimeters (TLDs)

Thermoluminescent dosimeter (TLD) is a type of detector which is used for dosimetry and also measuring neutron flux distributions in the workplace (Fig. 2.12a). The ionizing radiation creates free electrons (or holes) that may be trapped in metastable levels in the crystal structure which depends on the characteristic of the crystal. Thermoluminescence (TL) is the emission of light happening when electrons (or holes) are released from the traps and recombine with holes (or electrons); the escape probability is greatly increased by raising the phosphor temperature by using of the TLD reader system. The system provides a means for measuring TL by the controlled heating of the irradiated crystal. Consequently TL emission is detected and plotted as a function of time during the TLD temperature linear increase. The obtained curve is named Glow Curve (GC) which is shown in Fig. 2.12 b. In the glow curve, peaks correspond to the various energies of the emptied traps, which depend on the type of crystal and radiation. Therefore, the glow curve shape may be different changing the crystal or changing the type of

radiation. The area of each peak is proportional to the trap population and consequently, to the absorbed dose.

TLD-600 is sensitive to both gammas and neutrons due to $^{6}Li(n_{th},\alpha)^{3}H$ reaction with cross section about 940 barn, while TLD-700 is sensitive to gamma by total neutron cross section value of 14.7 barn. The thermal neutron-induced TL signal can be found by subtracting the TLD-700 glow curve from the TLD-600 one. In Fig. 2.13a, new application of the Bonner sphere as GSI-ball which is an extended-range rem-counter as dosimeter and consisting of a polyethylene Bonner sphere 31.8 cm in diameter with an inner lead layer 1 cm in thickness and pairs of TLDs 600/700 at the center of GSI-ball. This GSI-ball was applied for determining fluence response for 500 and 800 A MeV deuteron beams in Cave C at GSI. In Fig. 2.13b, measured and calculated fluence response by using Fluka code and fluence-to-dose conversion function for the quantity H*(10) from Sannikov and Savitskaya is shown (Sannikov, 1994).

a)

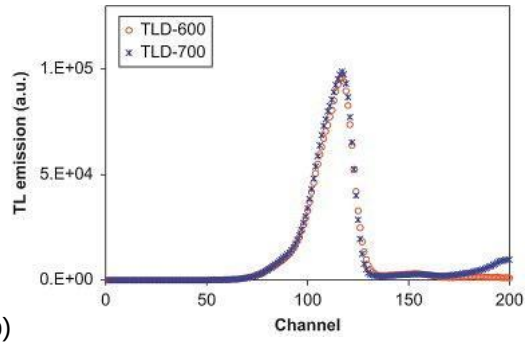

b)

Figure 2.12: a) Different types of TLDs (powder, chips and pellets) ; b) Glow Curves of TLD-600 and TLD-700.

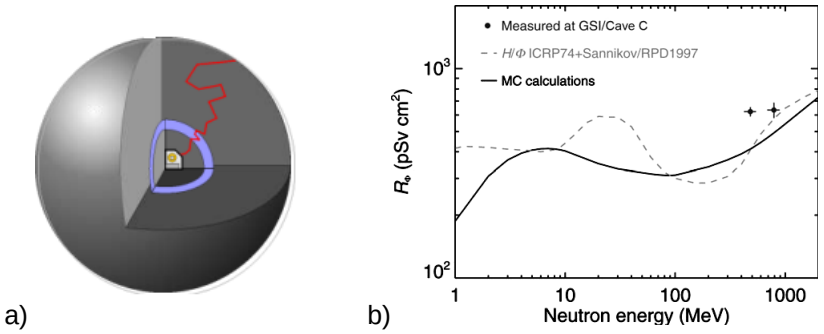

Figure 2.13: a) The GSI-ball is an extended-range rem-counter as dosemeter including pairs of TLDs 600/700 at the center of GSI-ball; b) Measured and calculated fluence response the GSI ball for 500 and 800 A MeV deuteron beams in Cave C at GSI and fluence-to-dose conversion function for the quantity H*(10) from Sannikov and Savitskaya (Fehrenbacher, 2007; Sannikov, 1994).

BSS based on TLD-600 (^{6}LiF:Mg,Ti) and TLD-700 (^{7}LiF:Mg,Ti) detectors are usually applied in mixed fields for determination of neutron components for particularly application around LINAC in the treatment room (Vega Carrillo, 2010) or in a reactor environment where the fluence rate is high and low sensitivity is needed (Sweezy, 1998).

The TLD readout due to neutrons for each Bonner sphere was applied by Vega Carrillo (2010) to unfold the neutron spectrum. This was carried out using unfolding code and response matrix which are obtained via MC calculations, and the results are shown in Figs. 2.14a,b.

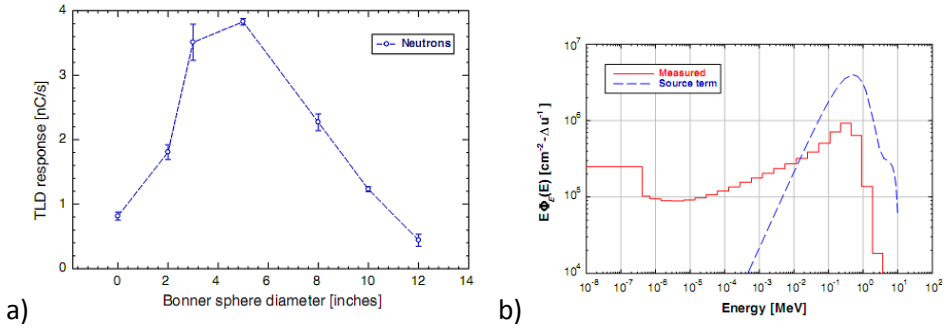

Figure 2.14: a) TLD neutron response for each Bonner sphere; b) Neutron spectrum produced in the LINAC head, and to100 cm from isocenter (Vega Carrillo, 2010).

Neutron spectrum at 100 cm from isocenter has been measured in the treatment room with an 18 MV LINAC. Neutrons are produced mainly due to photons incident with head materials, beam line LINAC and phantom usually above 10 MeV.

Measured spectrum is the contribution of those neutrons leaking out of a lion's head, scattered from materials in the treatment room, like the phantom, and the room returned neutrons (Vega Carrillo, 2010).

2.3.5.12 Superheated drop or Bubble detector

Superheated drop detector (SDD) is a miniature bubble chamber for neutron detection as dosimeter and also is known as bubble interactive neutron spectrometer (BINS) for purposes neutron spectrometry.

SDD was discovered in 1952 when Glaser did his initial work with bubble chambers. He found that radiation could induce the formation of bubbles or tiny droplets in a superheated liquid which are dispersed in a clear polymer (Glaser, 1952). The use of SDD was first introduced by Apfel in 1979. In the research, he investigated superheated droplets of CCL_2F_2 which are created in material with high viscosity and nucleation of these droplets was observed due to neutron irradiation (Apfel, 1979). The thermal neutron response of CCL_2F_2 based superheated emulsion detectors as follows:

$$^{35}\mathrm{Cl} + n_{th} \rightarrow {}^{35}\mathrm{S} + {}^{1}\mathrm{H} + 17\ \mathrm{keV} \tag{2.8}$$

According to the reaction the bubble nucleation generated in a superheated liquid if the neutron energy deposited is greater than a threshold value of W (Roy, 2003) (2.15a). Also threshold *W*, the energy required to create a bubble can be calculated through Eq. (2.10):

$$W = \frac{16\pi\gamma^3(T)}{3(p_v - p_0)^2} \tag{2.9}$$

where $\gamma(T)$ is the surface tension between liquid and vapor, p_v is the vapor pressure of the superheated liquid and p_0 is the ambient pressure. The difference between p_v and p_0 is called the degree of superheat of the liquid. According to Eq. (2.10), threshold *W* changes with temperature. Bubbles can be counted either visually or with a specially-designed reader, to give a measure of the number and energy of the incident neutrons (2.15b).

There are some compounds for superheated emulsion detector such as CF_3CH_2F(HFC-134A) and C_2HCIF_4 (HCFC-124) which are sensitive to neutron and C_3F_6 (hexafluoropropene), C_4F_8 (C-318), CCl_2F_2 (R-12), $C_2Cl_2F_2$(R-114) and C_2H_3 CIF_2 (R-142B) which are sensitive to neutron and gamma (Vaijapurkar, 2010). Such as these detectors used for 3-D dosimetry of photon- emitting brachytherapy sources and lead to study the novel position-sensitive systems for assessing the bubble spatial distribution (d'Errico, 2006). For reaching the aim, the optical tomography was proposed in 2008 by d'Errico and the satisfactory results obtained with this technique lead to apply scattered light for the bubble counting of superheated emulsions for individual dosimetry (d'Errico, 2008).

a) 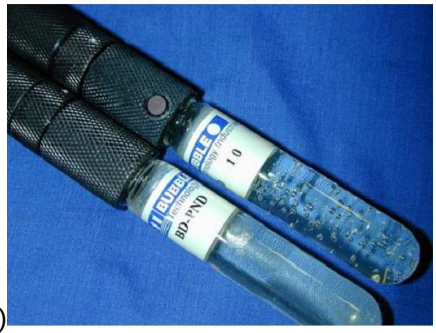 b) 

Figure 2.15: a) The commercial superheated detector (emulsion) before and after irradiation; b) The commercial bubble reader (BDR-III automatic reader).

The BINS spectrometer is based on SDD. By increasing the temperature of SDD, energy response thresholds of the detector decrease. The response of SDD covered the 0.1-10 MeV neutron energy range and is insensitivity to gamma irradiation. Neutron spectra can be obtained from measuring data and known response matrix by using unfolding codes such as MAXED.

In recently research, two superheated emulsion detectors (R-114 and C-318) were applied for determination neutron spectra from the ^{9}Be(p,xn) reaction at 0º direction in the framework of TRASCO-BNCT project. The unfolding of the data was performed by means of MAXED code and the spectrum was shown in Fig. 2.16. The obtained spectrum was compared with another technique and there was a good agreement at 0º (Di Fulvio, 2012).

Bubble Detector has many advantages. It is the only neutron dosimeter where the response is independent of dose rate and energy, with zero sensitivity to gamma radiation. Bubble Detectors are so compact, lightweight, and rugged, that they can be clipped to a coat or shirt pocket, placed in areas with limited access, or used in close proximity to a neutron source for a quick assessment. With an isotropic angular response, neutron dose can be accurately measured regardless of the direction of neutrons relative to the detector. Bubble Detectors are ideal for purposes personal dosimetry and radiation protection, providing the user with an immediate measurement of the neutron at emergency conditions. Disadvantages include the limitations temperature and reader is necessary for counting bubbles which are quite expensive.

The BINS spectrometer needs to have an unfolding code for achieving neutron spectra. Moreover changes in temperature cause threshold changes and effect on neutron spectra.

Bubble Detector can be used in the center of the Bonner sphere set for measuring neutron spectra in neutron field which are still a new idea for future work.

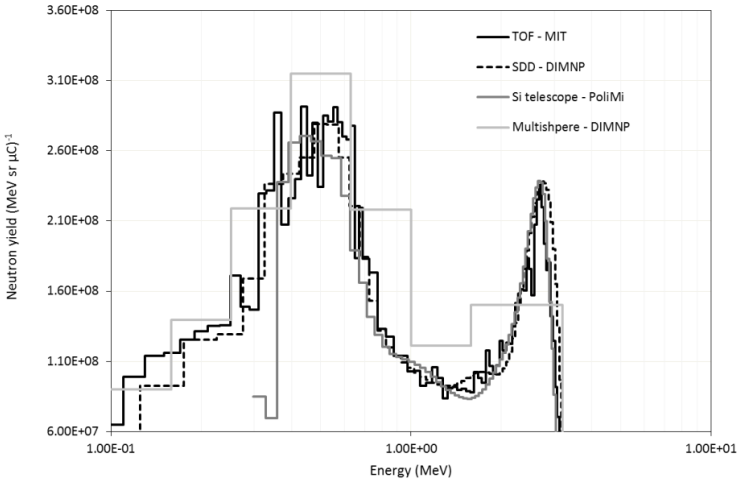

Figure 2.16: Neutron yield energy distribution measured with the BINS system at 0°, compared with other technique (Di Fulvio, 2012).

2.3.5.13 Track detector

The CR-39 plastic track detector is a $C_{12}H_{18}O_7$ polymer with density 1.3 g·cm^{-3}. Neutron interaction with CR-39 detector which is inelastic scattering on C-12 nucleus causing decay into three α particles:

$$^{12}\mathrm{C} + n \rightarrow n + 3\alpha \quad (Q = -7.37\ \mathrm{MeV}) \tag{2.10}$$

The cross section of the reaction is about 190 mb for neutron at E_n = 14.5 MeV. The presence of three α particle tracks outgoing from a single point allows us to separate these reactions from other neutron interactions with CR-39 nuclei. After exposure, the detector is etched in NaOH solution at 70°C for 7 h. After the etching, charged particle tracks become visible and can be investigated using a microscope (Fig. 2.17a). As is well known, the main parameter of track detector is the ratio of etching rates at the start of the track and at the end of the track (v_T/v_B). This ratio is a function of energy loss (stopping power, *dE*/*dx*). Track diameter is related to this ratio by a parametric equation (Samogyi, 1973). Identification of a particle depends on the track diameter which die/decks make it. The critical angle of registration (Θ_c = arcsin(v_B/v_T)) is also an important characteristic. Θ_c is the minimum angle of particle incidence on the detector which can cause the track formation. It is easy to show that the detection efficiency for a given type of particles is determined by the relation (Fleisher, 1975):

$$\eta = 1 - \sin\Theta_c \tag{2.11}$$

CR-39 nuclear coupled to a boron converter can be used for measuring neutron flux through the $^{10}B(n,\alpha)^{7}Li$ nuclear reaction, which can also be applied and placed in the Bonner sphere. For example, two kinds of boron converters were applied, the first made by natural boron and a second one enriched in ^{10}B (Caresana, 2007) (Fig. 2.17b). In Table 2.2, a list of passive detectors used as central detectors for BSS is presented.

a) 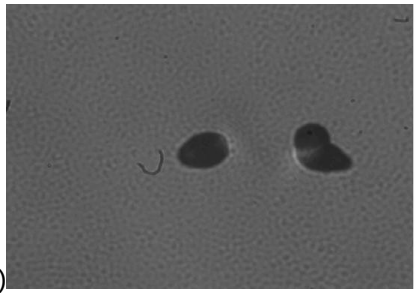 b) 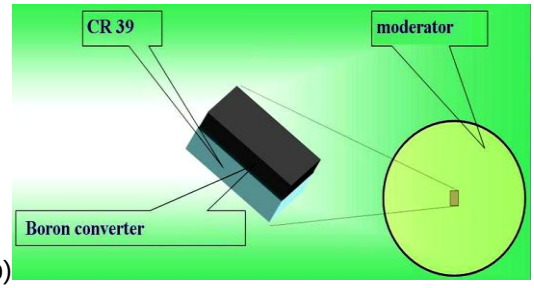

Figure 2.17: a) Microphotographs of tracks in CR-39 detector exposed to dT-neutron; b) CR-39 nuclear coupled to a boron converter which is placed inside the Bonner sphere.

Table 2.2: Passive devices for the determination of neutron spectrum by using BSS.

Passive device	Thermal neutron	Epithermal neutron	Fast neutron
Pairs of thermoluminescence dosimeters (TLD-600, TLD-700)	×	×	×
Activation of gold foils	×		
Track detectors (CR-39)	×	×	×

References

Amgarou, K., et al. (2009). Neutron spectrometry with a passive Bonner sphere system around a medical LINAC and evaluation of the associated unfolding uncertainties. *IEEE Transactions on nuclear science*, 56(5), pp. 2885-2895.

Amgarou, K., et al. (2010). Response matrix evaluations of a passive Bonner sphere system used for neutron spectrometry at pulsed, intense and complex mixed fields. *(http://iopscience.iop.org/1748-0221/5/09/P09002).*

Amgarou, K., et al. (2011). Experimental characterization of the neutron spectra generated by a high-energy clinical LINAC. *Nuclear Instruments and Methods in Physics Research A,* 629, pp.329–336.

Alevra, A.V., et al. (1988). Experimental determination of the response of the four Bonner sphere sets to monoenergetic neutrons. *Radiation Protection Dosimetry*, 23, pp. 249-252.

Alevra, A.V., et al. (1992). Experimental determination of the response of four Bonner sphere sets to monoenergetic neutrons (II). *Radiation Protection Dosimetry*, 40 (2), pp. 91-102.

Alevra, A.V and Thomas, D. J. (2003). Neutron spectrometry in mixed fields: multisphere spectrometers. *Radiation Protection Dosimetry*, 107 (1–3), pp. 37-72.

Apfel, R.E., et al. (1979). The Superheated Drop Detector. *Nuclear Instruments and Methods in Physics Research, 1*62, pp. 603-608.

Atanackovic, J., et al. (2012). Neutron spectrometry and dosimetry study at two research nuclear reactors using Bonner sphere spectrometer (BSS), Rotational spectrometer and Cylinder nested neutron spectrometer (NNS). *Radiation Protection Dosimetry*, pp. 1-11.

Aroua, A., et al. (1992). Evaluation and test of the response matrix of a multisphere neutron spectrometer in a wide energy range. *Part 1. Calibration*, *Nuclear Instruments and Methods in Physics Research A*, 321, pp. 298-304.

Baard, J.H., et al. (1989). Nuclear Data Guide for Reactor Neutron Dosimetry. Kluwer Academic, Dordrecht, The Netherlands.

Bedogni, R. (2009). Characterization of the neutron field at the ISIS-VESUVIO facility by means of a Bonner sphere spectrometer. Nuclear Instruments and Methods in Physics Research A, 612, pp. 143-148.

Bramblett, R.L., et al. (1960). A new type of neutron spectrometer. *Nuclear Instruments and Methods in Physics Research,* 9, pp. 1-12.

Batchelor, R.G., et al. (1960). Fast Neutron Physics, Part 1, Interscience, New York, 413.

Brooks, F.D., et al. (2002). Neutron spectrometry historical review and present status. *Nuclear Instruments and Methods in Physics Research A,* 476, pp. 1-11.

Byerly, P.R., et al. (1960). Fast Neutron Physics, Part 1, Interscience, New York, pp. 657.

Caresana, M., et al. (2007). Sensitivity study of CR39 track detector in an extend rang Bonner sphere spectrometer. *Radiation Protection Dosimetry,* 126, pp. 310-313.

Chadwick, J., et al. (1932). The Existence of a Neutron. Proc. Roy. Soc, A, 136, pp. 692.

Caizergues, R., et al. (1972). Calcul de la réponse des sphères de Bonner pour les détecteurs à LiI, He et Mn, *Rapport CEA-R-4400* (in French).

Chiojdeanu, C.F., et al. (2009). Boron neutron capture therapy set up for a linear accelerator, *Romanian Journal of Physics,* 54, (7–8), pp. 641-648.

Dearnaley, G., et al. (1963). Progress in Fast Neutron Physics, The University of Chicago Press, Chicago, pp. 173.

d'Errico, F., et al. (1997). Advances in Superheated Drop (Bubble) Detector Techniques. *Radiation Protection Dosimetry*, 70, pp. 103-108.

d'Errico, F., et al. (2003). Neutron spectrometry in mixed field: Superheated drop (bubble) detector. *Radiation Protection Dosimetry*, 107 (1-3), pp. 111-124.

d'Errico, F. (2006). Status of radiation detection with superheated emulsions. *Radiation Protection Dosimetry*, 120, 1-4, pp. 475-479.

d'Errico, F., et al. (2008). Optical readout of superheated emulsions. *Radiation Measurements*, 43, 2-6, pp. 432-436.

Dietz, E., et al. (1993). Neutron response of an ^{3}He proportional counter. *Nuclear Instruments and Methods in Physics Research A,* 332, pp. 521-528.

Di Fulvio, A., et al. (2012). Application of the BINS Superheated Drop Detector Spectrometer to the ^{9}Be(p,xn) Neutron Energy Spectrum Determination. Proceedings of ION BEAMS '12 Multidisciplinary Applications of Nuclear Physics with Ion Beams June 6th-8th, Laboratori Nazionali di Legnaro, Padua, Italy.

Domingo, C., et al. (2010). Neutron spectrometry and determination of neutron ambient dose equivalents in different LINAC radiotherapy rooms. *Radiation Measurements*, 45, pp.1391-1397.

Dubeau, J., et al. (2010). A new type of neutron spectrometer using nested moderator. (Toronto), UOIT, Oshawa, ON, 25 & 26 June, International Workshop on Real Time Measurement, Instrumentation & Control [RTMIC].

Elevant, T.H., et al. (1986). Silicon surface barrier detector for fusion neutron spectroscopy. *Review of Scientific Instruments*, 57, pp. 1763-1765.

Elevant, T.H., et al. (2002). Fusion neutron energy spectra measured by time of flight neutron method. *Nuclear Instruments and Methods in Physics Research A,* 476, pp. 485-489.

Ejiri, H., et al. (1991). Low-background measurement of fast neutrons by means of Ge detectors*. Nuclear Instruments and Methods in Physics Research* A, 302, pp. 482-*488.*

Fehrenbacher, G., et al. (2007). Measurement of the fluence response of the GSI neutron ball in the high-energy neutron fields produced by 500 AMeV and 800 AMeV deuterons. *Radiation Protection Dosimetry*, 126 (1–4), pp. 497-500.

Fleisher, R. L., et al. (1975). Nuclear Tracks in Solids. Principles and Applications. *University of California Press*, v. 1.

Glaser, D.A. (1952). Some effects of Ionizing radiation on the formation of bubbles in liquids. *Physical Review*, 87 (4), pp. 665-665.

Goldhagen, P. (2002). Measurement of the energy spectrum of the cosmic-ray induced neutrons aboard an ER-2 high-altitude airplane. *Nuclear Instruments and Methods in Physics Research,* 476(1–2), pp. 42-51.

Garny, S., et al. (2011). Measurement of neutron spectra and neutron doses at the Munich FRM II therapy beam with Bonner spheres. *Radiation Measurements,* 46, pp. 92-97.

Gressier, V., et al. (2005). Recent developments in neutron metrology at the Institute for radiological Protection and Nuclear Safety (IRSN). Report CCRI(III)/05-18.

Grosshoeg, G., et al. (1979). Neutron Ionization Chambers. *Nuclear Instruments and Methods in Physics Research,* 162, pp. 125-160.

Harvey, J.A., et al. (1979). Scintillation detectors for fast neutron physics. *Nuclear Instruments and Methods in Physics Research,* 162. pp. 507-530.

Harvey, W.F., et al. (1993). Multisphere neutron spectroscopy measurements at the Los Alamos National Laboratory Plutonium Facility. *Radiation Protection Dosimetry*, 50, pp. 13-30.

Hawkes, N.P., et al. (1993). A 2.5 MeV neutron spectrometry system with a tangential line of sight for the D-D phase at the JET tokamak. *Nuclear Instruments and Methods in Physics Research A,* 335, pp. 533-546.

Hertel, N.E., et al. (1985). The response of Bonner spheres to neutrons from thermal energies to 17.3 MeV. *Nuclear Instruments and Methods in Physics Research A,* 238, pp. 509-516.

Howell, R.M., et al. (2010). Calibration of a Bonner sphere extension (BSE) for high-energy neutron spectrometry. *Radiation Measurements*, 45, 10, pp. 1233–1237.

Iguchi, T., et al. (1994). Neutron spectrometry using a ^{3}He gas ionization chamber. *Nuclear Instruments and Methods in Physics Research A,* 353, pp. 152-155.

Jacobs, G.J., et al. (1980). Calibration measurements with the multisphere method and neutron spectrum analyses using the SAND-II program. *Nuclear Instruments and Methods in Physics Research,* 175, pp. 483-489.

Klein, H., et al. (2003). Neutron Neutron spectrometry in mixed fields: NE213/BC501A liquid scintillators spectrometers. *Radiation Protection Dosimetry*, 107, 1-3, pp. 95-109.

Kluge, H., et al. (1982). The neutron energy spectrum of a ^{241}Am-Be(Alpha,n) source and resulting mean fluence to dose equivalent conversion factors. *Radiation Protection Dosimetry*, 2, pp. 85-93.

Knoll, G.F. (2000). *Radiation detection and measurement*, 3rd ed, Wiley.

Kralik, M., et al. (1992). Specification of Bonner sphere systems for neutron spectrometry, *Radiation Protection Dosimetry*, 70, pp. 279-284.

Kuijpers, L., et al. (1977). On the determination of fast neutron spectra with activation techniques; its application in a fusion reactor blanket model. *Nuclear Instruments and Methods in Physics Research*, 144, pp. 215-224.

Liu, J.C., et al. (1990). Neutron spectral measurements at ORNL. *Radiation Protection Dosimetry*, 30, pp. 169-178.

Marek, M., et al. (1998). Determination of the geometric and spectral characteristic of BNCT beam (Neutron and gamma-ray). *Proceedings 8th International Symposium on Neutron Capture Therapy for Cancer*, La Jolla, USA, September. 13-18.

Mares, V and Schraube, H. (1994). Evaluation of the response matrix of a Bonner sphere spectrometer with lie detector from thermal energy of 100 MeV. *Nuclear Instruments and Methods in Physics Research A*, 337, pp. 461-473.

Marsh, J.W. (1995). High resolution measurements of neutron energy spectra from Am-Be and Am-B neutron sources. *Nuclear Instruments and Methods in Physics Research A, 366,* pp. 340-343.

Mazrou, H., et al. (2008). Characterization of the CRNA Bonner sphere spectrometer based on ^{6}LiI scintillator exposed to an ^{241}Am–Be neutron source. *Radiation Measurements*, 43, pp. 1095-1099.

Mirzajani, N., et al. (2009). Set up of a Bonner sphere Spectrometer for an accelerator-based BNCT Facility, *Proceedings of Young Researchers BNCT Meeting,* September 29- October 2, Mainz, Germany.

Mourgues, M., et al. (1974). La mesure des neutrons par compteur à helium-3 sous modérateur sphérique. *Proceedings of the Second Symposium on Neutron Dosimetry in Biology and Medicine, Neuherberg/Munchen*, 30 Septempber – 4 October, Vol. II, pp. 907-931, (in French).

Muller, H., et al. (2002). Monte Carlo calculations and experimental results of Bonner sphere systems with a new cylindrical helium-3 proportional counter, *Nuclear Instruments and Methods in Physics Research A*, 476 (1–2), pp. 411-415.

Murray, R.B., et al. (1958). Use of $Li^{6}I$(Eu) as a scintillation detector and spectrometer for fast neutrons. *Nuclear Instruments and Methods in Physics Research,* 2, pp. 237-248.

Perey, F.G. (1978). The STAY'SL Code. Oak Ridge Report ORNL/TM-6062.

Takeda, N., et al. (1999). A development of NRESPG Monte Carlo code for the calculation of neutron response function for gas counters. *Nuclear Instruments and Methods in Physics Research A,* 422, 1-3, pp. 69-74.

Roy, S. C., et al. (2003). Use of Superheated Liquid in Neutron Detection. *Current Science*, 84 (4), pp. 516-528.

Sanna, R., et al. (1973). Thirty one group response matrices for the multisphere neutron spectrometer over the energy range thermal to 400 MeV. *USAEC, HASL-267, March*.

Sannikov, A.V. (1994). Calculated response functions of indium loaded Bonner spectrometer, *Report CERN/TIS-RP/IR/94–05*, 18 March.

Sannikov, A.V., et al. (1997). Ambient dose equivalent conversion factors for high energy neutrons based on the ICRP60 Recommendations. *Radiation Protection Dosimetry*, 70(1–4), pp. 383-386.

Samogyi, G., et al. (1973). Track Diameter Kinetics in Dielectric Track Detectors. *Nuclear Instruments and Methods,* 109, N 2, pp. 211-232.

Silari, M. (2001). Design, calibration and tests of an extended-range Bonner sphere Spectrometer. Ph.D. thesis, Technischen Universitat, Wien, Austria.

Seghour, A., et al. (1999). Neutron spectrometry at Strasbourg University Reactor. *Nuclear Instruments and Methods in Physics Research A,* 420, pp. 243-248.

Shalev. S., et al. (1969). The wall effect in ^{3}He counters. *Nuclear Instruments and Methods,* 71, pp. 292-296.

Shalev, S and Cuttler,,J. M., (1972). The energy distribution of delayed fission neutrons. Nuclear Science *and Engineering*, pp. 51-52.

Spaepen, J., et al. (1961). Neutron Time-of-Flight Methods, Euratom, Brussels, Belgium.

Sweezy J.E., et al. (1998). Performance of multisphere spectrometry systems. *Radiation Protection Dosimetry*, 78, pp. 263-272.

Tagziria, H., et al. (2003). Neutron spectrometry in mixed fields: proportional counter spectrometers. *Radiation Protection Dosimetry*, 107 (1-3), pp. 73-93.

Thomas, D.J. (2002). Characterization of a gold foil based Bonner sphere set and measurements of neutron spectra at a hospital LINAC. *Nuclear Instruments and Methods in Physics Research A,* 476 (1–2), pp. 31-35.

Thomas, D.J., et al. (2002). Bonner sphere spectrometers—a critical review. *Nuclear Instruments and Methods in Physics Research A,* 476, pp. 12-20.

Tripathy, S.P., et al. (2007). Activation foils unfolding for neutron spectrometry: comparison of different deconvolution methods. *Nuclear Instruments and Methods in Physics Research A,* 583, pp. 421-425.

Ueda, H., et al. (2011). The optimization study of Bonner sphere in the epi-thermal neutron irradiation field for BNCT. *Radiation Protection Dosimetry*, 69, 12, pp. 1657-1659.

Uwamino, Y., et al. (1985). Two types of multi-moderator neutron spectrometers: gamma-ray insensitive type and high efficiency type, *Nuclear Instruments and Methods in Physics Research A,* 239, pp. 299-309.

Vaijapurkar, S.G. (2010). Bubble detector for neutron and gamma discrimination. *Radiation Protection and Environment (RPE)*, 33, 3, pp. 94-99.

Vega-Carrillo, H.R., et al. (2008). Calculation of Response matrix of a BSS with ^{6}LiI scintillator. *Revista Mexicana De Fisica*. S, pp. 54-57.

Vega Carrillo, H.R., et al. (2010). Neutron spectrum and doses in a 18 MV LINAC. *Radioanalytical and Nuclear Chemistry*, 283, pp. 261-265.

Wiegel, B., et al. (2002). NEMUSF the PTB Neutron Multisphere Spectrometer: Bonner spheres and more. *Nuclear Instruments and Methods in Physics Research A,* 476, pp. 36-41.

Wiegel, B., et al. (2009). Intercomparison of radiation protection devices in a high-energy stray neutron field, Part II: Bonner sphere spectrometry. *Radiation Measurements,* 44, pp. 660-672.

Zaborowski, H. L., et al. (1981). Dosimétrie et spectrométrie neutroniques avec les sphères de Bonner; établissement d'une matrice lognormale de référence. *Proceedings of the Fourth Symposium on Neutron Dosimetry,* Neuherberg. Germany, 1.

3. Monte Carlo calculation of the energy response functions of BSS-UNIPI

3.1 Overview of the Monte Carlo code

3.1.1 Historical development

Enrico Fermi was the first scientist which involved the method of random sampling in studying the neutron transport in nuclear fissile material in 1930s. Then, in 1944 Nicholas Metropolis and Stanislaw Ulam applied the statistical sampling technique to numerically solve quantitative problems and named this method as Monte Carlo (MC) at the Los Alamos National Laboratory (LANL) (Gregg, 2000).

In 1948, the first run on a digital computer was performed on ENIAC; a pre-release of the first FORTRAN compiler was used for Monte Carlo in 1957. Moreover, Monte Carlo codes were adapted to vector computers in the 1980s, clusters and parallel computers in the 1990s, and teraflop systems in the 2000s. Recent advances include hierarchical parallelism and combining threaded calculations on multicore processors with message-passing between different nodes. In additional, the past 65 years of Monte Carlo history represent a huge investment in the research and development of random number generators, random sampling methods, criticality calculation methods, variance reduction techniques, physics interaction modeling, geometric ray-tracing, parallel computing methods, physics interaction data libraries, and code development (Gregg, 2000).

Nowadays the MC method has found widespread application in different scientific fields such as nuclear engineering, astrophysics, radioactive heat transfer, aerospace engineering, chemistry, biology, medical physics, health physics, electrical engineering, mathematics, environmental engineering, economics and business modeling.

There are very large efforts devoted to the verification and validation of Monte Carlo codes all over the word. With the advances in computing, Monte Carlo codes have evolved with new capabilities and new ways to use such as represented by the codes MCNP (Monte Carlo N-Particle), Fluka (FLUktuierende KAskade), Geant4 (GEometry ANd Tracking) and etc. (Gregg, 2000; Ferrari, 2005; Agostinellia, 2003).

The MCNP was originally a neutron–photon transport code which was used for several nuclear processes. It has the capability to simulate particle interactions involving neutrons, photons, and electrons. MCNP code can be used for calculations of multiplication factor, reaction rates, saturated activities, neutron fluxes and spectra, power peaking factors, reaction rate distributions, shielding, etc. Its main advantage is the ability to handle complicated geometries. For example, it can be applied for solving photon transport problems like brachytherapy dosimetry (Williamson, 2005), diagnostic X-ray applications (Boone, 1988), neutron transport problems like the calculation of the response functions of Bonner sphere

spectrometer (Mares, 1994; Mirzajani, 2010), or simulation of reactor or accelerator and many other problems(Gregg, 2000). With particular regard to the nuclear filed, the specific subject of the application includes radiation protection and dosimetry, radiation shielding, radiography, medical physics, nuclear criticaly safety, detector design and analysis, accelerator target design, fission and fusion reactor design, decontamination and decommissioning (Battistoni, 2007).

This chapter presents a brief about Monte Carlo N-Particle, calculation of the response matrix BSS-UNIPI for 51 mono energy bins (1 meV to 100 MeV) and response to an ^{241}Am-Be source (point or disc source). Finally, the response of the BSS-UNIPI set (3 and 10 in.), based on activation foils, to mono energetic neutrons as disc source, will be described.

3.1.2. Monte Carlo N-Particle eXtended (MCNPX)

MCNPX (Monte Carlo N-Particle eXtended) was developed at Los Alamos National Laboratory (USA), and is capable of simulating interactions for 34 different types of particles (nucleons and ions), including 20–150 MeV neutrons and 2000+ heavy ions at all energies, (Pelowitz, 2008). The software is very capable of modeling many types of radiation transport problems and uses standard evaluated data libraries of neutrons, photons and protons (some extended to 150 MeV), along with physics models where libraries are not available.

Some software components are necessary to perform calculations in MCNPX and the user must be provided and insert an input file which contains the definition of geometry (surfaces and cells), sources, materials and tallies. The source can be parameterized by several variables including spatial location, energy, and direction. The material cell can also have various attributes including shape, location, and material composition. A plotting is available to check geometries easily. Cross section tables and physical models are used in order to sample all generated particles random-walk interactions according to the probabilities of different mechanisms. The code permits to specify the information required by Monte Carlo calculation through proper tally cards. MCNPX offers several types of tallies, such as current across a surface, flux at a point, heating in a region, track length estimate of the cell flux, etc. Each one is defined by a proper letter and number: for example, F4 tally is the track length estimate of the cell flux and it was applied in this study (Pelowitz, 2008). The F4 tally is a Monte Carlo estimation of the average flux in a volume and it is calculated as follows.

$$\mathrm{F4} = \int_V \int_E \int_{4\pi} \Phi(r, E, \Omega) dE d\Omega \frac{dV}{V} \tag{3.1}$$

where $\Phi(r,E,\Omega)$ is the energy and angular distribution of the fluency as a function of position r, direction Ω, energy E, and V is the cell volume (cm^3). F4 tally is in units of particles·cm^{-2} (Pelowitz, 2008). MCNPX has only a few tally types, but other quantities can be directly computed by using the FM (tally Multiplier card). The FM4

card as multiplication factor is used to calculate response function $R_i(E)$ for each Bonner sphere i:

$$R_i(E) = n_\rho V \int_0^E \sigma(E)\Phi(E)dE = C\int_0^E \sigma(E)\Phi(E)dE \quad (i = 1,.....,18) \tag{3.2}$$

where n_ρ is the atom number density (in atoms barn^{-1} cm^{-1}), $\sigma(E)$ is the microscopic cross-section of a particular reaction (in barn units, 1 barn = 10^{-24} cm^2), $\Phi(E)$ (cm^{-2} MeV^{-1}) is the fluence energy distribution and C is a constant multiplier. Then, the obtained results were multiplied in the source surface area to obtain the BSS response functions normalized for neutron incident flounce (cm^2). Thomas (1992) found a change in the Bonner sphere response about 1% with change in the polyethylene density (ρ) considering the ratio $(dR_i / R_i(E))/(d\rho/\rho)$ which is a function of the neutron energy and the Bonner sphere diameter. These parameters must be carefully verified, especially if the Bonner sphere is produced by a non specialized manufacturer. Then, the response function of a given Bonner sphere can be corrected for the density change, by attributing to the Bonner sphere a different diameter than the real one, according to the following relation (Alevra, 2003):

$$R_i(D, E, \rho + \Delta\rho) = R_i(D + \Delta D, E, \rho) \tag{3.3}$$

$$\left(\frac{\Delta D}{D}\right)_\rho = \left(\frac{\Delta\rho}{\rho}\right)_D \tag{3.4}$$

In this chapter the F4 tally and the multiplication factor card FM4 are used for the calculation response function of BSS-UNIPI based on ^{6}LiI(Eu) and passive detectors.

3.2 Calculation of response functions of BSS-UNIPI based on ^{6}LiI(Eu)

3.2.1 MCNPX model

In the study, MCNPX version 2.6e was used for the calculations. The simulation of the BSS-UNIPI system was done in detail according to the detector layout. BSS-UNIPI consists of a set of nine polyethylene Bonner spheres (ρ = 0.939 g cm^{-3}) of 7.62 cm (3") to 38.1 cm (15") diameter with a central thermal detector (^{6}LiI(Eu) scintillator) and associated electronics.

The thermal detector (4 mm x 4 mm cylindrical scintillator) contains ^{6}LiI(Eu), the light pipes, the photomultiplier tube, detector's container, and the polyethylene Bonner spheres. The materials considered for the simulation were ^{6}LiI crystal scintillation detector, plexiglas light pipe, polyethylene, air and aluminum. The elemental composition (weight percentage) of PMMA light pipe $(C_5H_8O_2)_n$ is

assumed to be C (60%), H (8%) and O (32%) with a mass density of 1.18 g cm^{-3}. The air composition (atomic fraction) was considered to be N (0.792), O (0.208) with a mass density of 1.2048 $x10^{-3}$ g cm^{-3}. The material composition (weight percentage) of the crystal scintillator ^{6}LiI is assumed to be 4.36% ^{6}Li, 0.18% ^{7}Li and 95.46% I, with a mass density of 3.494 g cm^{-3}. Polyethylene $(CH_2)_n$ was assumed to consist of C (85.7%) and H (14.3%) with a mean mass density of 0.939 g·cm^{-3}. In the MC calculations, the photomultiplier tube and the preamplifier were regarded as made of air. Geometry and materials of the ^{6}LiI(Eu) crystal scintillation detector and its MCNP model are shown in Figs. 3.1 and 3.2.

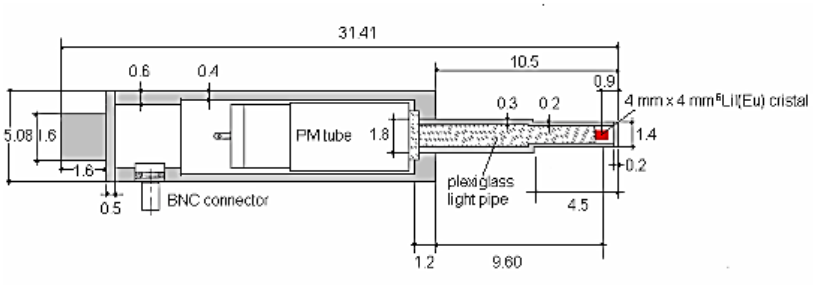

Figure 3.1: Geometry and materials of ^{6}LiI(Eu) crystal scintillation detector (all dimensions are in cm) .

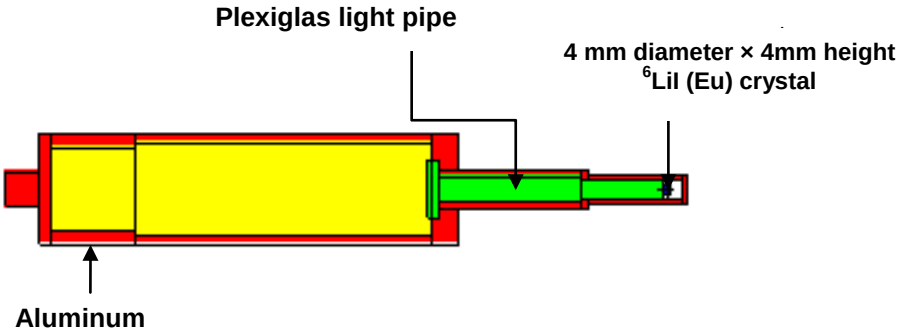

Figure 3.2: MCNP model of ^{6}LiI (Eu) crystal scintillation detector.

The energy neutron cross sections used by the standard MCNPX package (Pelowitz, 2008) are extracted from Evaluated Nuclear Data Files (ENDF) and also from Lawrence Livermore National Laboratory (LLNL) according to the following detail:

1. ^{6}Li, ^{7}Li, ^{1}H, ^{12}C (natural) and ^{27}Al from ENDF/B-VI;

2. ^{153}I from LLNL;
3. Poly 60t (hydrogen in polyethylene at 294 K) for polyethylene and PMMA (polymethyl methacrylate and Plexiglas) from ENDF/B-VI.

The S(α,β) treatment option was used to account for the carbon and hydrogen chemical binding at room temperature during thermal neutron scattering within the polyethylene Bonner sphere.

^{6}Li(n,t)α reaction has a Q-value of 4.79 MeV at neutron thermal energies, triton carries out 2.73 MeV and the alpha particle 2.06 MeV. The reaction cross-section for thermal energy is about four orders of magnitude larger than fast neutrons, as it is shown in Fig. 3.3. In the simulation only the ^{6}Li(n,t) events were considered, ignoring the contribution of all other nuclear reactions such as ^{6}Li (n,γ) and ^{6}Li (n,p) (Tanner, 2004).

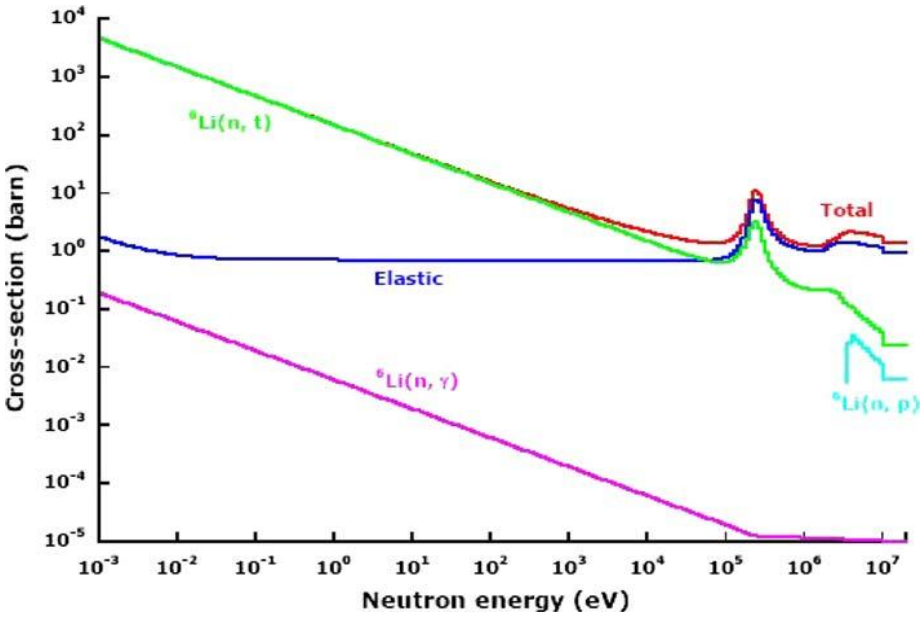

Figure 3.3: Cross-sections for neutron interactions on ^{6}Li (Tanner, 2004).

The response, $R_i(E)$ (cm^2), of each detector-sphere with respect to the considered neutron incidence energy, E, was defined as the number of the ^{6}Li(n,t)^{4}He reactions in the sensitive detector volume per incident neutron fluence. As mentioned before, $R_i(E)$ can be obtained by using equation (3.2) and considering the Li atom density (n_{Li}), the volume of the ^{6}LiI(Eu) crystal scintillation (V_{Li}) (in cm^3) and the cross section $\sigma(n,t)$ (in barn) of the ^{6}Li(n,t)^{4}He reaction.

3.2.2 The response matrix of the BSS-UNIPI based on ^{6}LiI(Eu)

The knowledge of the response matrix (the set of the energy response functions) for every neutron spectrometer is essential in both dosimetry and spectrometry application. Since BSS-UNIPI set is used in the range from thermal up to hundreds of MeV neutrons in workplaces, the determination of the response is fundamental. Moreover, each Bonner sphere has a unique energy dependence of the response function, which can be obtained through measurements or calculations. The measurements are usually performed in standardized monoenergetic neutron fields, and calculations are done using Monte Carlo codes such as MCNPX, Fluka and Geant4, as mentioned before (Mares, 1994; Agosteo, 2004; Garny, 2009). However the precise calculation of the spectrometer response functions is necessary for unfolding process. Thus the response matrix of the BSS-UNIPI set was determined in the large interval energy neutron by Monte Carlo code.

In previous works, the response function matrix for BSS like our system was calculated and are available in the literatures. Sanna was the first scientist who calculated thirty one group response functions for BSS from thermal to 400 MeV using the discrete ordinates code DTF-IV (Sanna, 1973). Later Hertel and Davidson calculated neutron responses for Bonner spheres to 17.3 MeV neutron energy with a 4 mm x 4 mm and 12.7 mm x 12.7 mm ^{6}LiI scintillator using an adjoin transport technique (Hertel, 1985). Mares and Schraube calculated the neutron responses of a Bonner sphere system with a 4 mm x 4 mm ^{6}LiI scintillator using the MCNP4 Monte Carlo code in the energy range from thermal to 100 MeV by considering 51 mono energy bins and 33 sphere diameters (Mares, 1994). Finally Vega Carrillo calculated the response functions of a Bonner sphere spectrometer based on 4 mm x 4 mm ^{6}LiI scintillator for from thermal to 100 MeV and 23 mono energy bins using MCNP 4C and MCNPX 2.4.0 codes (Vega Carrillo, 2008).

In this work, Monte Carlo simulations were performed by considering the realistic geometric model of the detector and 51 mono energy bins (from 1 meV to 100 MeV). All irradiations were considered by a parallel neutron beam to the axis of the detector has a circular area of radius d/2 for each Bonner sphere (d is the diameter of each Bonner sphere) and only bare laterally, in vacuum condition. Due to the moderator Bonner sphere shape the response of the detector to the source was isotropic. The absence of moderators around the bare detector caused different responses when changing its orientation with respect to the neutron beam. Thus, the bare configuration is the most difficult to validate. Mares calculated this response function in lateral irradiation geometry, i.e. with the neutron beam perpendicular to the detector axis. The experimental calibration factor shows a ±11% variability (1 stdev) with 8 neutron energies from thermal to 14.8 MeV (Mares, 1994). Due to the neutrons scattered in the light pipe and aluminum cover which substantial effect on the response, this work irradiation of bare detector was carried out with the neutron source at lateral with axis the bare detector.
Geometry splitting and Russian roulette as variance reduction methods were applied to obtain low statistical uncertainties in the results for the high number (51) of energy bins at a reasonable CPU time in this work. The method consists of subdividing the polyethylene Bonner sphere into many sub-cells and assigning to

them increasing importance values from external surface towards the central detector, so to preferentially consider the neutron migration in this direction. The whole response matrix of BSS-UNIPI was calculated with this method with a final relative statistical uncertainty below 3%, on a total CPU time of 3 months. The result for 8 in. Bonner sphere was compared with Mares (1994) and Vega-Carrillo (2008) response function (Figs. 3.4 and 3.5).

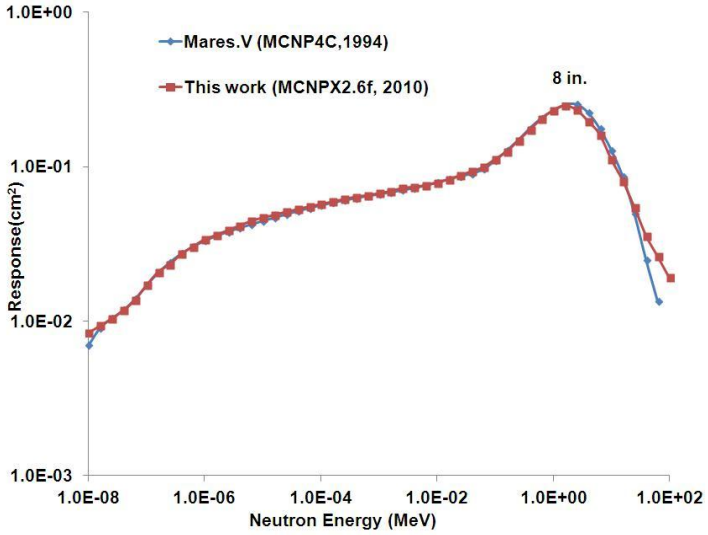

Figure 3.4: Comparison of the calculated response function (8 in. Bonner sphere) with Mares (1994).

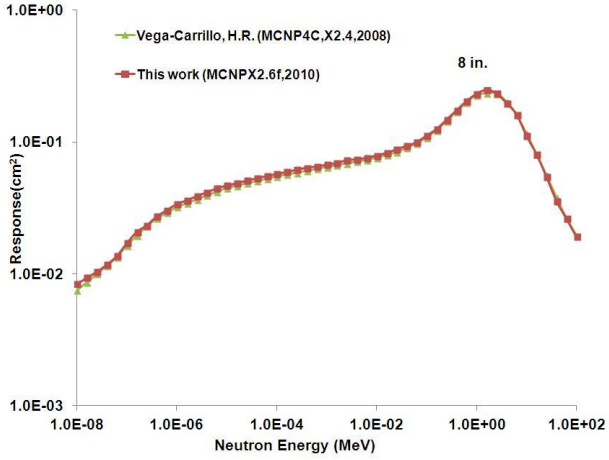

Figure 3.5: Comparison of the calculated response function (8 in. Bonner sphere) with Vega-Carrillo (2008).

Figs.3.4 and 3.5 show that a very good agreement was observed between our response function and the response function calculated by other authors. Only a little difference can be seen in the fast neutron energy regain, mostly due to three reasons. The first, the density of the moderating polyethylene Bonner sphere was 0.95 g cm^{-3} for other authors and 0.939 g cm^{-3} in our calculation (see Eqs. 3.3 and 3.4). The second reason is the differences in the cross sections libraries which utilized in the calculation. Mares used the Monte Carlo code MCNP 4C with the ENDF/B-5 cross section library, while our calculation and Vega-Carrillo used MCNPX with ENDF/B-VI and LA150 cross section library. The third was differences of ^{6}Li atomic density in the scintillator: 1.74 $\times 10^{22}$ (atoms cm^{-3}) for Mares and 1.523×10^{22} (atoms cm^{-3}) for us and Vega-Carrillo calculation.

The obtained response functions (matrix) of BSS-UNIPI set, as results from MCNPX calculations, are reported in Table 3.1 and shown in Figs. 3.6, 3.7 and 3.8.

Table 3.1: The response matrix of BSS-UNIPI set with a 4 x 4 mm ^{6}LiI scintillator at 51 energy neutron bins from 0.01 eV to 100 MeV.

N	Neutron Energy (MeV)	Bare (detector)	3 in.	4 in.	5 in.	6 in.
1	1.0000E-08	1.8574E-01	6.1483E-02	4.3767E-02	3.0177E-02	1.9867E-02
2	1.5850E-08	1.8269E-01	6.9044E-02	4.9485E-02	3.3890E-02	2.2444E-02
3	2.5120E-08	1.7935E-01	7.6751E-02	5.4814E-02	3.7637E-02	2.5274E-02
4	3.9810E-08	1.7400E-01	8.7596E-02	6.2739E-02	4.2769E-02	2.8586E-02
5	6.3100E-08	1.6783E-01	1.0365E-01	7.4103E-02	5.0903E-02	3.3885E-02
6	1.0000E-07	1.5920E-01	1.2920E-01	9.2294E-02	6.3402E-02	4.2116E-02
7	1.5850E-07	1.4877E-01	1.5722E-01	1.1376E-01	7.7529E-02	5.1674E-02
8	2.5120E-07	1.3650E-01	1.7441E-01	1.2733E-01	8.7394E-02	5.7501E-02
9	3.9810E-07	1.2293E-01	1.9654E-01	1.4611E-01	1.0127E-01	6.6521E-02
10	6.3100E-07	1.0883E-01	2.1260E-01	1.6152E-01	1.1140E-01	7.3896E-02
11	1.0000E-06	9.5068E-02	2.2624E-01	1.7551E-01	1.2301E-01	8.1300E-02
12	1.5880E-06	8.1739E-02	2.3516E-01	1.8721E-01	1.3185E-01	8.8260E-02
13	2.5120E-06	6.9547E-02	2.4369E-01	1.9818E-01	1.4218E-01	9.4228E-02
14	3.9810E-06	5.8456E-02	2.4964E-01	2.0808E-01	1.5021E-01	1.0113E-01
15	6.3100E-06	4.8746E-02	2.5409E-01	2.1689E-01	1.5783E-01	1.0709E-01
16	1.0000E-05	4.0413E-02	2.5534E-01	2.2308E-01	1.6535E-01	1.1287E-01
17	1.5850E-05	3.3310E-02	2.5394E-01	2.2839E-01	1.7048E-01	1.1720E-01
18	2.5120E-05	2.7169E-02	2.5118E-01	2.3227E-01	1.7657E-01	1.2187E-01
19	3.9810E-05	2.1649E-02	2.4648E-01	2.3463E-01	1.8145E-01	1.2572E-01
20	6.3100E-05	1.7924E-02	2.4165E-01	2.3669E-01	1.8548E-01	1.3000E-01
21	1.0000E-04	1.4450E-02	2.3624E-01	2.3665E-01	1.8912E-01	1.3329E-01
22	1.5850E-04	1.1640E-02	2.3053E-01	2.3790E-01	1.9266E-01	1.3826E-01
23	2.5120E-04	9.4151E-03	2.2330E-01	2.3659E-01	1.9572E-01	1.4252E-01
24	3.9810E-04	7.5534E-03	2.1651E-01	2.3576E-01	1.9890E-01	1.4494E-01
25	6.3100E-04	5.9211E-03	2.0901E-01	2.3394E-01	2.0039E-01	1.4686E-01
26	1.0000E-03	4.8370E-03	2.0162E-01	2.3250E-01	2.0188E-01	1.5052E-01
27	1.5850E-03	3.8912E-03	1.9459E-01	2.3060E-01	2.0375E-01	1.5356E-01
28	2.5120E-03	3.0993E-03	1.8719E-01	2.2788E-01	2.0506E-01	1.5654E-01
29	3.9810E-03	2.4819E-03	1.7967E-01	2.2465E-01	2.0585E-01	1.5896E-01
30	6.3100E-03	1.9987E-03	1.7214E-01	2.2133E-01	2.0753E-01	1.6276E-01
31	1.0000E-02	1.6007E-03	1.6529E-01	2.1882E-01	2.0857E-01	1.6476E-01
32	1.5850E-02	1.2730E-03	1.5843E-01	2.1595E-01	2.1116E-01	1.7023E-01
33	2.5120E-02	1.0080E-03	1.5178E-01	2.1367E-01	2.1360E-01	1.7527E-01
34	3.9810E-02	8.2328E-04	1.4460E-01	2.1197E-01	2.1555E-01	1.8105E-01
35	6.3100E-02	6.7353E-04	1.3700E-01	2.0914E-01	2.2209E-01	1.8971E-01
36	1.0000E-01	6.1181E-04	1.2926E-01	2.0721E-01	2.2917E-01	2.0144E-01
37	1.5850E-01	8.1327E-04	1.1945E-01	2.0310E-01	2.3447E-01	2.1523E-01
38	2.5120E-01	2.4122E-03	1.0719E-01	1.9675E-01	2.3994E-01	2.3238E-01
39	3.9810E-01	5.1066E-04	9.1577E-02	1.8355E-01	2.3960E-01	2.4531E-01
40	6.3100E-01	2.7110E-04	7.4329E-02	1.6333E-01	2.2991E-01	2.5368E-01
41	1.0000E+00	2.0541E-04	5.7068E-02	1.3732E-01	2.0909E-01	2.4883E-01
42	1.5850E+00	1.8067E-04	4.0922E-02	1.0798E-01	1.7894E-01	2.2784E-01
43	2.5120E+00	1.6052E-04	2.7397E-02	7.8296E-02	1.3957E-01	1.8993E-01
44	3.9810E+00	9.2612E-05	1.7170E-02	5.2222E-02	9.9514E-02	1.4461E-01
45	6.3100E+00	5.5543E-05	1.0936E-02	3.5448E-02	7.0132E-02	1.0710E-01
46	1.0000E+01	3.4308E-05	5.5554E-03	1.8951E-02	4.0933E-02	6.6105E-02
47	1.5850E+01	2.3508E-05	4.0174E-03	1.3564E-02	2.8604E-02	4.6466E-02
48	2.5120E+01	7.1604E-06	2.4564E-03	8.2816E-03	1.8268E-02	2.9909E-02
49	3.9810E+01	7.8865E-06	1.3943E-03	4.8507E-03	1.0829E-02	1.8397E-02
50	6.3100E+01	6.9705E-06	1.1063E-03	3.6996E-03	8.2563E-03	1.3918E-02
51	1.0000E+02	6.3731E-06	8.2374E-04	2.7870E-03	6.0773E-03	1.0231E-02

Table 3.1: (continued).

N	Neutron Energy (MeV)	7 in.	8 in.	10 in.	12 in.	15 in.
1	1.0000E-08	1.3105E-02	8.3995E-03	3.2279E-03	1.2230E-03	2.6441E-04
2	1.5850E-08	1.4612E-02	9.3461E-03	3.6168E-03	1.3534E-03	2.8904E-04
3	2.5120E-08	1.6254E-02	1.0383E-02	3.9554E-03	1.4829E-03	3.2547E-04
4	3.9810E-08	1.8437E-02	1.1744E-02	4.5209E-03	1.7035E-03	3.6974E-04
5	6.3100E-08	2.1619E-02	1.3679E-02	5.4268E-03	2.0328E-03	4.3415E-04
6	1.0000E-07	2.6976E-02	1.7054E-02	6.7210E-03	2.4855E-03	5.3393E-04
7	1.5850E-07	3.3345E-02	2.0819E-02	8.1387E-03	3.0453E-03	6.5121E-04
8	2.5120E-07	3.7025E-02	2.3316E-02	9.1243E-03	3.3551E-03	7.3757E-04
9	3.9810E-07	4.3068E-02	2.7201E-02	1.0461E-02	3.9280E-03	8.3621E-04
10	6.3100E-07	4.7984E-02	3.0332E-02	1.1749E-02	4.3239E-03	9.3465E-04
11	1.0000E-06	5.2408E-02	3.3788E-02	1.2811E-02	4.7461E-03	1.0194E-03
12	1.5880E-06	5.7076E-02	3.6013E-02	1.3932E-02	5.1372E-03	1.0966E-03
13	2.5120E-06	6.1595E-02	3.8688E-02	1.5112E-02	5.5246E-03	1.2170E-03
14	3.9810E-06	6.5349E-02	4.1425E-02	1.5878E-02	6.3134E-03	1.2738E-03
15	6.3100E-06	6.9207E-02	4.4399E-02	1.7063E-02	6.3064E-03	1.3553E-03
16	1.0000E-05	7.3284E-02	4.6594E-02	1.8193E-02	6.6829E-03	1.4261E-03
17	1.5850E-05	7.6343E-02	4.8569E-02	1.8745E-02	6.9048E-03	1.4831E-03
18	2.5120E-05	7.9779E-02	5.0820E-02	1.9607E-02	7.2281E-03	1.5796E-03
19	3.9810E-05	8.2647E-02	5.2853E-02	1.9930E-02	7.6322E-03	1.6254E-03
20	6.3100E-05	8.6175E-02	5.5097E-02	2.0984E-02	8.0598E-03	1.6987E-03
21	1.0000E-04	8.9306E-02	5.6969E-02	2.2213E-02	8.1897E-03	1.7715E-03
22	1.5850E-04	9.1697E-02	5.9125E-02	2.3154E-02	8.5071E-03	1.8088E-03
23	2.5120E-04	9.4004E-02	6.1402E-02	2.3791E-02	8.7041E-03	1.9034E-03
24	3.9810E-04	9.7661E-02	6.3591E-02	2.4577E-02	9.0310E-03	1.9906E-03
25	6.3100E-04	1.0023E-01	6.5037E-02	2.5752E-02	9.4695E-03	2.0798E-03
26	1.0000E-03	1.0308E-01	6.6996E-02	2.6148E-02	9.6811E-03	2.0825E-03
27	1.5850E-03	1.0624E-01	6.9155E-02	2.7495E-02	1.0228E-02	2.1825E-03
28	2.5120E-03	1.0872E-01	7.2411E-02	2.8371E-02	1,0447E-02	2.2923E-03
29	3.9810E-03	1.1235E-01	7.3734E-02	2.9303E-02	1.1092E-02	2.3527E-03
30	6.3100E-03	1.1527E-01	7.5609E-02	3.0565E-02	1.1178E-02	2.4430E-03
31	1.0000E-02	1.1877E-01	7.8758E-02	3.2136E-02	1.1934E-02	2.5862E-03
32	1.5850E-02	1.2297E-01	8.2374E-02	3.2994E-02	1.2366E-02	2.6886E-03
33	2.5120E-02	1.2845E-01	8.7744E-02	3.4824E-02	1.3343E-02	2.8484E-03
34	3.9810E-02	1.3407E-01	9.3085E-02	3.8078E-02	1.4372E-02	3.0972E-03
35	6.3100E-02	1.4365E-01	9.9162E-02	4.1844E-02	1.6021E-02	3.4999E-03
36	1.0000E-01	1.5413E-01	1.1156E-01	4.7841E-02	1.8142E-02	3.9617E-03
37	1.5850E-01	1.7222E-01	1.2477E-01	5.6478E-02	2.1981E-02	4.9104E-03
38	2.5120E-01	1.9533E-01	1.4707E-01	7.0316E-02	2.8703E-02	6.5456E-03
39	3.9810E-01	2.1768E-01	1.7314E-01	9.1739E-02	3.9908E-02	9.9424E-03
40	6.3100E-01	2.3920E-01	2.0336E-01	1.2241E-01	5.9761E-02	1.7180E-02
41	1.0000E+00	2.5472E-01	2.3055E-01	1.5770E-01	8.9310E-02	3.1936E-02
42	1.5850E+00	2.4980E-01	2.4694E-01	1.9505E-01	1.2847E-01	5.8632E-02
43	2.5120E+00	2.2104E-01	2.3192E-01	2.0839E-01	1.5893E-01	9.0565E-02
44	3.9810E+00	1.7890E-01	1.9613E-01	1.9555E-01	1.6725E-01	1.1227E-01
45	6.3100E+00	1.3728E-01	1.6100E-01	1.7348E-01	1.6479E-01	1.2776E-01
46	1.0000E+01	9.0478E-02	1.1095E-01	1.3944E-01	1.4825E-01	1.4175E-01
47	1.5850E+01	6.4470E-02	8.0408E-02	1.0122E-01	1.1623E-01	1.1873E-01
48	2.5120E+01	4.2253E-02	5.4222E-02	7.1811E-02	8.2816E-02	9.0562E-02
49	3.9810E+01	2.7168E-02	3.5549E-02	5.0124E-02	6.1602E-02	7.2205E-02
50	6.3100E+01	2.0056E-02	2.6114E-02	3.7025E-02	4.4942E-02	5.4623E-02
51	1.0000E+02	1.4700E-02	1.9093E-02	2.7386E-02	3.3816E-02	4.0868E-02

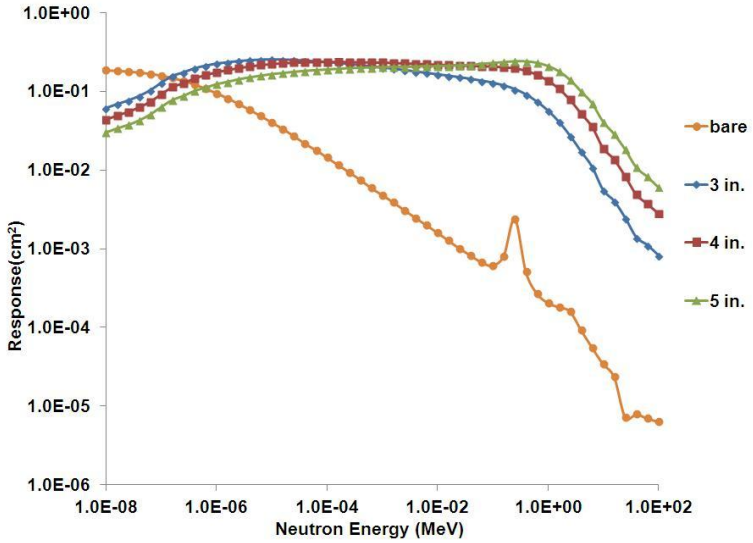

Figure 3.6: Response functions for bare detector, 3, 4 and 5 in. Bonner sphere.

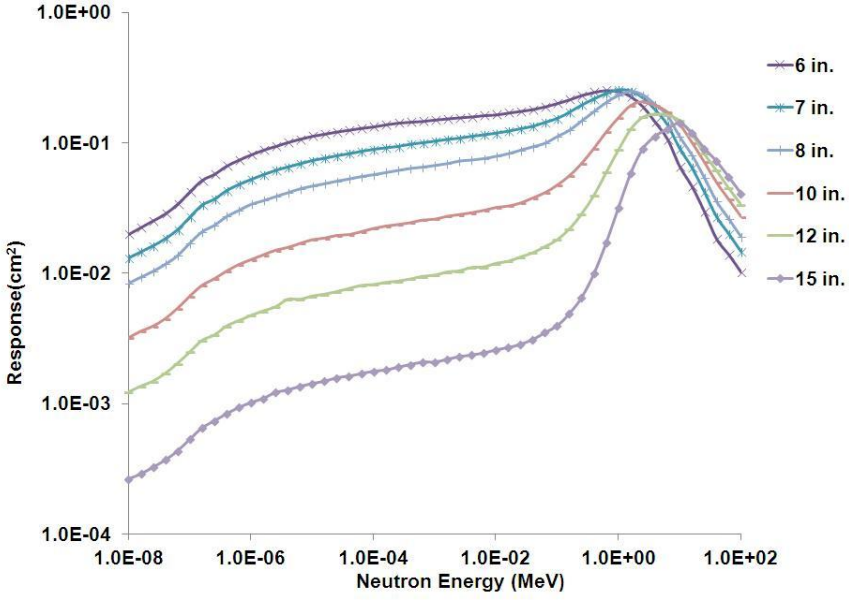

Figure 3.7: Response functions for 6, 7, 8, 10, 12 and 15 in. Bonner sphere.

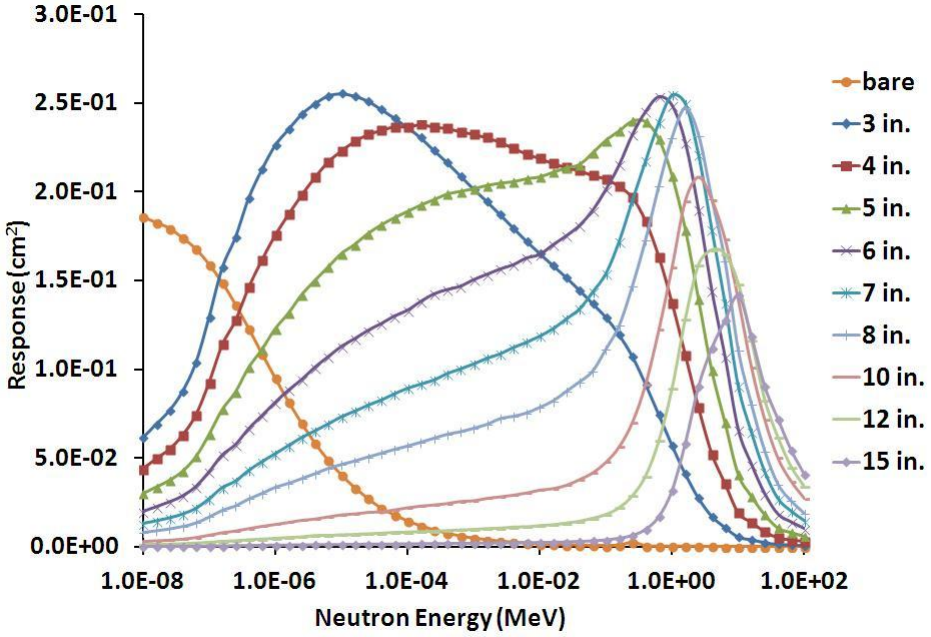

Figure 3.8: Response of matrix of the BSS-UNIPI set.

It can be clearly seen in Figs. 3.6, 3.7 and 3.8 that for each Bonner sphere the corresponding response function has a maximum at the energy of those neurons that are better thermalized by the Bonner sphere itself. Lower energy neutrons are more frequently captured by polyethylene, while higher energy neutrons are more likely to escape from the Bonner sphere assembly. Small Bonner spheres generate a more intense response for low energy incident neutrons, while larger Bonner spheres provide a more intense response to high energy neutrons. The response function peak energy, uniquely related to the Bonner sphere diameter, shifts to higher energies as the Bonner sphere diameter increases. The bare detector response has the shape of ^{6}Li cross section (Fig. 3.6).

The response functions of the Bonner spheres with diameters greater than 8 in. Bonner sphere presents similarities with an overlapping above 20 MeV (Figs. 3.7 and 3.8). Consequently, the energy resolution of the BSS is quite poor in this region. For this reason, it is possible to use only a small number of Bonner spheres in some cases, which are usually enough to provide all the achievable spectrometric information. Because sometimes the additional information brought by further Bonner spheres is very low. Five or six, well-chosen, polyethylene Bonner spheres are thus usually enough to determine a neutron spectrum from

thermal up to 20 MeV. When more Bonner spheres are used, the system answer can be “redundant” (Alevra, 2003).

The response matrix BSS-UNIPI will be used as input for the unfolding codes which are used for calculating neutron spectrum as it will be explained in the next chapters.

3.2.3 BSS-UNIPI response to ^{241}Am-Be neutron source

Other simulations were performed to investigate the variation of BSS response to an ^{241}Am-Be neutron source. The different irradiation geometries were considered and all the Bonner spheres were exposed to an ^{241}Am-Be (ISO 8529-1 standard) neutron source in the following conditions:

1. ^{241}Am-Be neutron source as a disc with radius (d/2) (diameter of Bonner sphere (d)) with the axis parallel and perpendicular to the detector axis.
2. ^{241}Am-Be neutron source as a point source.

All irradiations are considered in a vacuum. The fluence energy distribution of the ^{241}Am-Be (ISO-8529-1) neutron source is shown in Fig. 3.9. As can be seen, the most of emitted neutrons (~85%) have energies higher than 1 MeV. The mean fluence energy is around 4.4 MeV.

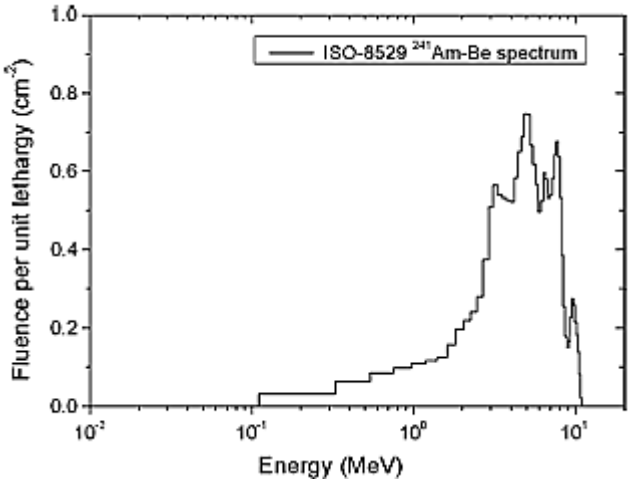

Figure 3.9: Neutron energy spectrum of ^{241}Am-Be (ISO-8529-1).

The number of histories was large enough (nps = 10^7) to have statistical uncertainties of the MCNPX results less than 3%. The ^{6}LiI(Eu) scintillation detector inside the center of 10 in.Bonner sphere with the disc-shaped of an ^{241}Am-Be

neutron source are shown in Fig. 3.10. Results are shown in Table 3.2 and Fig. 3.11.

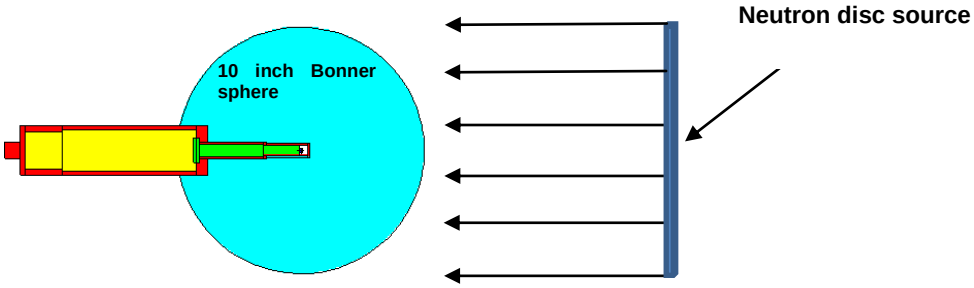

Figure 3.10: View of the Bonner sphere System: ^{6}LiI(Eu) scintillation detector inside the center of 10 in. Bonner sphere and an ^{241}Am-Be neutron source (disc-shaped) with the axis parallel to the detector axis.

Table 3.2: The calculated response of BSS-UNIPI to disc-shaped ^{241}Am-Be neutron source with the axis parallel to the detector axis.

Sphere diameter (inch)	Absolute response (counts per neutron)	Relative error (%)	Response (cm^2)	8in. Relative Response
3	6.33E-04	1.4	3 E-02	1.56E-01
4	8.78E-04	1.1	7 E-02	3.85E-01
5	9.27E-04	1.1	1.2 E-01	6.34E-01
6	8.28E-04	1.1	1.5 E-01	8.17E-01
7	7.09E-04	1.2	1.8 E-01	9.51E-01
8	5.71E-04	1.3	1.9 E-01	1.00E+00
10	3.48E-04	1.6	1.8 E-01	9.54E-01
12	2.01E-04	2.1	1.5 E-01	7.94E-01
15	9.39E-05	3.2	1.1 E-01	5.79E-01

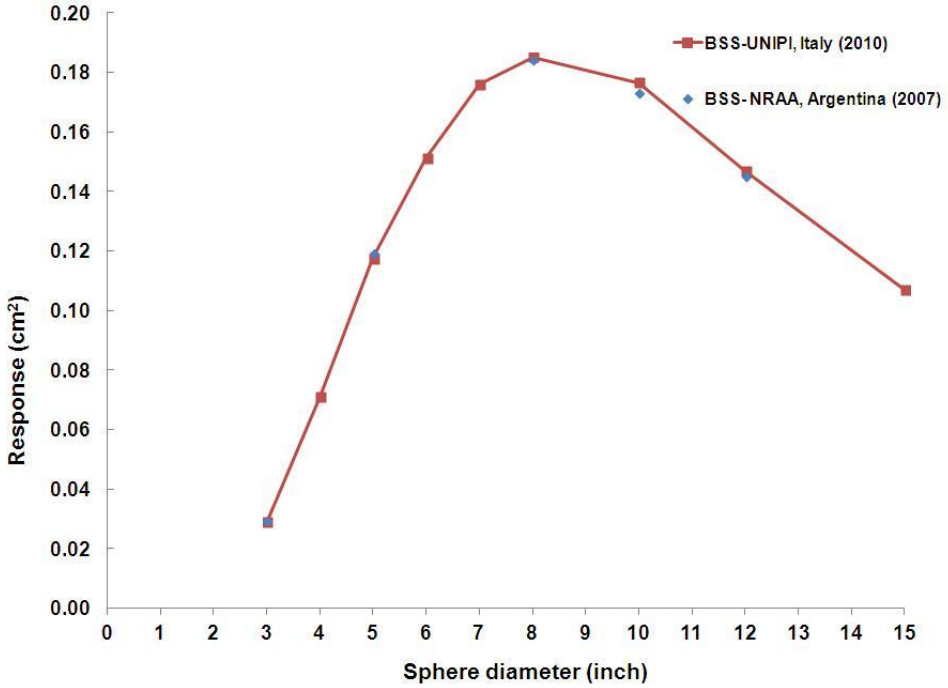

Figure 3.11: Comparison of calculating BSS-UNIPI response with BSS-NRAA.

Due to the typical shape of the Bonner sphere, the responses directly depend on neutron energy source. By considering combining effects resulting, firstly, from the increasing number of neutron collisions with the moderator as the moderator thickness increases and, secondly, the process of absorption the moderator before the neutron has a chance to reach the detector. There is an optimal value of moderator thickness for neutrons of fixed energy. For ^{241}Am–Be energy spectrum which has a mean energy value about 4.4 MeV, the maximum response is achieved for 8 in. Bonner sphere (Fig. 3.11). For this reason the detector response was normalized to 8 in. Bonner sphere response (Table 3.2).

Our results have been compared to BSS-NRAA (Cruzate, 2007) which consist of seven Bonner spheres (2, 3, 5, 8, 10, 12, 12+lead in.) with high-density polyethylene (0.95 g cm^{-3}), and a cylindrical 4 mm (diameter) by 4 mm (height) ^{6}LiI(Eu) active scintillator (Fig. 3.11). The results were in a good agreement with the calculated BSS-NRAA response to ^{241}Am–Be with the same geometry irradiation.
In order to investigate the angular response of BSS-UNIPI, it was exposed to the same ^{241}Am–Be source but with the source axis perpendicular to the detector axis (Fig. 3.12). The results of the calculated angular responses (0°and 90°) of BSS-UNIPI set to ^{241}Am–Be is shown in Fig. 3.13.

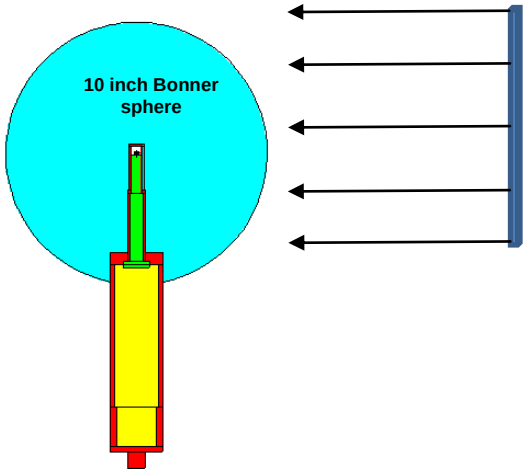

Figure 3.12: BSS-UNIPI (10 in. Bonner sphere) exposed to disc-shaped ^{241}Am-Be neutron source with the axis perpendicular to the detector axis.

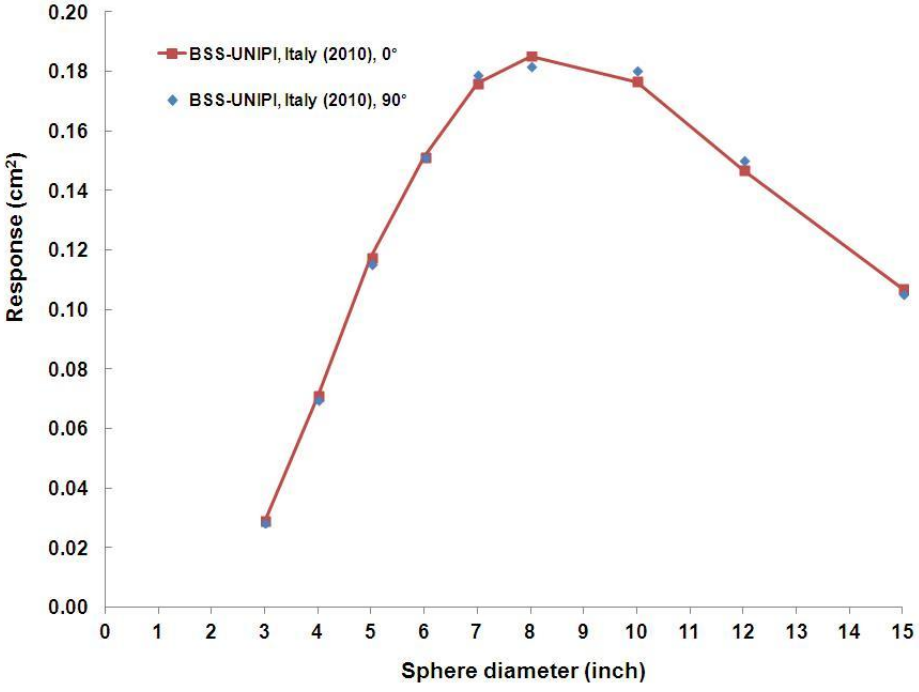

Figure 3.13: The angular responses (0° and 90°) of BSS-UNIPI set to ^{241}Am–Be.

As can be seen in Fig. 3.13, the response of BSS-UNIPI is particularly independent of the directions (0° and 90°) of the beam to the detector: the difference achieved does not exceed 2%. This result confirmed the isotropic response of BSS. It is also shown that the neutron thermalization inside the Bonner sphere eliminates the anisotropies given by the two different considered incidence neutron direction. To validate the calculated responses through comparison with measured responses in the broad neutron field of an ^{241}Am-Be will be shown in chapter 5.

Finally, the BSS-UNIPI set was simulated by considering ^{241}Am-Be (ISO 8529-1 standard) neutron source as point source at 100 cm source-to-detector. 8in. relative the calculated response BSS-UNIPI set to ^{241}Am-Be as point source compared with the same calculation and irradiation geometry by Mares (Fig. 3.14). It can be seen in Fig. 3.14 the result is in good agreement with literature results (Mares, 1994; Gualdrini, 2008).

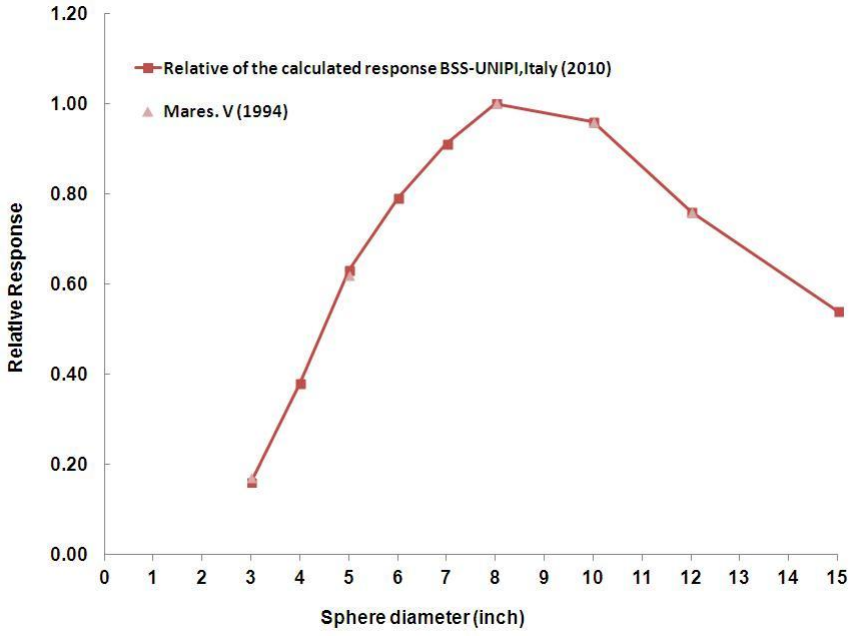

Figure 3.14: Comparison of 8in. relative the calculated response BSS-UNIPI set to ^{241}Am-Be as point source compared with the same calculation by Mares (1994).

3.3 Investigation of the activation-based BSS-UNIPI set (3 and 10 in.) response to monoenergetic neutrons

As mentioned before, active detectors have some limitations such as pulse pile-up, dead-time effect and radiofrequency interferences when applied at pulsed, intense and mixed fields (neutron-gamma). Most of these fields can be encountered in Linacs, cyclotrons and synchrotrons. BSS based on passive detectors can be used in these fields, especially for the assessment of neutron spectra in gamma field such as the Linac radiotherapy application. Some authors (Thomas, 2002; Fernandez, 2007, Esposito, 2008; Amgarou, 2009 and 2011) reported the use of BSS based on gold foils (Au -BSS) for measuring neutron leakage around LINACs.

The aim of this research was a priminary Monte Carlo investigation of the response function of the BSS-UNIPI set (3 and 10 in.) based on two activation foils (indium and gold) to 4 broad neutron energy bins (10^{-5}, 10^{-3}, 10^{-1} and 1 MeV). These activation foils are particularly suited for this application because they are insensitive to high-energy gamma ray. The considered activation foils have a disc shape and their characterization are in the following:

1. Indium: natural composition (^{115}In 95.7% and ^{113} In 4.3%), 15 mm diameter, 0.1 mm thick and 7.31 g cm^{-3} density;
2. Gold: ^{197}Au, 15 mm diameter, 0.1 mm thick and 19.3 g cm^{-3} density.

Every foils are placed horizontally (i.e., with the axis parallel to the detector axis) in the center of each Bonner sphere (3 and 10 in.) with a polyethylene support. Each Bonner sphere has its own inch aluminium support and was irradiated by a disc source whose axis is parallel to the detector axis with the same diameter of the Bonner sphere (Fig. 3.15). The input MCNPX file can be found in appendix A.

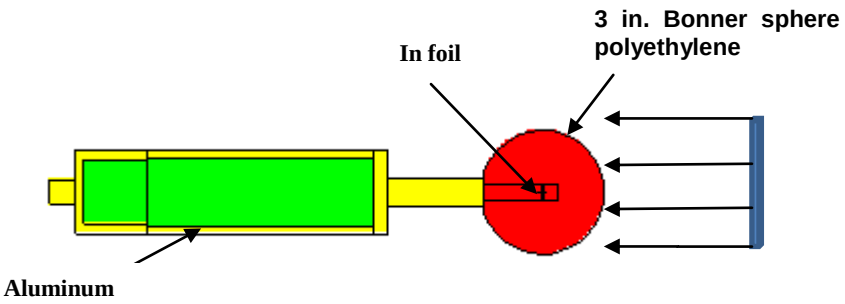

Figure 3.15: MCNP model of BSS (3 in. Bonner sphere) with an In foil as a passive detector.

The response, *R(E)*, of each detector-sphere with respect to the considered neutron incidence energy, *E*, was calculated as the number of the neutron capture reactions, as follows:

1. $^{115}In(n,\gamma)^{116m}In$ (σ_t = 161 barn, $T_{1/2}$ = 54.41 min);
2. $^{197}Au(n,\gamma)^{198}Au$ (σ_t = 98.8 barn, $T_{1/2}$ = 2.7 d)

For every foil, *R (E)* was normalized to the foil mass (i.e., $cm^2\ g^{-1}$) using the F4 tally and the associated FM card of the MCNPX code. The results, shown in Figs. 3.16 and 3.17, were compared with BSS based on gold (Au-BSS) and dysprosium (Dy-BSS) literature results (Bedogni, 2008; 2010).

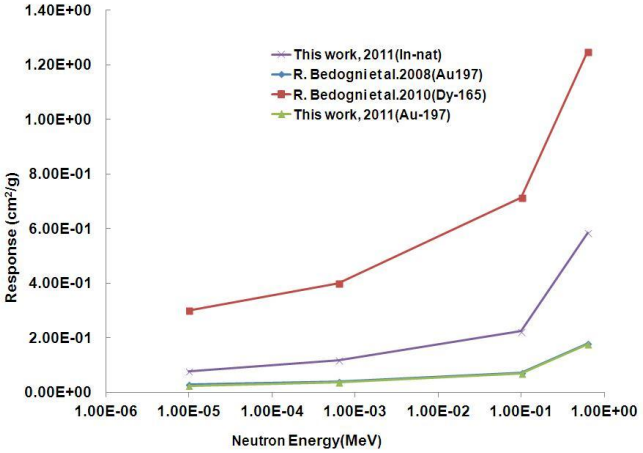

Figure 3.16: Response of Dy, Au and In foils in the 10 in. Bonner sphere with monoenergetic neutrons, in comparison to literature (Bedogni, 2008; 2010).

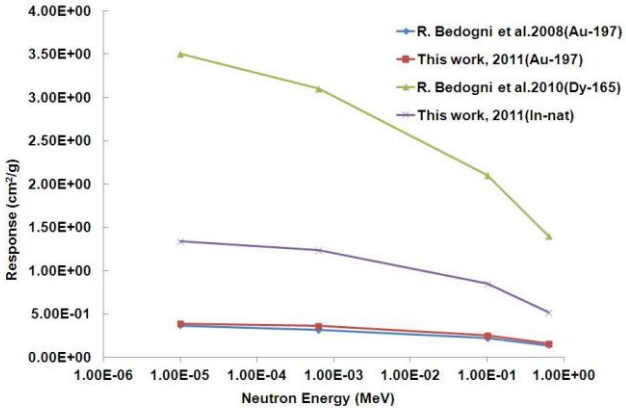

Figure 3.17: Response of Dy, Au and In foils in the 3 in. Bonner sphere with monoenergetic neutrons, in comparison to literature (Bedogni, 2008; 2010).

According to Figs. 3.16 and 3.17, it can be seen that the calculated response of Au has a good agreement with literature data (Bedogni, 2008). The response of Dy foils is higher than In and Au foils, due to higher neutron cross section (σ_t = 2700 barn) (Figure 3.18).

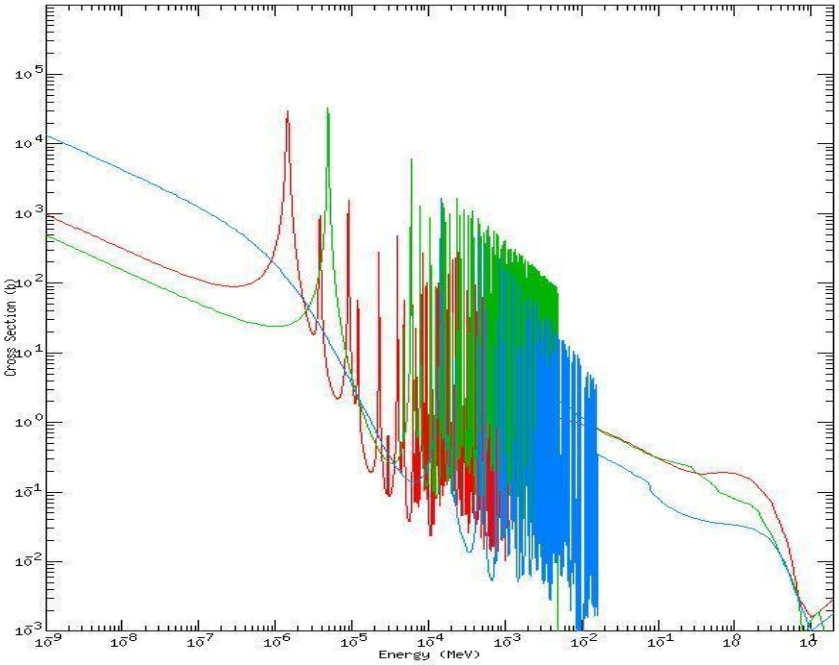

Figure 3.18: Cross sections of the interaction processes of neutrons with ^{115}In nuclei (red), ^{197}Au (green) and ^{164}Dy (blue) from ENDFB 6.1 data library.

The cross sections of the interaction processes of neutrons with ^{115}In nuclei (red), ^{197}Au (green) and ^{164}Dy (blue) are shown (data are from ENDFB 6.1 data library). As can be seen, although thermal cross-sections of Au and In are lower than Dy for thermal neutrons, they have a very high cross section in the epidermal region.

In addition, it should be kept in mind that the different half-lives of ^{116m}In (54.41 min), ^{198}Au (2.696 d) and ^{165}Dy (2.334 h) play a crucial role in the experimental procedures.

The present study shows that the characteristics of In-BSS and Au-BSS are suited for operational measurements around neutron producing facilities, where short irradiations and short measurement times are desirable. They can also be used with or without cadmium cover to evaluate the thermal and epithermal neutron. But Au is sensitive to the gamma with energy above 10 MeV, due to the reaction ^{197}Au(γ,n)^{196}Au ($T_{1/2}$=6.18d), the use of In-BSS is recommended for this situation.

The conclusion of these simulations indicate that the In-BSS can be a valied determinate to the unwanted neutron production (threshold for (γ, n) reactions in high-*Z* material in 7 MeV) of every high-energy LINACs used in radiotherapy medical treatment.

References

Amgarou, K., et al. (2009). Neutron spectrometry with a passive Bonner sphere system around a medical LINAC and evaluation of the associated unfolding uncertainties. *IEEE Transactions on nuclear science*, 56, 5, pp. 2885-2895.

Amgarou, K., et al. (2011). Experimental characterization of the neutron spectra generated by a high-energy clinical LINAC. *Nuclear Instruments and Methods in Physics Research A,* 629, pp. 329-336.

Agosteo, S., et al. (2004). The response of a Bonner sphere spectrometer to charged hadrons. *Radiation Protection Dosimetry*, 110 (1-4), pp. 161-168.

Agostinelli, S., et al. (2003). Geant4 - a simulation toolkit. *Nuclear Instruments and Methods in Physics Research A*, 506, pp. 250-303.

Alevra, A.V. and Thomas, D. J. (2003). Neutron spectrometry in mixed fields: multisphere spectrometers. *Radiation Protection Dosimetry*, 107 (1-3), pp. 37-72.

Battistoni, G., et al. (2007). The FLUKA code: Description and benchmarking. *Proceedings of the Hadronic Shower Simulation Workshop 2006*, Fermilab 6–8 September 2006, AIP Conference Proceeding 896, pp. 31-49.

Bedogni, R., et al. (2008). Determination and validation of a response matrix for a passive Bonner sphere spectrometer based on gold foils. *Radiation Measurements,* 43, pp. 1104-1107.

Bedogni, R., et al. (2010). Design and experimental validation of a Bonner sphere Spectrometer based on Dysprosium activation foils. *Radiation Measurements,* 45, pp. 1201-1204.

Boone, J.M., et al. (1988). Monte Carlo simulation of the scattered radiation distribution in diagnostic radiology. *Medical Physics,* 15, pp. 713-720.

Brown, F.B., et al. (2011). Recent Advances and Future Prospects for Monte Carlo. *Progress in nuclear science and technology*, 2, pp. 1-4.

Cruzate, J.A., et al. (2007). Bonner sphere Spectrometer. *Proceedings of the Workshop on uncertainty assessment in computational dosimetry: a comparison of approaches*, Bologna, Italia, 8-10, October.

Esposito, A., et al. (2008). Determination of the neutron spectra around an 18MVmedical LINAC with a passive Bonner sphere spectrometer based on gold foils and TLD pairs. *Radiation Measurements*, 43, pp. 1038-1043.

Fernández, F., et al. (2007). Neutron measurements in a Varian 2100 LINAC facility using a Bonner sphere system based on passive gold activation detectors. *Radiation Protection Dosimetry*, 126 (1-4), pp. 361-365.

Ferrari, A., et al. (2005). FLUKA: a multi-particle transport Code. Stanford Linear Accelerator Center, Stanford University, Stanford, *Report No. SLAC-R-773*.

International Organization for Standardization (2001). Reference neutron radiations, part 1: characteristics and methods of production. ISO 8529-1, Geneva, Switzerland, 2001.

Garny, S., et al. (2009). Response functions of a Bonner sphere spectrometer calculated with GEANT4. *Nuclear Instruments and Methods in Physics Research A,* 604, pp*.* 612-617.

Gregg, C., et al. (2000). MCNP software quality then and now. *Proceedings of 10th International conference software quality*, 16-18, October, New Orleans, USA, LA-UR-00-2532.

Gualdrini, G., et al. (2008). Bonner sphere Spectrometry: main achievements from the "CONRAD Computational Dosimetry Study. *Proceedings of the 12th Congress of the International Radiation Protection Association*, Buenos Aires, Argentina, October 19-24.

Mares, V. and Schraube, H. (1994). Evaluation of the response matrix of a Bonner sphere spectrometer with Lil detector from thermal energy to 100 MeV. *Nuclear Instrumental Method A*, 337, pp. 461-473.

Mirzajani, N., et al. (2010). Progress towards Bonner sphere spectrometry of the INFN-LNL SPES-BNCT. *INFN- LNL Annual Report.* pp. 135-136.

Pelowitz, D.B. (2008). MCNPX User's Manual Version 2.6.0. LA-CP-07-1473.

Ranft, J. (1972). Estimation of Radiation Problems around High-Energy Accelerators Using Calculations of the Hadronic Cascade in Matter*. Particle Accelerators*, 3, pp. 129-161.

Ranft, J. (1964). Monte Carlo calculation of the nucleon-meson cascade in shielding energies between 10 and 1000 GeV, *CERN Report.* pp. 64-47.

Sanna, R.S. (1973). Thirty One Group Response Matrices for the Multisphere Neutron Spectrometer Over the Energy Range Thermal to 400 MeV, *U. S. Atomic Energy Commission*, Report HASL-267.

Tanner, R.J., et al. (2004). Intercomparison of the usage of computational codes in radiation dosimetry. *Radiation Protection Dosimetry,* 1, 110 (1-4), pp. 769-780.

Thomas, D.J., et al. (1992). Use of the program ANISIN to calculate response functions for a Bonner sphere set a ^{3}He detector. NPL Report RSA(EXT) 31, National Physical Laboratory, Teddington, UK.

Thomas, D.J. (2002). Characterization of a gold foil based Bonner sphere set and measurements of neutron spectra at a hospital LINAC. *Nuclear Instruments and Methods in Physics Research A,* 476 (1–2), pp. 31-35.

Vega-Carrillo, H.R., et al. (2008). Calculation of Response matrix of a BSS with ^{6}LiI scintillator. *Revista Mexicana de Física S*, pp. 54-57.

Williamson, J.F., et al. (2005). Quantitative dosimetry methods for brachytherapy. *Brachytherapy Physics,* pp. 233-294.

4. Unfolding procedures

4.1 Overview

The unfolding process is the most delicate part of the BSS-based spectrometry, as mentioned before in Chapter 2. The function $\Phi(E)$ which is determined by the unfolding techniques is the spectral particle fluence, often simply referred to as a spectrum. The unfolding techniques are methods for solving undetermined equation systems, as the following:

$$A_i = \sum_{j=1}^{N} R_{ij}(E)\Phi(E_j) \qquad (i = 1,\ldots, M) \tag{4.1}$$

The subscript i is related to the channel number, *i.e.* to the individual Bonner sphere of the BSS set. The A_i indicated the data obtained from measurements, *e.g.* using the Bonner spheres. The $R_{ij}(E)$ is the response matrix of the BSS, while $\Phi(E)=(\Phi_1,....,\Phi_\nu,.....,\Phi_N)$ is the group fluence vector and $\Phi_\nu=\Phi_\nu(E)$. The N components Φ_ν can be considered as average fluence values in the intervals between the energies E_ν and $E_{\nu+1}$. Eq. (4.1) has no unique solution for $N>M$. An unique exact solution of the discrete spectrum $\Phi_\nu(E)$ exists only in the case of equal dimensions $N=M$ and with a non-singular response matrix R. However, in few-channel measurements, as in Bonner sphere spectrometry, it would be desired to have $N>M$. In this case, Eq. (4.1) becomes strongly underdetermined with an infinite manifold of possible solutions Φ_ν. So, a more sophisticated unfolding procedure is required. There are some possibilities to overcome these difficulties. First, all the information available on the spectrum must be used within the unfolding algorithm. Sometimes a precalculated fluence vector Φ_0 is known; other times a smoothing condition for the fluence can be formulated.

In general, there are two ways of implementing the *a priori* information about the measured neutron spectrum for almost all the unfolding codes:

1. By taking an initial guess or default spectrum, with non-negative value of each of $\Phi_\nu(E)$ for the chosen neutron energy bins E_ν - $E_{\nu+1}$, to start the iteration process;
2. By representing the unknown spectrum with a parameterized function based on physical meaning.

For the first case, the initial guess spectrum can be obtained from Monte Carlo simulations of the given situation or from previous measurements performed in limited energy ranges with complementary neutron spectrometry systems.

In the second case, the chosen parameters must not exceed the number of available measurements, A_i, and should be enough to describe correctly the main features of the neutron spectrum.

To date, the problem of the neutron spectrum unfolding from the BSS measurements has been extensively studied, giving rise to a number of independent methods, based on least squares, Monte Carlo, maximum entropy and Bayesian approach procedures, as well as on genetic and neutral network algorithms. A number of unfolding codes have been developed such as Gravel (Matzke, 1994), Unfana (Weise, 1995), MAXED (Reginatto, 2002), FRUIT (Bedogni, 2007), Ann (Vega-Carrillo, 2009) and Msandb (Simmer, 2010). Here only the unfolding codes MAXED and FRUIT, which were used in this work, are briefly described.

4.2 Neutron spectrum unfolding code: MAXED

MAXED is the main unfolding code used for this work. MAXED is an unfolding code written in FORTRAN based on "maximum entropy deconvolution" method. It was developed at EML (Environmental Measurements Laboratory, DoE, USA) for the unfolding of Bonner sphere data, but later modified to accommodate proton recoil measurements (Reginatto, 2002). Advantages of MAXED include:

1. It is the only mathematically consistent method of incorporating *a priori* information into the solution;
2. It makes use of the estimated variances for each detector's count rate in the unfolding process;
3. The algorithm leads to a solution spectrum that is always a non-negative function;
4. The solution spectrum can be written in closed form (Reginatto, 2002).

Disadvantages of MAXED, the user interface is poor. When neutron spectrometry measurements are performed, some information is known about both the neutron source and the physics that governs the neutron interactions. This *a priori* information, usually derived from calculations or independent measurements, needs to be incorporated into the deconvolution process in a mathematically consistent way. In the language of MAXED, the initial estimate of the spectrum that incorporates all the *a priori* information is called the "default spectrum". The challenge of neutron spectrum unfolding is to take the default spectrum and to modify it as minimally as possible so that it becomes consistent with the measurement data (Reginatto, 2002). This minimally modified spectrum that is consistent with the measurements is called the "solution spectrum". MAXED uses the maximum entropy principle to find a spectrum which fits the data within experimental errors in a mathematically rigorous, consistent and unbiased way.
The set of possible solution spectra are defined by two constraints. First, the sum of the solution spectrum f_n elements each one multiplied by the response matrix elements R_{mn} yields the measurement M_n within some discrepancy ε_m:

$$M_m + \varepsilon_m = \sum_{n=1}^{N} R_{mn} f_n \tag{4.2}$$

The second constraint is that the discrepancies ε_m are bound by some value Ω:

$$\sum_{m=1}^{M} \frac{\varepsilon_m^2}{\sigma_m^2} = \Omega \tag{4.3}$$

The value Ω is chosen by the user in MAXED. In Eq. (4.3), the discrepancies are squared to be positive and normalized to the standard uncertainty of each measurement σ_m. Setting Ω to the number of detectors *M* essentially requires that the average uncertainty normalized discrepancy is:

$$\frac{1}{M} \sum_{m=1}^{M} \frac{\varepsilon_m^2}{\sigma_m^2} = 1 \tag{4.4}$$

Eq. (4.4) states that the discordance between the calculated flux spectrum and the measurements should be the same as the measurement uncertainty on average. It's reasonable that the solution spectrum cannot be more precise than the measurements that were used to determine it.

The solution spectrum satisfies Eqs. (4.3) and (4.4). The maximum entropy principle states that from all admissible spectra satisfying the set of constraints, *i.e.* the measurements, one should choose the one that maximizes the entropy *S* of the distribution:

$$S = -\sum_{n}^{M} \left(f_i \ln \frac{f_i}{f_i^{DEF}} + f_i^{DEF} - f_i \right) \tag{4.5}$$

where f_i and f_i^{DEF} are the discretized output and default spectrum. Any *a priori* information about the neutron spectrum is contained in the default spectrum.

The information from the measurements is used to modify the default spectrum in order to produce an output spectrum that fits the data within the experimental uncertainties. If the data contains no information about a portion of the spectrum, the unfolded output for that portion of the spectrum will be the same as the default spectrum.

The program does not apply any smoothing procedure to the unfolded spectrum, and none is needed to get a smooth spectrum if the estimates of the experimental uncertainties are realistic. Since no smoothing is applied, MAXED preserves any structure in the default spectrum which is finer than the resolution of the spectrometer. MAXED also uses a process called "simulating annealing" to assure that it finds the globally optimal solution.

4.3 Neutron spectrum unfolding code: FRUIT

The FRUIT code was applied in this work for unfolding purposes. The code FRUIT (FRascati Unfolding Interactive Tool) was written using the LabView software and developed in the framework of collaboration between INFN-LNF and UAB[12]. The main characteristics of FRUIT include:

1. FRUIT models a generic neutron spectrum as the superposition of elementary spectra described by a set of positive parameters, having physical meaning. This approach to Bonner sphere spectrometry was previously used in the MITOM code (Tomás, 2004);
2. The limited amount of *a priori* information needed about the neutron spectrum to obtain meaningful solutions. Besides the Bonner sphere response functions, the counts and related uncertainties, the user is only asked to introduce qualitative information on the type of ‘‘radiation environment’’, on the basis of a check-box input section. It is worth underlying that no ‘‘default spectrum’’ is asked to the user. The code generates itself a default spectrum, needed to start the iterative procedure, on the basis of the radiation environment selected by the user. The main achievement is that, taking advantage on a flexible convergence algorithm (based on a variable tolerance principle), the results do not depend on the numerical values of this spectrum. This allows overcoming a drawback of many existing codes (Thomas, 2004; Reginatto, 2002), i.e. the need to provide realistic *a priori* information such as a detailed ‘‘default spectrum’’,;
3. The iterative convergence procedure varies the parameters describing the spectrum on the basis of a ‘‘variable tolerance’’ which may be changed by the user according to the progress of the run. The progressive reduction of this tolerance during the run allows to rapidly restricting the whole ‘‘parameter space’’ to a meaningful subspace containing the final solution;
4. User-friendliness and visual operation: the code continuously displays all quantities involved in the unfolding process and their variation (the plot of the spectrum, the measured and unfolded Bonner sphere counts, the parameters, the tolerances and the dosimetric integral quantities, etc.).

Relevant achievements of the FRUIT code are:

1. A high level of interactivity, allowing the user to follow and modify the convergence process;
2. The possibility to modify the convergence tolerances during the run, allowing a rapid achievement of meaningful solutions;
3. The reduced dependence of the results of the initial hypothesis.

As with all unfolding codes, when using FRUIT one must provide the response matrix of the BSS system. According to the specified radiation environment, the

[12] Universitat Autónoma de Barcelona (Spain)

code selects the appropriate physical model to unfold the experimental data: fission, evaporation, evaporation and high-energy components, Gaussian. A neutron spectrum in FRUIT is described as the linear superposition of up to four components as follows:

$$\varphi(E) = P_{th}\varphi_{th}(E) + P_e\varphi_e(E) + P_f\varphi_f(E) + P_{hi}\varphi_{hi}(E) \tag{4.6}$$

where $\varphi_{th}(E)$ is the thermal Maxwellian component, $\varphi_e(E)$ the epithermal one, $\varphi_f(E)$ the fast one and $\varphi_{hi}(E)$ the high energy component. P_{th}, P_e, P_f and P_{hi} represent the fraction of thermal, epithermal, fast and high-energy neutrons, respectively. As the sum of the four fractions must be equal to one as normalization constraint, only three of them are independent.

The iterative process starts when the code generates automatically an initial parameter array depending on the radiation environment chosen. From this array, the code derives a first trial until spectrum. Then, the measured count rates are compared with those calculated by folding the trial spectrum with the BSS response matrix to obtain a set of convergence indexes. In each iteration, the code generates a new spectrum by randomly changing one of the parameters. If the new parameter set fulfills the acceptance criteria defined in FRUIT, the new spectrum is accepted as a new solution. The user can, at any moment, interrupt the process and re-start it using this accepted solution, increasing or decreasing the tolerance. This allows to rapidly restricting the whole parameter space to a meaningful subspace containing the final solution. After few interventions, the solution is found and the user can stop the code and get the results. The code provides three output files, containing the final spectrum parameters, the numerical unit spectrum and the summary of all results (Bedogni, 2007). The latter contains:

1. The final value of the deviation between measured and calculated normalized readings;
2. The mean fluence to ambient dose equivalent conversion coefficient $\bar{h}^*_\varphi$ and its uncertainty, calculated using the following expression:

$$\bar{h}^*_\varphi = \frac{\int_0^{E_{\max}} \phi(E) h^*_\varphi(E) dE}{\int_0^{E_{\max}} \phi(E) dE} \tag{4.7}$$

3. The fluence or the equivalent averaged mean energy, $\bar{E}_\varphi$ or $\bar{E}_H$, respectively, characterizing the hardness of the measured neutron spectrum. These quantities are defined as:

$$\bar{E}_{\varphi} = \frac{\int_{0}^{E_{\max}} \phi(E) E dE}{\int_{0}^{E_{\max}} \phi(E) dE} \tag{4.8}$$

$$\bar{E}_{H} = \frac{\int_{0}^{E_{\max}} h_{\varphi}^{*}(E) E dE}{\int_{0}^{E_{\max}} h_{\varphi}^{*}(E) dE} \tag{4.9}$$

In this work, the FRUIT unfolding code, version 5, was selected as a proper tool to obtain the neutron energy spectrum of an ^{241}Am-Be from the experimental data. Then MAXED deconvolution code and FRUIT unfolding, version 5, was applied for the determination of the angular neutron energy spectrum of an accelerator-based BNCT.

References

Bedogni, R., et al. (2007). FRUIT: an operational tool for multisphere neutron spectrometry in workplaces. *Nuclear Instruments and Methods in Physics Research A*, 580, pp.1301-1309.

Matzke, M. (1994). Unfolding of pulse-height spectra: the HEPRO program package, *Report PTB-N-24,* Physikalisch Technische Bundesanstalt, Braunschweig, Germany.

Reginatto, M., et al. (2002). Spectrum unfolding, sensitivity analysis and propagation of uncertainties with the maximum entropy deconvolution code MAXED. *Nuclear Instruments and Methods in Physics Research A*, 476, pp. 242-246.

Simmer, G., et al. (2010). Iterative unfolding for Bonner sphere spectrometers using the MSANDB code – Sensitivity analysis and dose calculation. *Radiation Measurements,* pp. 451-459.

Thomas, D.J., et al. (2004). Neutron spectrometry for radiation protection. *Radiation Protection Dosimetry,* 110 (1–4), pp. 141-149.

Tomás, M., et al. (2004). MITOM: a new unfolding code based on a spectra model method applied to neutron spectrometry. *Radiation Protection Dosimetry,* 110 (1–4), pp. 545-548.

Vega-Carrillo, H.R., et al. (2009). Spectra and dose with ANN of ^{252}Cf, ^{241}Am–Be, and ^{239}Pu–Be. *Journal of Radioanalytical and Nuclear Chemistry*, 281, pp. 615-618.

Weise, K. (1995). Mathematical foundation of an analytical approach to Bayesian-Statistical Monte Carlo spectrum unfolding, *Report PTB-N-24, Physikalisch-Technische Bundesanstalt*, Braunschweig, Germany.

5. Experimental characterization of BSS- UNIPI

5.1 General characteristics of BSS-UNIPI

The Bonner sphere set was designed at DICI[13] of Pisa University and manufactured by the Legnaro National Laboratories (LNL) of the INFN. The spectrometer consists of a set of 9 polyethylene Bonner spheres with diameters of 3, 4, 5, 6, 7, 8, 10, 12 and 15 in. (Fig. 5.1). The mean polyethylene density was measured to be 0.939 g·cm^{-3} (relative error: 0.01%).

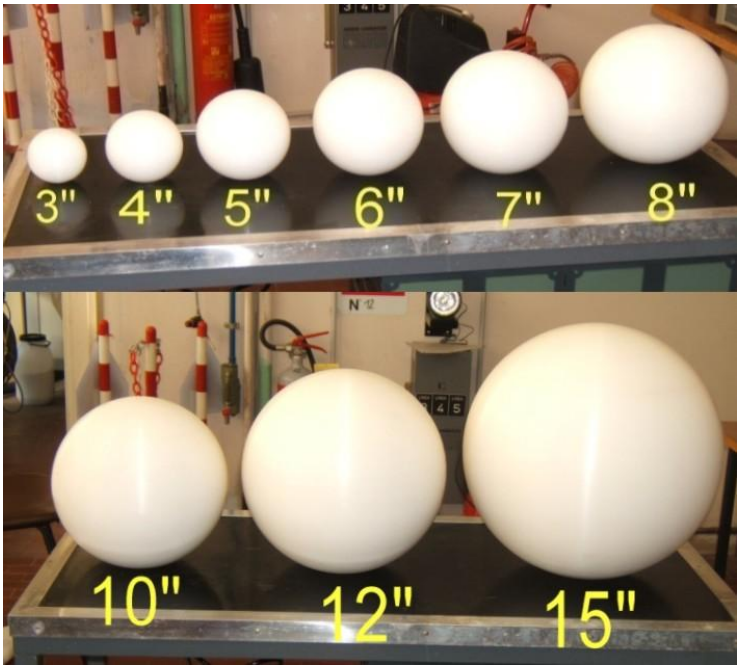

Figure 5.1: The Bonner sphere set of UNIPI (3, 4, 5, 6, 7, 8, 10, 12 and 15 in. diameters).

The neutron detector consists of a ^{6}LiI(Eu) (96% ^{6}Li enrichment) cylindrical 4 mm (diameter) x 4 mm (height) scintillator, connected through a Plexiglas light pipe to a magnetically shielded photomultiplier. A cross sectional view of the detector and the related data logger are shown in Figs. 5.2a and b.

[13] Department of Civil and Industrial Engineering

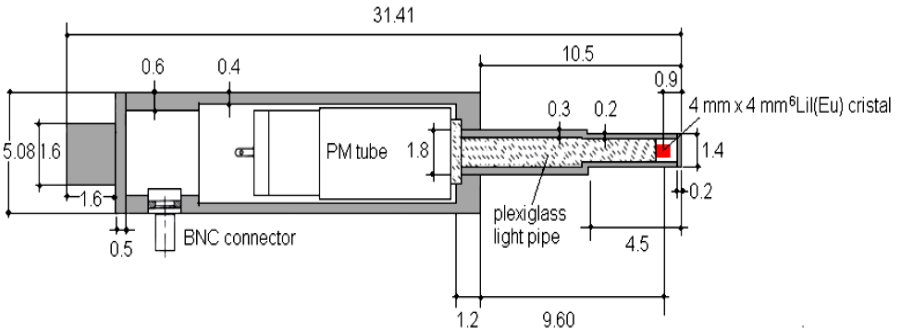

(a)

(b)

Figure 5.2: (a) Cross sectional view of the detector; (b) the detector and the related data logger.

Thermal neutrons are detected through the $^{6}Li(n,\alpha)^{3}H$ reaction (Q value = 4.78 MeV). The electric pulse is collected by a single-channel analyzer system (Ludlum scaler Ratemeter, mod. 2200) after a pulse height analysis; and it is counted by the same scaler which works also as a data logger. Then the counting rate is displayed on the unit of this system (Figs. 5.3 a and b). The neutron reaction rate is proportional to the number of pulses in the scintillator, which are registered by the scaler separating the gamma background from the neutron induced events. The scaler operating parameters are determined referring to the suggestion of the instrument manufacturer.

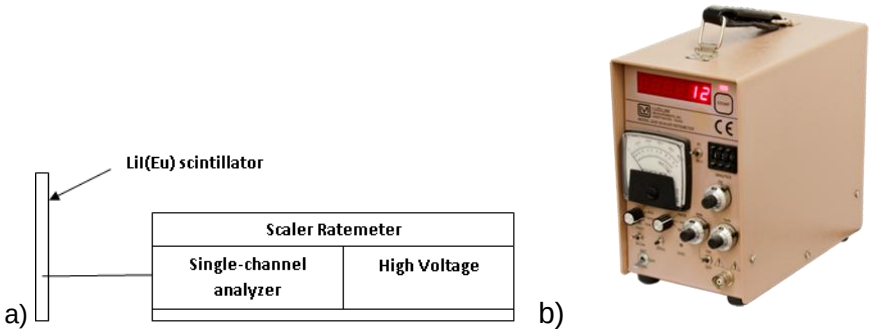

Figure 5.3: a) Schematic diagram of the acquisition chain for the ^{6}LiI(Eu) scintillator; b) Ludlum scaler Ratemeter, mod. 2200.

According the calibration certificate of the scaler manufacturer, the operating parameters have been optimized and measured by a ^{137}Cs gamma source and an ^{241}Am-Be neutron source. Using a ^{137}Cs gamma source (0.19 MBq), the scaler gain was adjusted to have 10 mV the high pulse using an oscilloscope while the photomultiplier operation voltage was set to 500 V. In order to perform measurements at the required height of the Bonner spheres from the ground, a dedicated inch holder was designed and built at the DICI, as shown in Fig. 5.4.

Figure 5.4: View of the inch holder for the Bonner spheres manufactured at DICI.

5.2 Discrimination of background and gamma

The ^{6}LiI(Eu) detector, due to its high density and atomic number of iodine, is sensitive to photons. If the gamma radiation field has high intensity and energy, it is possible to have pulses in the 4.78 MeV region, where the neutron peak arises. For this reason, the external gamma field or the 2.2 MeV gamma originating from neutron capture in polyethylene have to be considered. In order to have a negligible photon sensitivity of the detector (0-2 cpm) for background radiation, its response must be checked by introducing a discrimination threshold as the suggestion of the instrument manual. A specific procedure allows the experimental verification of the photon discrimination threshold in a gamma radiation field. The manual indicates a counting rate of 0-10 cpm in a 1 R/h gamma field by using a ^{137}Cs (0.19 MBq). As a result of measurements in gamma field, the photon discrimination threshold was set to be 1.44 V with high voltage 500 V.

5.3 Calibration in neutron radiation field

According to manufacturer's specifications, the BSS-UNIPI was calibrated by exposing 10 in. Bonner sphere to an ^{241}Am-Be neutron source at 100 cm source-to–detector distance (SDD): the manual recommend that sensitivity must be 60 cpm/mrem/h in neutron filed. For a 30 mCi ^{241}Am-Be (1.11 GBq), 4.62 cpm counting rate is expected in the considered irradiation condition. Using the high voltage and threshold values previously determined, the results of the measurements are shown in Table 5.1.

In order to investigate the response of the BSS-UNIPI to ^{241}Am-Be, this measurement was repeated for 3, 6, 8 and 15 in. and the results are shown in Table 5.2 and Fig. 5.5.

Table 5.1: Results of the measurements for exposing 10 in. Bonner sphere to an ^{241}Am-Be neutron source (1.11 GBq) at 100 cm (SDD).

Irradiation Time (min)	Net counts	Count rate (cpm)
20	92	4.60
20	97	4.85
20	90	4.50
	Average	4.65
	Error (1 σ)	4%

Table 5.2: Results of BSS-UNIPI set (3, 6, 8, 10 and 15 in.) exposed to an ^{241}Am-Be source (1.11 GBq) at 100 cm (SDD) and 20 min acquisition time.

Sphere diameter (inch)	Count rate (cpm)	Error (1σ %)
3	1.5	4.7
6	4.5	6.7
8	5.9	3.9
10	4.6	3.9
15	2.6	2.2

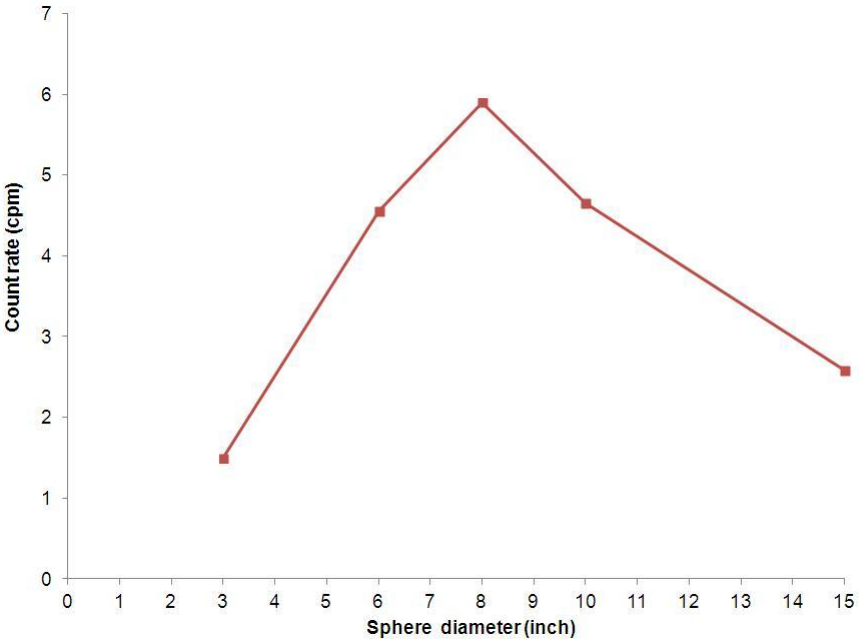

Figure 5.5: BSS-UNIPI set (3, 6, 8, 10 and 15 in.) measurements (count rate) with an ^{241}Am-Be neutron source for 1200 s irradiation time.

As it can be seen in Fig. 5.5 and explained before in Chapter 3, since an ^{241}Am-Be neutron source has a mean neutron emission energy value around 4.4 MeV, the maximum responses is achieved for 8 in. Bonner sphere, as expected.

5.4 Evaluation of the fluence response

The data reported in Table 5.2 can be used to calculate the fluence response R_Φ defined as the ratio between the reading, M, of a measuring instrument and the fluence , Φ (n.cm-^{2}), for evaluating the fluence using the following Eq. (5.1) :

$$\Phi = BtF(\theta)\frac{e^{-\Sigma r}}{4\pi r^2} \tag{5.1}$$

where B is the neutron emission rate of the 30 mCi ^{241}Am-Be neutron source ($6.6 \cdot 10^4$ s^{-1}), t is the irradiation time (1200 s), $F(\theta)$ = 1.023 is the assumed anisotropy correction factor for the considered ^{241}Am-Be source, r = 100 cm is the distance between the center of the source and the center of the detector, Σ = $8.9 \cdot 10^{-5}$ cm^{-1} is the macroscopic cross section of the air averaged on the Am-Be neutron emission spectrum. The fluence (Φ) obtained from Eq. (5.1) about 640 n·cm^{-2} and the result of the fluence response (R_φ) was shown in Table 5.3. In additional, the responses of the BSS-UNIPI calculated by MCNPX for an ^{241}Am-Be ISO neutron spectrum (see Chapter 2) are compared to the experimental results (Fig. 5.6 and Table 5.3).

Table 5.3: Comparison of measured and MCNPX calculated response (cm^2) of BSS-UNIPI for an ^{241}Am-Be neutron source.

Sphere diameter (inch)	$R_{\Phi,E}(cm^2)$ (Experimental	Relative response	$R_{\Phi,C}(cm^2)$ (Calculated)	Relative response	$\frac{R_{\Phi,E}}{R_{\Phi,C}}$
3	0.047	0.25	0.028	0.16	1.67
6	0.142	0.77	0.151	0.83	0.94
8	0.184	1.00	0.182	1.00	1.01
10	0.145	0.79	0.180	0.99	0.81
15	0.081	0.44	0.105	0.58	0.77

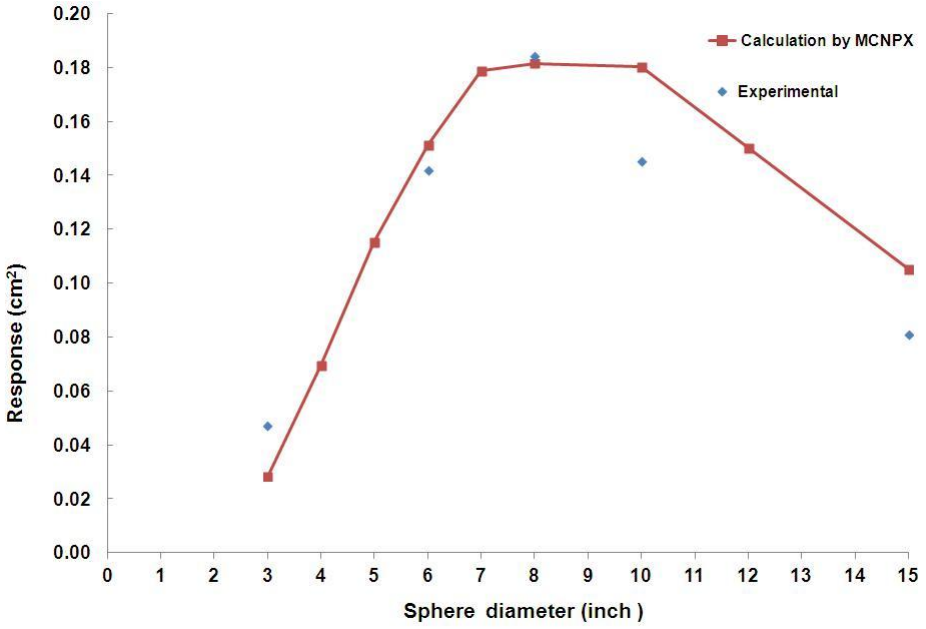

Figure 5.6: Comparison of measured and MCNPX calculated response (cm^2) of BSS-UNIPI.

Table 5.3 indicates that large discrepancies are found between experimental values and the MCNPX calculation, especially for 3 in. Bonner sphere. However, the difference may be explained by an underestimation of the neutron backscattering effect induced by the presence of supporting materials inside the irradiation room which are difficult to simulate by MC calculations. Their contributions, in this case, may not be negligible. Indeed, the best way to estimate realistically the neutron scattering contributions can be obtained by applying the shadow cone technique, which will be explained in the 5.6 section.

5.5 Unfolding data

The experimental results were unfolded with the FRUIT unfolding code (Bedogni, 2007), version 5, for obtaining the neutron spectrum.

The main characteristics of this code are the parameterization of the neutron spectrum on the basis of physically meaningful parameters and the implementation of a variable tolerance convergence procedure to evaluate the dependence of the results from the priori information. The ^{241}Am–Be neutron spectrum and related numerical characterization were obtained by unfolding the spectrometer count rates using the FRUIT unfolding code in comparison with ISO standard spectrum (ISO-8529-1); they are shown in Fig. 5.7 and Table 5.4.

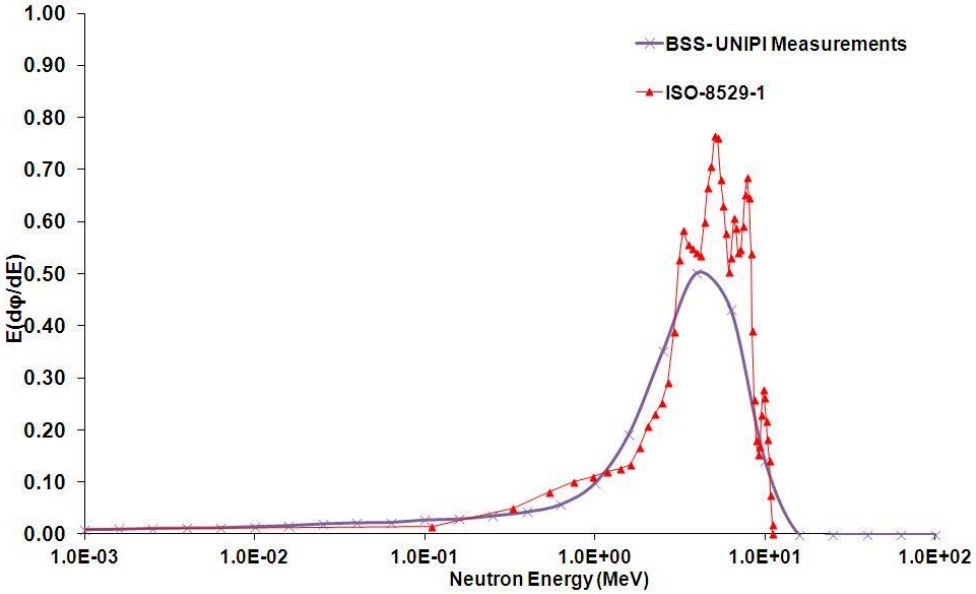

Figure 5.7: Comparison of unfolded neutron spectrum obtained from the experiments for ^{241}Am–Be with ISO spectrum.

Table 5.4: Comparison between the integral quantities ($H^*(10)$, E_φ, E_H) for ^{241}Am-Be neutron spectrum obtained by measurements with the ISO reference values.

	E_φ (MeV)	E_H (MeV)	$H^*(10)$ (pSv·cm^2)
ISO 8592-1	4.16	4.40	391
BSS-UNIPI	4.07	3.48	352 ± 5

The obtained results are shown in Table 5.4 in terms of the relevant integral quantities of the neutron spectrum: the average fluence to ambient dose equivalent conversion factor, $H^*(10)$; the average fluence neutron energy E_φ; the average ambient dose equivalent neutron energy, E_H. The integral quantities ($H^*(10)$, E_φ, E_H) have been compared to the ISO 8529-1 reference values.

As it can be seen in Fig. 5.7 and Table 5.4, the contributions of scattered neutrons which are produced by interaction of neutrons with walls, floor, roof, air and also all structures around the experiment set up, affected the final spectrum, both shape and numerical quantities. Thus they must be evaluated and determined by proper methods and their contribution should be eliminated from the measurements. For solving this problem, in the next the section shadow cone technique will be applied

for the determination and elimination of the neutron scattering in a neutron field (^{241}Am–Be) to obtain a more precise ^{241}Am–Be neutron spectrum.

5.6 Analysis of the application of the shadow cone technique for the determination of neutron spectrum with Bonner sphere spectrometer

5.6.1 Overview

Neutron sources generally are not applied in empty places. Thus, their spectrum determination is affected by walls, floor, roof, air and also all structures around the experiment set up which can determine a neutron scattering contributions (Eisenhauer, 1985; ISO 8529-2, 2000; IAEA, 2000). The scattered neutrons have a lower energy spectrum than the original neutron field and this spectrum can vary with the distance from the source. Consequently, these neutrons must not be considered as a proper part of the field but as a background component, thus requiring an appropriate correction coefficient.

There are different techniques to determine the neutron scattering contributions: computational, semi-empirical and empirical methods (Eisenhauer, 1985; ISO 8529-2, 2000; IAEA, 2000). One of the empirical types is the shadow cone technique. This method is based on the use of different shadow cones which are placed between the source and the detector at a suitable distance: the cone removes any direct radiation emitted by the source, so that only the scattered neutrons can reach the detector. Therefore it is possible to directly measure the neutron source intensity by subtracting the shadow cones neutron counts from the total counts obtained without the cone.

Previous works have been focused on the shadow cone technique. Bedogni (2007) applied this method for larger Bonner spheres and the polynomial technique for smaller Bonner spheres and, more recently, Khabaz (2011) studied the shadow cone technique applied to BSS with BF_3 thermal detector. In this work the application of the shadow cone technique for BSS-UNIPI was considered using an ^{241}Am–Be neutron source. In particular, the distance between the neutron source and the shadow cone front face was experimentally investigated to obtain a minimum neutron scattering contribution, following the ISO recommendations (ISO 8529-2, 2000). After finding the best set up to evaluate the neutron scattering contribution with the shadow cones, the FRUIT unfolding code (Bedogni, 2006), version 5, was applied to obtain the neutron energy spectrum (an ^{241}Am–Be) from the experimental data.

5.6.2 The shadow cone method

The shadow cone method, as explained before, permits to evaluate experimentally the contribution of scattered neutrons from walls, ceiling, floor, air and other objects

in the neutron installation. Having fixed the source-to-detector distance *l*, the counts due to the contribution of direct neutrons, $N_D(l)$, were obtained from the difference between the counts measured without the shadow cone, $N_T(l)$, and the counts measured with the shadow cone, $N_S(l)$, then multiplying it for a correction factor, $f(l)$, which accounts for air attenuation (air out scattering):

$$N_D(l) = \left[N_T(l) - N_S(l)\right] f(l) \tag{5.3}$$

The distance *l* is taken between the center of the source and the detector. Generally, measurements are made at a distance *l* greater than twice the shadow cone length so that the coefficient $f(l)$ is essentially one (ISO 8529-2, 2000; IAEA, 2000).

These shadow cones were designed in this thesis and two of them were used in the experiments: the first one (indicated as shadow cone I) was designed for larger Bonner spheres, considering 8 in. Bonner sphere as the reference; the second one (indicated as shadow cone II) was designed for smaller Bonner spheres, considering 5 in. Bonner sphere as the reference. Each cone consists of two parts, as recommended by ISO (ISO 8529-2, 2000): a 20 cm long front end made of iron and a 30 cm long rear section made of borated polyethylene (2% of boron). The geometrical parameters of the two shadow cones, described in Fig. 5.8, are shown in Table 5.5.

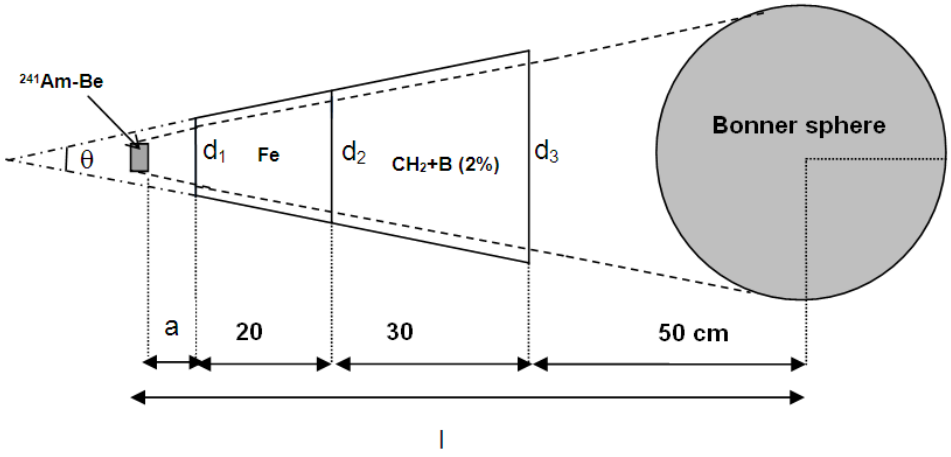

Figure 5.8: Geometrical specification of the shadow cones consisting of two parts (20 cm of iron and 30 cm of 2%-borated polyethylene) and schematic diagram of the irradiation condition with the shadow cone and the neutron source.

Table 5.5: Geometrical details of the shadow cones: cone angle θ; front end diameter of the iron cone d_1: rear diameter of the iron cone (or front end diameter of the borated polyethylene cone) d_2; rear diameter of the borated polyethylene cone d_3.

Cone	θ (º)	d_1 (cm)	d_2 (cm)	d_3 (cm)
I	10.6	11.0	14.7	20.3
II	10.5	3.9	7.6	13.1

For what the concerns the source-to-detector distance, ISO recommends that the ratio between the scattered and the direct neutron counts (N_S /N_D) should not exceed 40% (ISO 8529-2, 2000). No other indications exist about the distance *a* between the source and the shadow cone source front face: for this reason the experimental analysis of the effect of the variation of this distance on the final neutron energy spectrum was examined.

5.6.3 Experimental measurements

An ^{241}Am–Be neutron source (1.11 GBq, corresponding to a neutron emission rate of $6.6 \cdot 10^4$ s^{-1}) was used for the experiments. The effect of different distances between the source and the shadow cone front face (*a*) was investigated, while the distance between the rear face of the cone and the neutron detector was fixed to be 50 cm (see Figs. 5.8 and 5.9).

Figure 5.9: shadow cone II positioned between 5 in. Bonner sphere and an ^{241}Am–Be neutron source which is visible on the right side of the picture.

In the first step, measurements were performed with 6, 8, 10 and 12 in.Bonner spheres which were positioned at the center of the irradiation room (dimensions 6.0 m × 4.0 m × 4.0 m). The shadow cone I was placed between the neutron source and the detector, following the set up showed in Fig. 5.8. The source and the detector were placed at a 120 cm height from the floor. A measurement time of 3600 s was chosen for each test. In order to account for the scattered neutrons contribution, the measurements were performed with and without the shadow cone I and the counts due to neutrons directly emitted by the source (N_D) was obtained by Eq. (5.3). The statistical uncertainty of the results is lower than 2%.

In the second step, measurements were performed with 3, 4 and 5 in. Bonner spheres with the shadow cone II placed between the source and the Bonner sphere, with the same irradiation conditions as mentioned before (Fig. 5.9).

5.6.4 Results and discussion

The obtained ratio N_S/N_D, i.e. the ratio between the scattered neutron counts and the direct neutron counts, for the 6, 8, 10 and 12 in. Bonner spheres using shadow cone I at different distances *a* between the source and the shadow cone front face, are shown in Table 5.6.

Table 5.6: Scattered to direct neutron counts ratio (N_S/N_D) for 6, 8, 10 and 12 in. Bonner spheres using the shadow cone I at different distances (a).

Sphere diameter (in.)	*a* (cm)					
	2	5	7	10	12	15
6	0.51	0.35	0.38	0.41	0.45	0.46
8	0.32	0.31	0.32	0.32	0.34	0.41
10	0.20	0.27	0.29	0.27	0.39	0.30
12	0.16	0.19	0.20	0.19	0.26	0.17

The results show that only the distances 5, 7 and 10 cm permit to satisfy the ISO recommended value ($N_S/N_D \leq 0.4$) for all the considered Bonner spheres (the N_S/N_D value at 10 cm distance with the 6 in. Bonner sphere can also be considered acceptable taking into account the uncertainty of the measurements, which is 3%). Following these results, the shadow cone I was applied to other Bonner spheres, at the distances of 5, 7 and also 10 cm. The results of N_S/N_D are shown in Fig. 5.10 and Table 5.7.

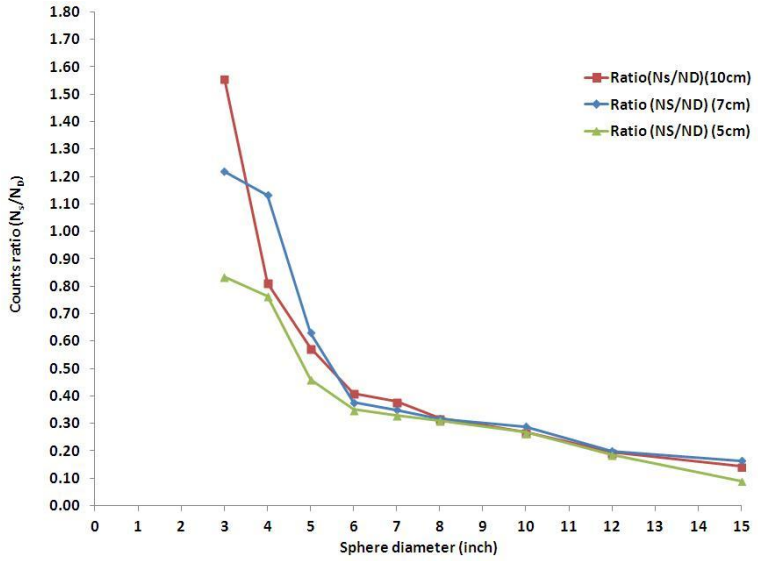

Figure 5.10: Scattered to direct neutron counts ratio (N_S/N_D) for 3 – 15 in. Bonner spheres using shadow cone I at different distances (5, 7 and 10 cm).

Table 5.7: Scattered to direct neutron counts ratio (N_S/N_D) for 3 – 15 in. Bonner spheres using the shadow cone I at different distances.

Sphere diameter (in.)	*a* (cm)		
	5	7	10
3	0.83	1.22	1.56
4	0.76	1.13	0.81
5	0.46	0.63	0.57
6	0.35	0.38	0.41
7	0.33	0.35	0.38
8	0.31	0.32	0.32
10	0.27	0.29	0.27
12	0.19	0.20	0.19
15	0.09	0.16	0.14

As it can be seen from Table 5.7, the ratio N_S/N_D decreases with increasing the sphere diameter: this ratio is higher than 0.4 for small Bonner spheres (3, 4 and 5 in.) at the considered distances, while being less than 0.4 for the 6-15 in. Bonner spheres. In all the situations the relevant statistical uncertainty is lower than 5%.

According to the experiments, the optimal distance of an ^{241}Am–Be neutron source to the shadow cone which in order to the N_S/N_D ratio was found to be 5 cm, but only for the larger Bonner spheres (diameter ≥ 6 in.).

To evaluate the scattered neutrons contribution for smaller Bonner spheres, the shadow cone II was placed between the neutron source and 3, 4 and 5 in. Bonner spheres at the optimal distance of 5 cm, in the same irradiation condition as the previous experiments. As can be seen in Table 5.8, the ratios N_S/N_D obtained for 3, 4 and 5 in. Bonner spheres dropped from 0.83 to 0.40, from 0.76 to 0.39 and from 0.46 to 0.37, respectively, satisfying the ISO recommended value (ISO-8529-2, 2000). In the same table the attenuation coefficient for the shadow cone, defined as the ratio between the detector counts registered with and without the cone (Rinard, 1991), is shown for both cone I and cone II.

Table 5.8: The ratio of scattered to direct neutron counts (N_S/N_D) and the attenuation coefficient for shadow cones I and II at the distance of 5 cm.

Sphere diameter (in.)	Cone I		Cone II	
	N_S/N_D	Attenuation coefficient (cm^{-1})	N_S/N_D	Attenuation coefficient (cm^{-1})
3	0.83	6.85E-03	0.40	1.09E-02
4	0.76	7.17E-03	0.39	1.11E-02
5	0.46	9.93E-03	0.37	1.14E-02
6	0.35	1. 16E-02	-----	-----
7	0.33	1.17E-02	-----	-----
8	0.31	1.25E-02	-----	-----
10	0.27	1.34E-02	-----	-----
12	0.19	1.61E-02	-----	-----
15	0.09	2.20E-02	-----	-----

As it can be seen in Table 5.8, the attenuation coefficient increases when shadow cone II was used for 3, 4 and 5 in. Bonner spheres. Thus a low attenuation coefficient does not necessarily means a high efficiency of the shadow cone and cannot be the unique parameter to be considered in the shadow cone method.

By using Eq. (5.2), Φ_{ref} has been calculated and considered for all Bonner spheres, being equal to about 1740 n cm^{-2} at 105 cm.

The calibration factor can be calculated for each Bonner sphere from Eq. (5.4) as follows:

$$f_i == \frac{N_{i,D}}{\Phi_{ref} R_{Am-Be}} \qquad (5.4)$$

where *i* indicated that for each Bonner sphere and the fluence response ($R_{Am\text{-}Be}$) has been calculated for each Bonner sphere by Monte Carlo simulations. f_i is obtained for each Bonner sphere as shown in Table 5.9.

The experimental results obtained for total, scattered and direct (difference between total and scattered) neutron counts by using shadow cone I for Bonner sphere diameters ≥ 6 in. and shadow cone II for Bonner sphere diameters < 6 in. are shown in Table 5.9 and Fig. 5.11.

Table 5.9: The total neutrons (N_T), scattered neutrons (N_S), direct neutron counts (N_D) and f_i for shadow cones I and II at the distance of 5 cm.

Sphere diameter (in.)	N_T	N_S	N_D	N_S/N_D	f_i
3	110	32	79	0.40	1.43
4	147	41	106	0.39	0.86
5	204	55	149	0.37	0.75
6	251	66	185	0.35	0.70
7	259	67	192	0.33	0.62
8	256	61	195	0.31	0.62
10	233	50	183	0.27	0.58
12	172	27	145	0.19	0.55
15	107	9	98	0.09	0.53

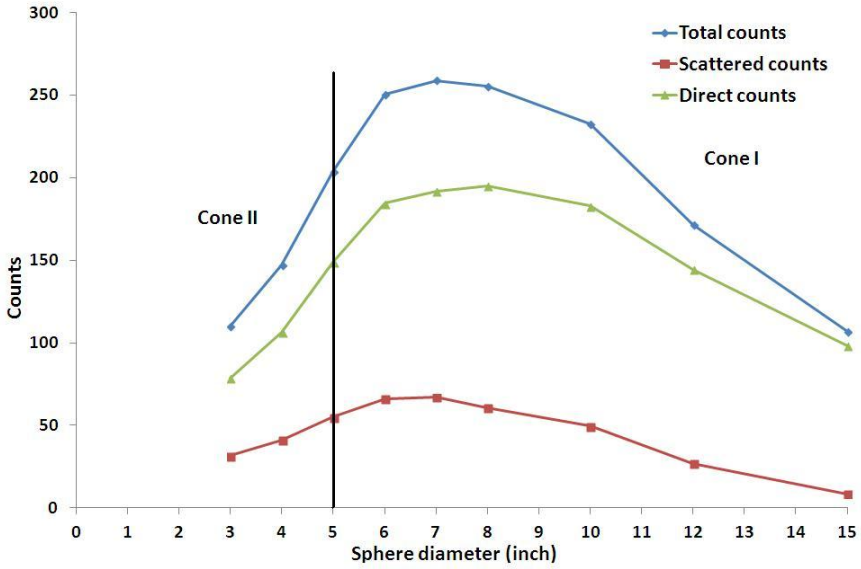

Figure 5.11: Experimental measurements for total, scattering and direct (the scattered subtracted from total) neutron counts from ^{241}Am–Be neutron source by using shadow cones I - II with 3600 s Irradiation time.

The BSS with only the shadow cone I and with the combination of the shadow cones I and II (i.e. shadow cone I for Bonner sphere diameters ≥ 6 in. and shadow cone II for Bonner sphere diameters < 6 in.) were used to determine the ^{241}Am–Be neutron spectrum by applying the FRUIT 5 unfolding code (Bedogni, 2007), version 5. The main characteristics of this code are the description of the neutron spectrum on the basis of physically meaningful parameters and the implementation of a variable tolerance convergence procedure to evaluate the dependence of the results from the *priori* information. The ^{241}Am–Be neutron spectra obtained by the present method in comparison with ISO standard spectrum (ISO-8529-1, 2001) are shown in Fig. 5.12.

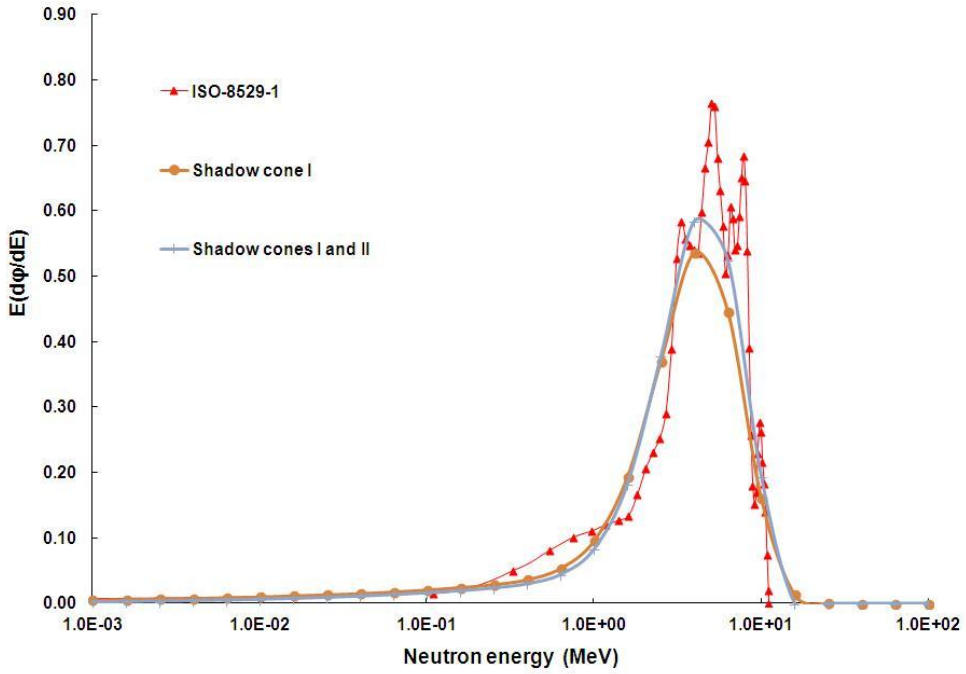

Figure 5.12: Comparison of experimental neutron spectra obtained from the unfolding of the two data set (using shadow cone I and shadow cones I – II, respectively) with ISO reference spectrum for an ^{241}Am–Be.

The advantage of using the combination of two shadow cones in comparison to using only one shadow cone is evident: the neutron spectrum obtained by applying only the shadow cone I produces a spectrum shifted to lower energies by the effect of the scattered neutrons, whereas using the shadow cone II also for smaller Bonner spheres produces a good agreement with the reference spectrum.

The obtained results reports in Table 5.9 in terms of the relevant integral quantities of the neutron spectrum: the average fluence to ambient dose equivalent conversion factor, $H^*(10)$; the average fluence neutron energy, E_φ; the average ambient dose equivalent neutron energy, E_H.

The integral quantities (H^* (10), E_φ and E_H) were compared to the reference value (ISO-8529-1, 2001) and to the results obtained with another technique (Bedogni, 2007), which uses the combination of the shadow cone method and the polynomial technique to evaluate the neutron scattered contribution with the smaller Bonner spheres. The improvement of the integral quantities (H* (10), Eφ and E_H) is evident by applying two shadow cones instead of only one shadow cone.

Table 5.10: Comparison between the experimental integral quantities ($H^*(10)$, E_φ and E_H) for ^{241}Am-Be neutron spectrum and ISO reference value.

	E_φ (MeV)	E_H (MeV)	$H^*(10)$ (pSv·cm^2)
ISO 8529-1	4.16	4.4	391
Shadow cone I	3.80	4.2	369 ± 3
Shadow cones I - II	4.16	4.4	389 ± 6
Bedogni (2007)	4.24	4.5	389 ± 8

5.6.5 Conclusions

In this section, the BSS and the shadow cone technique were experimentally investigated. The ^{241}Am–Be neutron spectrum was considered. The obtained results show that there are two factors which strongly influence the determination of the neutron spectrum: the size of the shadow cone and the source-to-shadow cone distance. To obtain a correct evaluation of the neutron scattering contribution, a minimum number of two cones are required in this work. The shadow cone I is recommended for larger Bonner spheres (6, 7, 8, 10, 12 and 15 in.) and a shadow cone II for smaller Bonner spheres (3, 4 and 5 in.). An optimal the source-to-shadow cone distance of 5 cm was found.

Finally, the experimental BSS data and the BSS response function matrix were used as the input for the unfolding code FRUIT 5. Our results showed that by using two shadow cones (I and II) with nine Bonner spheres, the obtained spectrum has a good agreement with the ISO reference spectrum.

The shadow cones **(**I and II) with BSS can also be used for the determination of the neutron spectrum in unknown neutron fields such as BNCT facility, as it will be explained in the next chapter.

References

Bedogni, R., et al. (2006). Neutron spectrometry and dosimetry for radiation protection around a high energy electron/positron collider. Ph.D. Thesis, Universitat Autónoma de Barcelona, Spain.

Bedogni, R., et al. (2007). FRUIT: an operational tool for multisphere neutron spectrometry in workplaces. *Nuclear Instruments and Methods in Physics Research. A*, 580, pp.1301-1309.

Eisenhauer, C.M., et al. (1985). Calibration techniques for neutron personal dosimetry. *Radiation Protection Dosimetry*. 10, pp. 43-57.

IAEA (2000), Calibration of radiation protection monitoring instrument. Safety Reports Series No. 16.

ISO(2001), ISO-8529-1. Reference neutron radiations-Part 1: Characteristics and methods of production. International Organization for Standardization, Geneva, Switzerland.

ISO(2000), ISO-8529-2. Reference neutron radiations—part 2: calibration fundamentals of radiation protection devices related to the basic quantities characterizing the radiation field. International Organization for Standardization, Geneva. Switzerland.

Khabaz, R. and Hashem Miri, S. (2011). Determination of ^{241}Am-Be using Bonner sphere Spectrometer by applying shadow cone technique in calibration, *Journal of Applied Sciences*, 11, pp. 2849-2855.

Khabaz, R. and Hashem Miri, S. (2011). Development of a Bonner sphere spectrometer with emphasis on decreasing the contribution of scattering by using a new designed shadow cone. *Journal of Radioanalytical and Nuclear Chemistry*, 289, pp. 789-795.

Rinard, P.M. (1991). Neutron interactions with matter. In Passive Nondestructive Assay of Nuclear Material, Los Alamos Technical Report NUREG/CR-5550, LA-UR-90-732, pp. 357-377.

6. Assessment of the angular neutron energy spectrum of an accelerator-based BNCT facility (TRASCO-BNCT project) by Bonner sphere spectrometer.

6.1 Overview

In the framework of the new stand-alone TRASCO-BNCT project, formerly included in the SPES (Study and Production of Exotic Species) one, BNCT facility construction is in progress at the Legnaro National Laboratories (LNL) of the Italian National Institute for Nuclear Physics (INFN).

The goal is the experimental treatment of skin melanoma (Pisent, 2006) and, at the next stage, the treatment of hepatic metastases in the explanted liver (Prete, 2008 and Ceballos, 2009) using an accelerator-based, high-flux thermal neutron beam facility. The experimental activity reported in this thesis has been carried out at the CN 5 MeV Van de Graaff accelerator at INFN-LNL, where the neutron source based on ^{9}Be(p,xn) reaction which is placed for the BNCT facility has been reproduced with a maximum proton current of 300 nA.

Detailed information and characterization of the neutron beam in terms of intensity and energy spectrum at different angles is requested in order to finally validate the neutron irradiation moderating system to obtain the design thermal neutron flux of the facility (Ceballos, 2009).

Neutron energy spectrum from the ^{9}Be(p,xn) reaction was first measured with incident 5 MeV protons on beryllium thick-target at 0º by using the standard Time-Of-Flight (TOF) techniques (Howard, 2001). Other techniques, using both the silicon telescope spectrometer (Agosteo, 2007, 2010) and BINS Superheated Drop Detector Spectrometer (d'Errico, 2009; Di Fulvio, 2011, 2012) were later exploited at INFN-LNL, mainly for measurements in the 100 keV- 5 MeV neutron energy range. In this thesis the BSS previously described, based on ^{6}LiI(Eu) thermal detector and with proper shadow cones was used for the characterization of the neutron spectrum below even 100 keV.

Other works reported the application of BSS to the spectral characterization of BNCT beams: FCB at MIT (USA), FiR at VTT (Finland), HFR at Petten (the Netherlands), LVR-15 at NRI (Czech Republic), at JRR-4[14] and NRI (JAEA Japan) (Voorbraak, 2003; Marek, 1998, 2011). To evaluate the neutron spectrum from BSS measurements, the response function for each Bonner sphere used together to the FRUIT and MAXED unfolding codes. Finally, the results are compared with those obtained by the other authors.

[14] Japan Research Reactor

6.2 The primary experimental measurements

The BSS-UNIPI was applied to measure the neutron spectrum produced at the CN Van de Graaff accelerator of the INFN-LNL by bombarding a beryllium target with 5 MeV incident protons. Neutrons are generated via four reactions: ^{9}Be(p,np) 2α, ^{9}Be(p,np)^{8}Be, ^{9}Be(p,n)^{9}B and ^{9}Be(p,nα)^{5}Li with threshold energies of 1.75, 1.85, 2.06 and 3.93 MeV, respectively (Howard, 2001).

The measurements were done at four different angles (0°, 40°, 80°, and 120°) measured between the proton beam line reference direction and the main axis of the BSS detector at 3 m source to detector distance. In order to perform measurements at the required height from the floor, an inch holder was used to position the center of each Bonner sphere in correspondence of the proton beam line (Fig. 6.1).

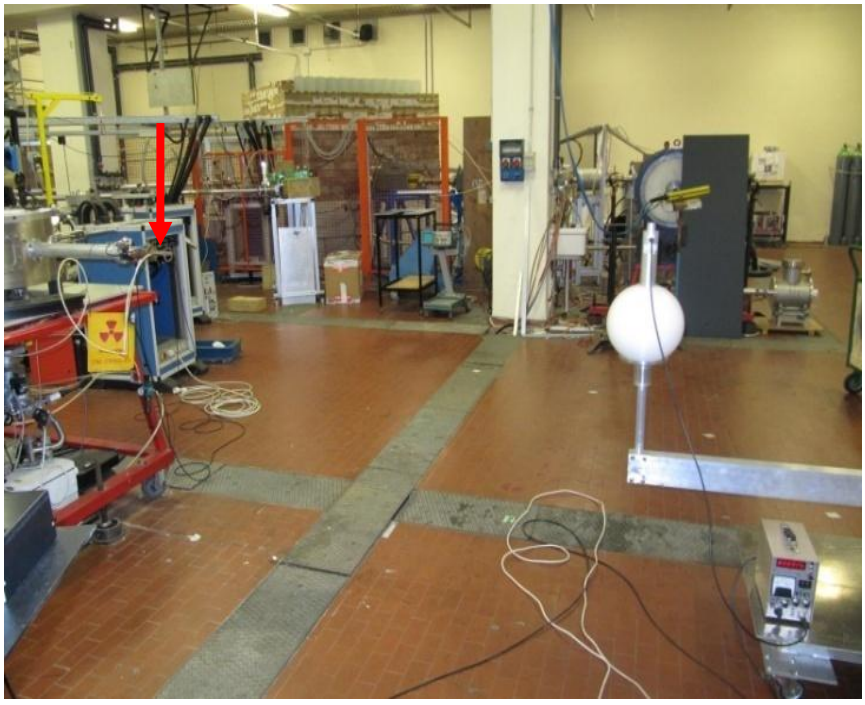

Figure 6.1: The 8 in. Bonner sphere positioned in the CN accelerator room (0° angle). The Be target is visible on the left side of the picture with red line.

Our experiments were performed at a constant proton beam current of about 60 nA: the counting time was varied in order to achieve an acceptable neutron count during measurements. The results are shown in Fig. 6.2. These first measurements included uncollided and collided neutrons. The shadow cone technique was

applied for the determination of the neutron scattering contribution in the next step. As can be seen, the maximum response was obtained with the 6 in. Bonner sphere for 0° angle and 5 in. Bonner sphere for the other investigated angles. A marked dependence of the response was found with the different angles for all Bonner spheres. The bare detector shows the same response at different angles (0°, 40°, 80°, and 120°), as expected.

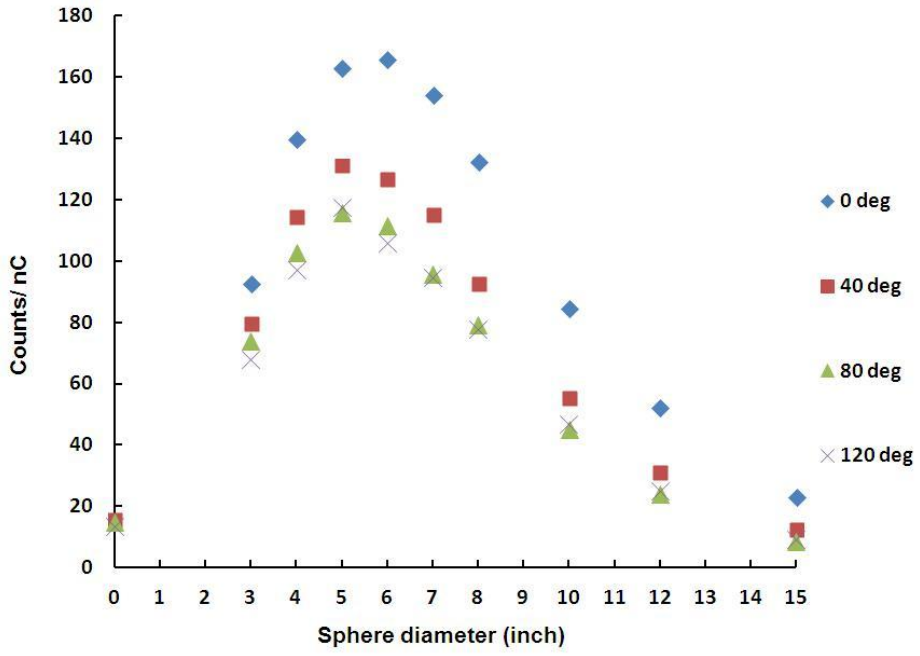

Figure 6.2: Dependence of the angular (0°, 40°, 80°, 120°) response of the BSS-UNIPI obtained for the ^{9}Be(p,n) reaction.

6.2.1 Unfolding procedures

Deconvolution of the data was performed with two codes, MAXED and FRUIT, at 0° angle. The MAXED code uses the maximum entropy method to find a neutron energy spectrum which fits the data within experimental errors in a mathematically rigorous, consistent and unbiased way. MAXED was used with an initial flat spectrum in lethargy and an upper energy cut-off of 3.2 MeV, based on the Q value of the Be(p,n) reaction, which represents a first physically reasonable guess of the measured neutron spectrum.

After running code, an educated guess spectrum was obtained and applied iteratively until a satisfactory solution of the least-squares minimization problem is found (Reginatto, 2002). Fig. 6.3 shows the result of unfolding data in comparison with the obtained spectrum by the TOF method.

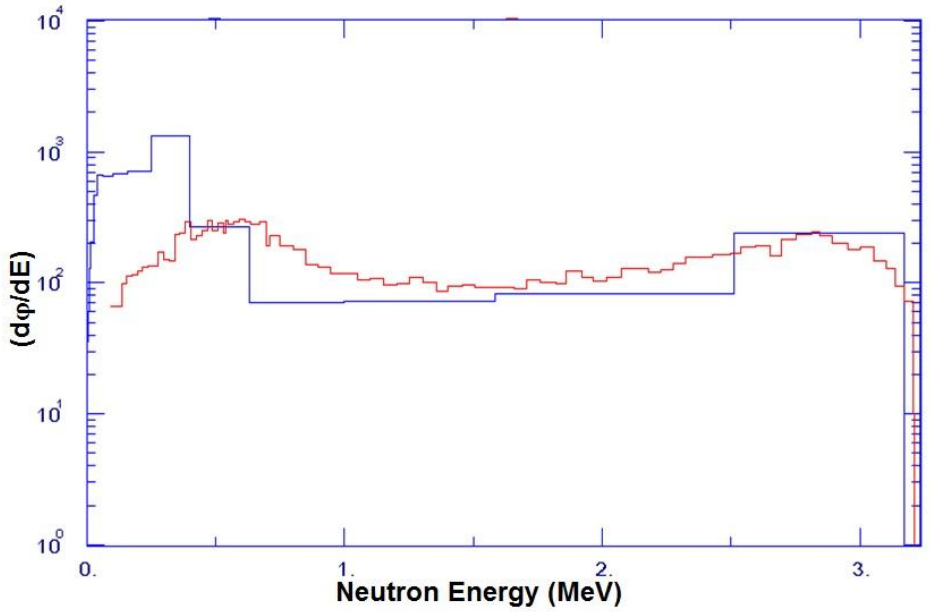

Figure 6.3: The unfolded neutron spectrum (blue) for 0° angle compared with that obtained through the TOF (red).

Analyzing the unfolded neutron spectrum for 0° angle, it is observed that the energy region below 100 keV does not show good agreement with the reference spectrum.

The FRUIT 5 unfolding code (Bedogni, 2007) was used to obtain neutron spectrum at 0º neutron emission angle. In order to use it in the parametric model, a prior spectrum was used for ^{9}Be(p,n) reaction with 5 MeV at 0º : this is the spectrum obtained by standard time-of-flight (TOF) techniques (Howard, 2001). Then, according to this spectrum the response matrix used for the unfolding was linearly rebinned, in the energy range 0.091 - 3.2 MeV. The response matrix, the rebinned energy, the BSS-UNIPI readings and their relative uncertainties were applied as input files for the FRUIT 5 code, but the result was not satisfactory.

Although the scattered neutrons have a lower energy spectrum than the primary neutron field, their contribution affects the neutron spectrum. The result obtained by the Maxed showed that it is necessary to apply shadow cone technique to subtract the scattered neutron contribution and obtain the exact spectrum.

6.3 Application of the shadow cone technique with BSS-UNIPI for the determination of the angular neutron energy spectrum of INFN-LNL SPES-BNCT facility

An important aspect of neutron filed characterization was the correct evaluation of the scattered neutrons contribution in the actual irradiation room. For this reason the BSS-UNIPI, based on ^{6}LiI(Eu) scintillator, coupled with the shadow cone technique. As described before in Chapter 5, the shadow cone method has been applied in order to evaluate and subtract the neutron scattering component due to accelerator room structures such as walls, air and the ancillary experimental apparatus (Eisenhauer, 1985; ISO 8529-2, 2000; IAEA, 2000).

Two shadow clones were designed, consisting of a 20 cm iron pot and a 30 cm polyethylene (2% boron enriched) part, as explained in Chapter 5.The first shadow cone I was designed for larger Bonner spheres and the other (II) was for smaller Bonner spheres to be used for investigation neutron spectra of the neutron beam in the LNL facility: shadow cone I for Bonner sphere diameter more than 6 in. and shadow cone II for Bonner sphere diameter less than 6 in. Each shadow cone was placed between the source and the detector at a suitable distance to determine the neutron scattering contribution, as suggested by the ISO 8529-2 standard. The geometrical details of the two shadow cones are shown in Table 6.1.

Table 6.1: Geometrical details of the shadow cones: cone angle θ; front end diameter of the iron cone d_1: rear diameter of the iron cone (or front end diameter of the borated polyethylene cone d_2); rear diameter of the borated polyethylene cone d_3.

Cone	θ (º)	d_1 (cm)	d_2 (cm)	d_3 (cm)
I	10.6	11.0	14.7	20.3
II	5.9	3.4	5.6	9.1

6.3.1 Experimental measurements

The measurements were performed at four different angles (0°, 40°, 80°, and 120°) using BSS-UNIPI with shadow cone technique. The experiments were done at a constant proton beam current of about 100 nA: In order to achieve an acceptable

neutron count the irradiation time was varied during the measurements with and without shadow cones. The shadow cone was placed between the source and the detector: the distance between source and shadow cone front face was set at 8 cm. This value was found to be in accordance with the ISO requirement that the ratio between the scattered and direct neutron counts is be less than 40% (Fig. 6.5).

Figure 6.4: The 5 in. Bonner sphere and shadow cone II positioned in the CN accelerator room of the INFN-LNL (120° angle). The Be accelerator target is on the left side of the picture.

The aim of these measurements was to obtain the net neutron spectrum at different angles with the impinging proton beam. The contribution of neutrons directly emitted by the target was obtained by subtracting the total neutron counts from the scattering neutron counts. The results for the total neutron, scattering and direct counts are shown in Figs. 6.5 and 6.6. The resulting statistical uncertainties were lower than 2% for all the different angles.

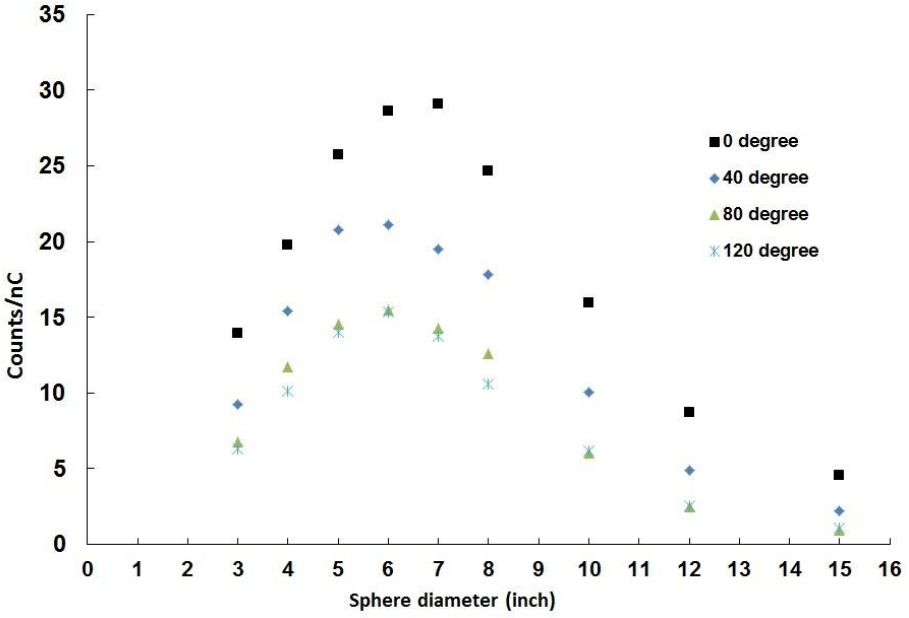

Figure 6.5: The dependence of the angular (0°, 40°, 80°and 120°) response of the BSS-UNIPI (total counts, i.e. without using shadow cones) obtained by ^{9}Be (p, n) reaction.

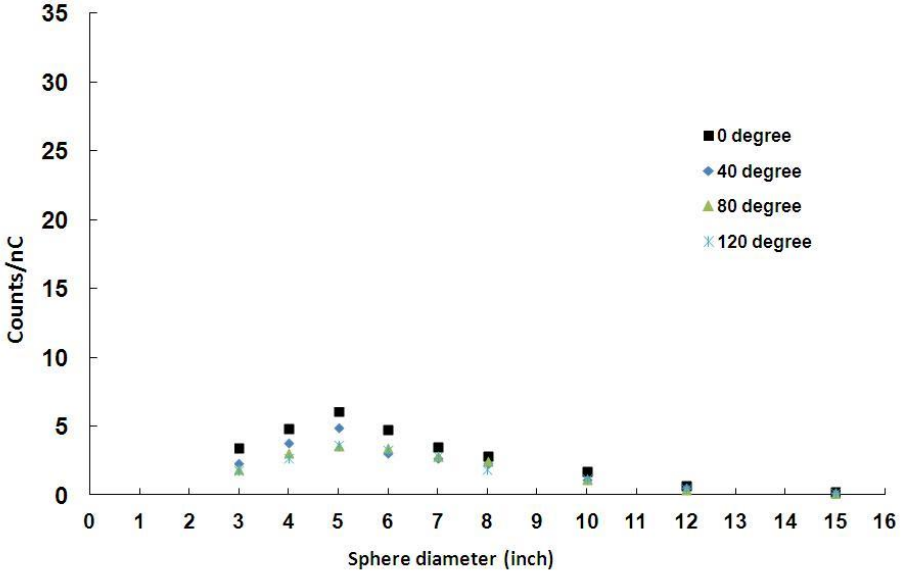

Figure 6.6: The dependence of the angular (0°, 40°, 80°and 120°) response of the BSS-UNIPI (scattering counts, i.e. using shadow cones) obtained by ^{9}Be (p, n) reaction.

The obtained results for neutrons directly emitted by the target for 0°, 40°, 80° and 120° with respect to the primary proton beam axis at the CN accelerator of INFN-LNL are shown in Fig. 6.7.

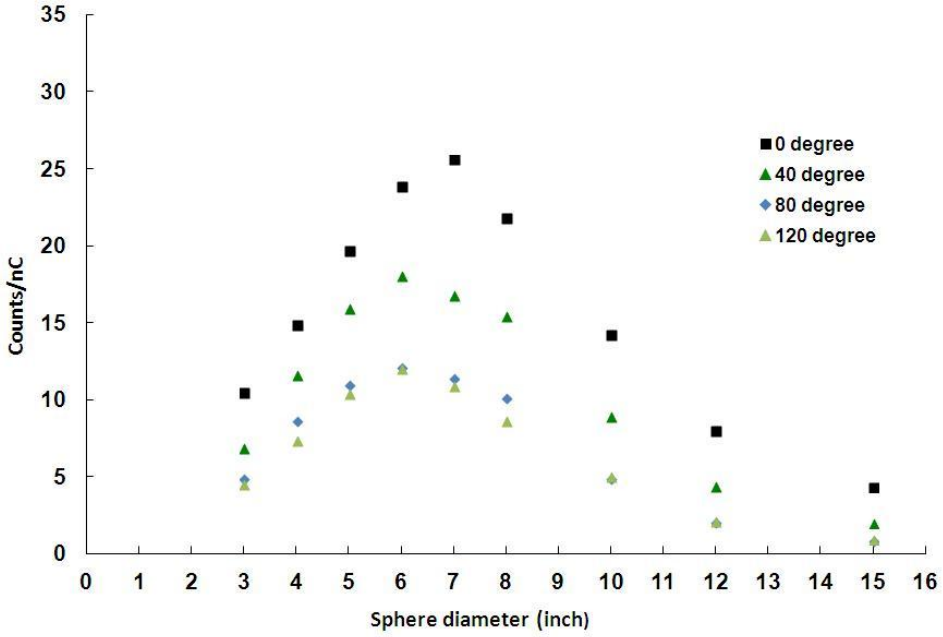

Figure 6.7: The dependence of the angular (0°, 40°, 80°and 120°) response of the BSS-UNIPI (direct counts) obtained by the ^{9}Be (p, n) reaction.

As can be seen, the maximum detector response for neutrons directly emitted by the target was obtained with the 7 in. Bonner sphere for 0° angle and 6 in. Bonner sphere for other investigated angles.

6.3.2 Unfolding procedures

The FRUIT 5 was used for 0º and MAXED code was applied to obtain neutron spectrum at 0º, 40°, 80° and 120° neutron emission angle. Then the results were compared to those of other authors.

As mentioned in the last section, the FRUIT 5 unfolding code was used for 0 degree in parametric models, default spectrum. MAXED requires a default spectrum as input to be used, as the information available about the spectrum requires a so-called start (guess, a-priori) spectrum, which represents a first

physically reasonable guess of the measured neutron spectrum. Tme-of-flight (TOF) measured spectrum was used as guess one for the first run.

6.3.3 Results and discussion

The resulting neutron spectra (0°, 40°, 80° and 120°) from unfolding of experimental data by MAXED and for 0° by FRUIT 5 are shown in Figs. 6.8-12.

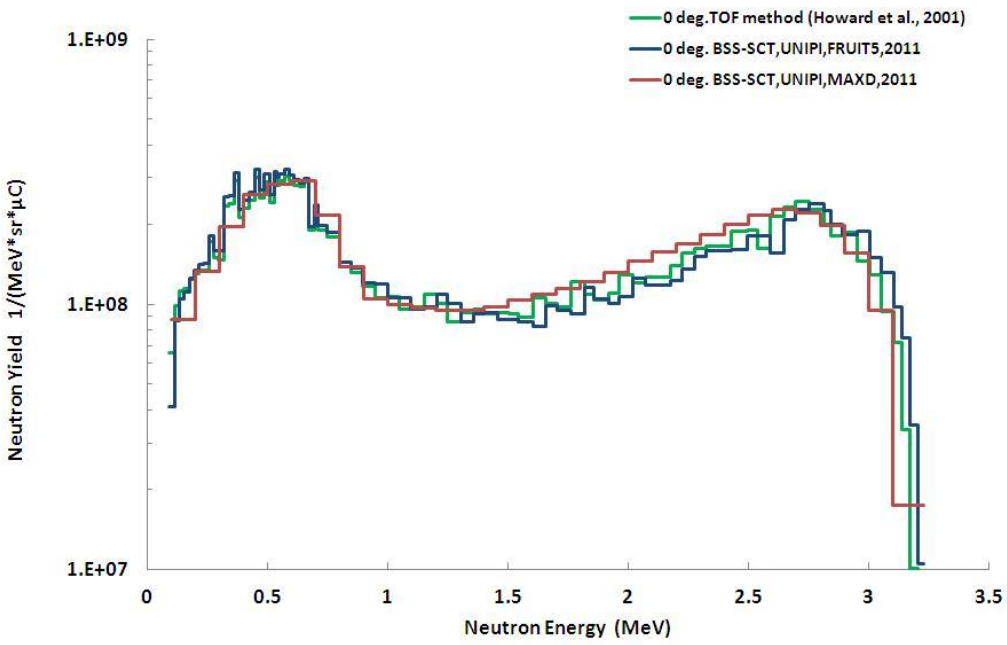

Figure 6.8: Neutron energy spectra obtained by the BSS-UNIPI coupled with the shadow cone technique using FRUIT 5 or MAXED codes at 0°in comparison with the TOF spectrum.

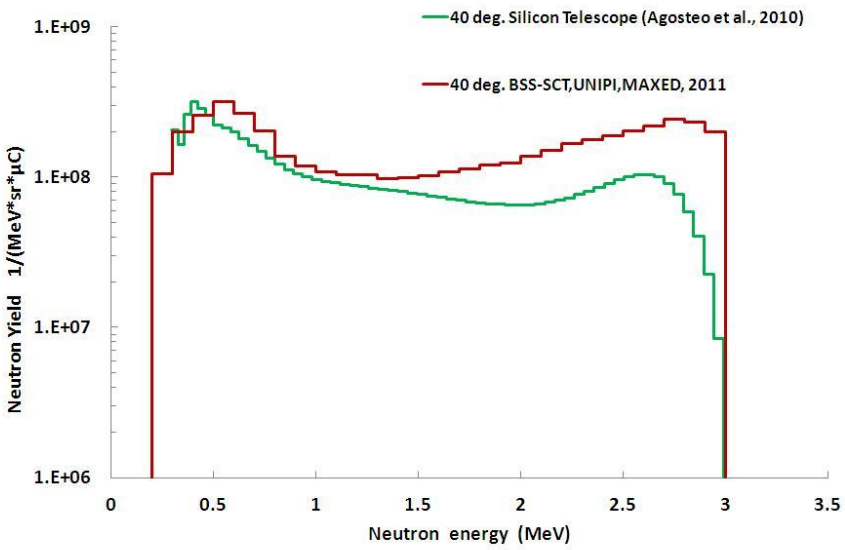

Figure 6.9: Neutron energy spectrum obtained by the BSS-UNIPI coupled with the shadow cone technique using MAXED code at 40°in comparison with a silicon telescope spectrometer.

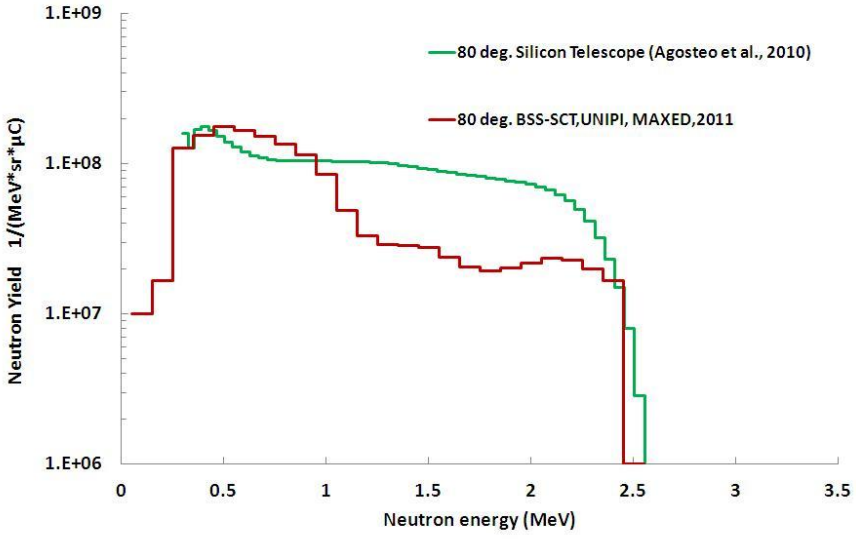

Figure 6.10: Neutron energy spectrum obtained by the BSS-UNIPI coupled with the shadow cone technique using MAXED code at 80° in comparison with a silicon telescope spectrometer.

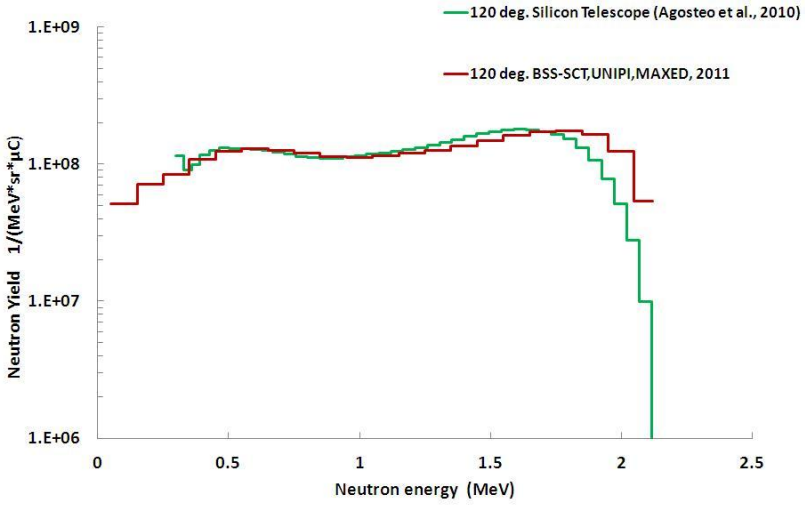

Figure 6.11: Neutron energy spectrum obtained by the BSS-UNIPI coupled with the shadow cone technique using MAXED code at 120°, in comparison with a silicon telescope spectrometer.

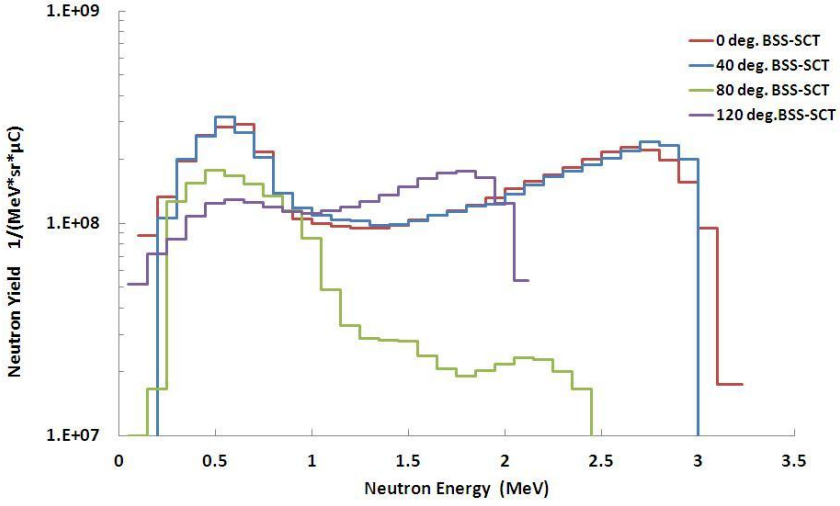

Figure 6.12: Neutron energy spectrum obtained by the BSS-UNIPI coupled with the shadow cone technique using MAXED code at 0°, 40°, 80° and 120°.

According to the kinetic energy of ^{9}Be (p,xn) reaction, the maximum values of the neutron energy are 3.2, 3.0, 2.5, and 2.1 MeV at 0°, 40°, 80° and 120°, respectively. Two broad neutron energy peaks (the first one around 500 keV and the second one in the 1.8 - 2.7 MeV intervals) depending on the angle can be seen in Figs. 6.8-12. Due to incident proton energies of interest between 3 and 5 MeV to beryllium target and taking into account that the isotope ^{9}Be that has the lowest neutron binding energy (~1.67 MeV), three main channels of neutron production exist via inelastic scattering. The three channels are compound nucleus break-up, direct-charge exchange, and multi-body break-up of ^{9}Be.

The first channel, compound nucleus breaks up, is obtained in the production of high energy neutrons and maybe the responsibility to produce the peak at the right of the spectrum displayed in Figs. 6.8-12. Higher energy neutrons (E >1 MeV) result from the compound nucleus formation process, whose energy threshold is 1.75 MeV. 5 MeV protons have created an intense high energy component since both ground and first excited state transitions of ^{9}B contribute to the ^{9}Be (p,n) ^{9}B reaction channel: the nominal threshold for excitation of the first excited state of ^{9}B is 4.64 MeV. Multi-body break-up imparts less energy to the neutron due to conservation of momentum in the system, and thus it contributes strongly to the low-energy component of the spectrum. Indeed, the three-body breakup of ^{9}Be can occur for incident proton energies as low as 1.85 MeV while protons slow down within the target. In addition to the reaction channels already cited, the neutron production increase around 500 keV should be instead ascribed to the 2.56 MeV reaction resonances, affecting protons slowed down within the target (Marion, 1959 and Howard, 2001). As the incident energy of the protons increases, there are more excited states of the compound nucleus decaying to the ground state by emitting mid-energy neutrons. This begins in the "valley" between the multi-body break up peak at 0.6 MeV and the peak due to compound nucleus break up.

In the TOF technique, neutron spectrum is obtained by the measurement process of neutron detection while for the other two techniques, neutron spectra are achieved through the unfolding of the measured data by using proper unfolding algorithms. In the monolithic silicon telescope, neutron spectra result from unfolding the measured data using a proper unfolding algorithm based on both a non-linear least squares method and the known detector response functions. The obtained spectrum showed a minimum detectable neutron energy about 300 keV, due to the attenuation of recoil-protons in the air gap between the polyethylene converter and the monolithic silicon telescope. Such a limitation is not present with the BSS-UNIPI spectra because the system, based on ^{6}LiI(Eu) scintillator, is sensitive to thermal and epithermal neutrons as well.

A spectrum was obtained using the BSS data coupled with the shadow cone technique with MAXED code and FRUIT 5 code for 0° as shown in Fig. 6.8, in good agreement with the TOF technique. On the other hand, the other unfolded spectra at 40°, 80° and 120° (Fig. 6.8-11) show a more limited energy resolution than for spectrum obtained by FRUIT 5 for 0°, because MAXED used the few-channel algorithm while FRUIT 5 used very detailed default spectrum as input. The agreements of the other unfolded spectra (40°, 80° and 120°) with a monolithic silicon telescope were on the whole satisfactory. The difference between BSS-

UNIPI coupled with the shadow cone technique and monolithic silicon telescope results could be related to the radiation measurement method and unfolding procedure.

6.3.4 Conclusions

The aim of this work was to characterize the neutron source of the accelerator-based BNCT by BSS-UNIPI and shadow cone technique facility which is being studied at the LNL-INFN.

Although a significant gamma component is produced by the ^{9}Be(p,xn) reaction, this is nonetheless the one ranked among the most suitable accelerator based neutron sources for BNCT, given the high neutron yield and the favorable thermo mechanical properties of beryllium.

The configuration of a Bonner spectrometer based on ^{6}LiI (EU) scintillator with shadow cone technique was validated for neutron spectrometry at the LNL-INFN.

While having a poor energy resolution, the ^{6}LiI(Eu) scintillator based BSS-UNIPI system, with its good gamma discrimination can be used for the spectrometric characterization of mixed radiation fields.

The BSS-UNIPI with the shadow cone technique was applied at a specific source-to-shadow cone distance of 8 cm at the LNL-INFN, in order to obtain the net neutron count and to evaluate the neutron spectrum. Data unfolded using the FRUIT 5 for 0° and MAXED deconvolution codes for (0°, 40°, 80° and 120°) were compared with neutron spectra measured either by the TOF method for 0°or using a compact monolithic silicon telescope spectrometer, coupled with a polyethylene converter at yield angles (40°, 80° and 120°). The obtained spectra are in satisfactory agreement with the previous technique.

References

Agosteo, S., et al. (2007). Neutron spectrometry with a monolithic silicon telescope. *Radiation Protection Dosimetry*. 126 (1-4), pp. 210-217.

Agosteo, S., et al. (2010). Improvement of the minimum detectable energy of a recoil-proton spectrometer based on a silicon telescope*. Radiation measurements.* 45, pp. 1281-1283.

Bramblett, R.L., et al. (1960). A new type of neutron spectrometer. *Nuclear Instruments and Methods in Physics Research.* 9, pp. 1-12.

Bedogni, R., et al. (2007). FRUIT: an operational tool for multisphere neutron spectrometry in workplaces. *Nuclear Instruments and Methods in Physics Research*. A, 580, pp.1301-1309.

Ceballos, C., et al. (2009). The BSA modeling for the accelerator-based BNCT facility at INFN LNL for treating shallow skin melanoma. *Applied Radiation* and *Isotopes*. 67 (7-8), pp. S274-S277.

d'Errico, F., et al. (2009). Angle and energy differential neutron spectrometry for the SPES BNCT facility. *Applied Radiation* and *Isotopes*. 67, pp. S141–S144.

Di Fulvio, A. (2011). Studio e realizzazione di tecniche di spettrometria e dosimetria neutronica: applicazione al progetto SPES-BNCT. Ph.D. thesis, University of Pisa, Pisa, Italy.

Di Fulvio, A., et al. (2012). Application of the BINS Superheated Drop Detector Spectrometer to the ^{9}Be(p,xn) Neutron Energy Spectrum Determination. Proceedings of ION BEAMS '12 Multidisciplinary Applications of Nuclear Physics with Ion Beams June 6th-8th, 2012, Laboratori Nazionali di Legnaro (Padua), Italy.

Eisenhauer, C.M., et al. (1985). Calibration techniques for neutron personal dosimetry. *Radiation Protection Dosimetry*. 10, pp. 43-57.

IAEA, Safety Reports Series No. 16, 2000.

ISO 8529-2 (2000). Reference neutron radiations—part 2: calibration fundamentals of radiation protection devices related to the basic quantities characterizing the radiation field. International Organization for Standardization, Geneva. Switzerland.

Howard, W.B. (2001). Measurement of the thick-target ^{9}Be(p,n) neutron energy spectra. *Nuclear science and engineering.* 138(2), pp. 145-160.

Marek, M., et al. (1998). Determination of the geometric and spectral characteristics of BNCT beam (neutron and gamma-ray). *Proceedings of the 8th International Symposium on Neutron Capture Therapy for Cancer*, La Jolla, CA, September, pp. 13-18.

Marek, M., et al. (2011). Bonner sphere spectrometer for characterization of BNCT beam. *Applied Radiation* and *Isotopes*. 69, pp. 1918–1920.

Marion, J.B., and J.S. Levin. (1959). Investigation of the ^{9}Be(p,n) ^{9}B and ^{9}Be(p,**a**-γ) ^{6}Li reactions. Physical Review., 115(1), pp.144-149.

Pisent, A., et al. (2006). Progress on the accelerator based SPES-BNCT project at INFN Legnaro, *Journal of Physics: Conference Series*. 41, pp. 391-399.

Prete, G., et al. (2008). Selective production exotic Species, Chapter XII – SPES applied Science, BNCT and LENOS. *Technical design report. INFN-LNL-224*, pp. 181-214.

Reginatto, M., et al. (2002). Spectrum unfolding, sensitivity analysis and propagation of uncertainties with the maximum entropy deconvolution code MAXED. Nuclear Instruments and Methods in Physics Research, A, 476, pp.242-246.

Voorbraak, W.P., et al. (2003). Recommendations For the Dosimetry of Boron Neutron Capture Therapy (BNCT). Report 21425/03.55339/C, NRG, Petten.

7. Summary, conclusions and prospects

The present work describes the characterization and the application of the BSS-UNIPI, based on ^{6}LiI (Eu), as neutron spectrometer. This spectrometer is useful to apply in investigating neutron beam in mixed fields, as found in BNCT. The main conclusions of the work are the following:

1 - The response matrix of BSS was calculated for 51 energy bins (from 1 meV to 100 MeV) by MCNPX code with a proper variance reduction method; the final statistical uncertainty was found to be less than 3%.

2 - For the assessment of the angle dependence, the response of the BSS-UNIPI to an ^{241}Am-Be neutron source was investigated in two directions of neutron beam (0º and 90º). The result shows that both directions are in good agreement and the difference achieved does not exceed 2%.

3 - The differential energy distribution of neutron source was determined by unfolding techniques. For this purpose, two unfolding codes, FRUIT 5 and MAXED, were selected and studied.

4 - The BSS-UNIPI was calibrated with respect to background and photon discrimination by using a ^{137}Cs (0.19 MBq) gamma source. This procedure allowed the experimental set up of the photon discrimination threshold. In particular, the neutron response of the instrument with the selected discrimination threshold was checked exposing the 10 in. Bonner sphere to a ^{241}Am–Be (1.11 GBq) neutron source at 100 cm source-to–detector distance.

5 - The fluence response of the BSS-UNIPI to ^{241}Am–Be (1.11 GBq) neutrons was measured and compared with calculations. The result showed that large discrepancies are found between MCNPX calculations and experimental values, due to underestimation of the room return effect on the measured response fluence. The total (uncollided + collided) neutron counts were unfolded by FRUIT 5. The obtained spectrum was compared with the ISO 8529-1 reference values. Numerical and final spectrum was not in agreement with the reference value ISO 8529-1 and showed that the neutron scattering contribution affects both shape and numerical quantity of spectrum.

6 - For this reason three shadow cones were designed, consisting of a 20 cm iron and a 30 cm polyethylene (2% boron enriched) parts. The first shadow cone I was designed for larger Bonner spheres and the other II for smaller Bonner spheres: shadow cone I for Bonner sphere diameter more than 6 in. and shadow cone II for Bonner spheres < 6 in. diameter. Each shadow cone was placed between the source and the detector at a suitable distance to determine the neutron scattering contribution, as suggested by ISO 8529-2 standard.

7 - The application of the shadow cone technique for the determination of neutron spectra with BSS-UNIPI was analyzed. The set of measurements were done with and without shadow cones. The scattered to direct neutron count ratio (N_S/N_D) for BSS were evaluated at different distances between the source and the shadow cone front face according to the recommended value ($N_S/N_D \leq 0.4$). An optimal

distance was found at 5 cm between the source and the shadow cone. The obtained data were unfolded by FRUIT 5 code, the results were compared and result showed that both shape and numerical quantity of final spectrum were in good agreement with the ISO 8529-1 reference value.

8 - The BSS-UNIPI, based on ^{6}LiI(Eu) scintillator, was used for measuring angular-dependent neutron energy spectrum produced by the ^{9}Be (p,xn) reaction, under 5 MeV proton beam in the framework of INFN TRASCO-BNCT project. Preliminary unfolding spectrum showed the effect of the contribution of neutron scattering on final spectrum. Subsequently, the experiment was repeated by using BSS-UNIPI couple with the shadow cone technique and data unfolded by two codes (FRUIT 5 for 0° and MAXED for all angles). The result showed that satisfactory agreement with other authors.

BSS-UNIPI, based on ^{6}LiI(Eu) scintillator, coupled with the shadow cone technique can be used for determination of the neutron spectrum in BNCT facility and other mixed fields. In future, BSS-UNIPI will be also developed and based on passive detector to be used in pulsed neutron fields and determine the unwanted neutron production of every high-energy LINACs used in radiotherapy medical treatments.

APPENDIX A - Input simulation file of MCNP

C Calculation of Neutron Rate for Indium activation foil with Bonner sphere Spectrometer (3 inch)

C cell specifications

1 1 -0.939 -1 2 -11 $ upper cylinder of Indium (Polyethylene (C2H4)n)

2 2 -7.31 -2 3 -11 $ Indium

3 1 -0.939 -3 4 -11 #2 $ The gap between Indium and (Polyethylene (C2H4)n)

4 3 -2.7 -4 5 -12 #3 $ inch support 1

5 3 -2.7 -5 6 -14 #4 $ inch support 2

6 3 -2.7 -6 7 -14 13 $ covered inch 1

7 4 -0.0012 -6 7 -13 #5 #6 $ inside the cover fill by air 1

8 4 -0.0012 -7 8 -15 #7 #6 $ inside the cover fill by air 2

9 3 -2.7 -7 9 -14 #8 $ covered aluminum 2

10 3 -2.7 -8 9 -14 #9 $ aluminum support 3

11 3 -2.7 -9 10 -16 #1 #2 #3 #4 #5 #6 #7 #8 #9 #10 $ aluminum support 4

12 1 -0.939 (-17 14 -5):(-17 11 12 5 -4):(-17 11 4 -1):(-17 1) $ 3 inch Bonner sphere

13 4 -0.0012 -18 17 #1 #2 #3 #4 #5 #6 #7 #8 #9 #10 #11 #12 $ free Bonner sphere

14 4 -0.0012 18 #13 $ outside the Bonner sphere

c surface specifications

1 PY 0.9 $ upper plane of (covered aluminum) 1

2 PY 0.005 $ upper plane of (Indium)

3 PY -0.005 $ bottom plane of (Indium) and upper plane of Polyethylene (C2H4)n

4 PY -3.6 $ covered aluminum

5 PY -9.6 $ covered aluminum

6 PY -10.5 $ upper plane of laluminum

7 PY -24.53 $ bottom plane of

8 PY -28.41 $ bottom plane of and upper plane of (covered

9 PY -28.91 $ bottom plane of covered aluminum 1

10 PY -30.51 $ bottom plane of covered aluminum 1 final

11 CY 0.50 $ cylinder about the y axis (Dysprosium)

12 CY 0.9 $ cylinder about the y axis (aluminum)

13 CY 2.14 $ cylinder about the y axis (covered aluminum) 3

14 CY 2.54 $ cylinder about the y axis (covered aluminum) 5

15 CY 1.94 $ cylinder about the y axis covered internal second after PM

16 CY 0.8 $ cylinder about the y axis (covered aluminum) final

17 SO 3.81 $ Bonner sphere

18 SO 50 $ free Bonner sphere

c data section

MODE N

imp:n 1 12r 0

SDEF POS=0 3.81 0 AXS=0 1 0 EXT=0 VEC=0 1 0 DIR=-1 RAD=d1 PAR=1 ERG=6.310E-01

si1 0 3.81

SP1 -21 1

c data section

c Materials

m1 6000.60c -0.857 $ Polyethylene (C2H4)n with density(0.939 g/cm3)

1001.60c -0.143

mt1 poly.01t

m2 49000.60c -1.0 $ Indium(In-nat) with density (7.31 g/cm3)

```
m3   13027.60c -1.0          $ Aluminum with density(2.7 g/CM3)
m4   7014.60c -0.7553
     8016.60c -0.2421
     6012.50c -0.0021
     18000.35c -0.0005      $ air with density (-0.0012)
c TALLIES
f4:n  2
fm4 (0.23905 2 102)          $ atom Cm^4/bg, reaction (n,gamma)
nps 10000000                 $ run 10000000 neutron histories in this calculation
Print                        $ print everything about the calculation
c end data section
```

APPENDIX B- Publications

Papers:

1. **N. Mirzajani,** R. Ciolini, A. Di Fulvio, F. d'Errico , Application of a Bonner sphere spectrometer for the determination of the angular neutron energy spectrum of an accelerator-based BNCT facility, Paper accepted for publishing in *Applied radiation and Isotopes (ARI) journal* in November (2012) and in progress .

2. A. Di Fulvio, R. Ciolini, **N. Mirzajani,** C. Romei, F. d'Errico, R. Bedogni, J. Esposito, D. Zafiropolous, P. Colautti, Setup of the BINS superheated drop detectors spectrometer and application to the Be (p,n) neutron energy spectrum determination, *ION BEAMS '12 Multidisciplinary Applications of Nuclear Physics with Ion Beam, June 6th-8th,* (2012), Laboratori Nazionali di Legnaro (Padova), Italy. Paper accepted for publishing in AIP conference proceeding and in progress.

3. C. Romei, R. Ciolini, A. Di Fulvio, **N. Mirzajani,** S. Selici, F. d'Errico, S.O. Souza, J. Esposito, P. Colautti, Analysis of the response of innovative neutron detectors with monoenergetic neutron beams, Proceedings of *ION BEAMS '12 Multidisciplinary Applications of Nuclear Physics with Ion Beams* June 6th-8th, (2012), Laboratori Nazionali di Legnaro (Padova), Italy. Paper accepted for in AIP conference proceeding and in progress.

4. **N. Mirzajani,** R. Ciolini, G. Curzio, Analysis of the application of the shadow cone technique for the determination of neutron spectra with Bonner sphere spectrometer. In press, accepted manuscript for publishing in *Journal of nuclear instrument and methods in physics research section A* (DOI:10.1016/j.nima.2013.04.030).

Reports:

5. R. Ciolini, G. Curzio, D. Mazed, **N. Mirzajani**, Development of a neutron Bonner sphere spectrometer system Part 1, DIMNP *Report, Atto del Dipartmento 006* (2010).

6. **N. Mirzajani**, R. Ciolini, A. Di Fulvio, J. Esposito, A. Del Gratta , G. Curzio. Progress towards Bonner sphere spectrometry of the INFN-LNL SPES-BNCT. *INFN-LNL Annual Report* ,pp*. 135-136,* (2010).

Proceeding conference:

7. **N. Mirzajani,** R. Ciolini, G. Curzio, F. d'Errico, A. Del Gratta, J. Esposito, Set up of a Bonner sphere Spectrometer for an accelerator-based BNCT Facility, *Young Researchers BNCT Meeting*, Mainz, Germany September 29- October 2, (2009).

8. A. Di Fulvio, R. Ciolini, **N. Mirzajani,** S. Selici, A. Del Gratta, F. Pazzagli and F. D'Errico, Neutron spectrometry of proton induced reaction on beryllium target with superheated emulsions: results and further developments. *Interdisciplinary Physics with Ion Beams: Status and Perspectives - LNL Users* Workshop-16-17 June, (2011).

9. **N. Mirzajani,** R. Ciolini, A. Di Fulvio, F. D'Errico ,J. Esposito, R. Bedogni, Investigation of the neutron beam of an accelerator-based BNCT facility by means of a Bonner sphere spectrometer, *14th International Congress of Radiation Research ,* Warsaw , Poland , August 28- September 1, pp.118 (2011).

10. **N. Mirzajani,** R. Ciolini, A. Di Fulvio, F. d'Errico , Application of a Bonner sphere spectrometer for the determination of the angular neutron energy spectrum of an accelerator-based BNCT facility, *Proceedings of 15th International Congress on Neutron Capture Therapy*- Tsukuba, Japan, September 10-14, pp.142, (2012).